DRYING AND CO-PELLETIZATION OF MICROALGAE WITH SAWDUST

by

Hasti Hosseinizand

B.A.Sc., Sharif University of Technology, 2010

M.A.Sc., Sharif University of Technology, 2012

A THESIS SUBMITTED IN PARTIAL FULFILLMENT OF

THE REQUIREMENTS FOR THE DEGREE OF

DOCTOR OF PHILOSOPHY

in

THE FACULTY OF GRADUATE AND POSTDOCTORAL STUDIES

(Chemical and Biological Engineering)

THE UNIVERSITY OF BRITISH COLUMBIA

(Vancouver)

August 2018

The following individuals certify that they have read, and recommend to the Faculty of Graduate and Postdoctoral Studies for acceptance, the dissertation entitled:

Drying and co-pelletization of microalgae with sawdust

submitted by	Hasti Hosseinizand	in partial fulfillment of the requirements
the degree of	Doctor of Philosophy	
in	Chemical and Biological Engineering	

Examining Committee:

Professor Shahab Sokhansanj, Chemical and Biological Engineering Department, UBC
Co-supervisor

Professor Jim Lim, Chemical and Biological Engineering Department, UBC
Co-supervisor

Professor Susan Baldwin, Chemical and Biological Engineering Department, UBC
Supervisory Committee Member

Professor Xiaotao Bi, Chemical and Biological Engineering Department, UBC
University Examiner

Professor Philip David Evans, Department of Wood Science, UBC
University Examiner

Professor Arun Mujumdar, Department of Mining and Materials Engineering, McGill
University Examiner

Additional Supervisory Committee Members:

Professor Timothy Durance, CEO of Enwave Company
Supervisory Committee Member

Abstract

Post-harvest handling of microalgae following mechanical dewatering is challenging due to the high moisture content of biomass (about 65-75% wet basis). Therefore, thermal drying is applied to decrease the moisture content to the safe value for storage, handling, and transportation. After drying, handling of dried microalgae powder is still difficult because of its low bulk density and possibility of blocking the flow of material inside handling equipment. Pelletization improves microalgal material characteristics by making high-density and homogenous pellets. The first goal of this research is to study the thin-layer drying mechanism of microalgae *Chlorella* at the temperature range of 40-140° C. The second goal is to study densification mechanism of pure and mixed microalgae with pine sawdust. The specific species used in this experimental investigation is *Chlorella vulgaris.* In the studied temperature range, microalgae drying from an initial moisture content of 65% wet basis occurred in the falling-rate period with no constant-rate phase. The results revealed that diffusion is the controlling mechanism in microalgae drying and all the water is entrapped in algal cells. This confirms the industrial experience that further mechanical dewatering to remove water is not effective. It was also understood that although the drying rate at 100-140° C is the highest, 60 and 80° C are the optimum drying temperatures to preserve microalgae surface color and chemical composition. Pelletization of pure *Chlorella* occurred in two distinct regions of particles' rearrangement and particles' deformation. However, there was no clear separation between the two regions when pure sawdust was pelletized. Adding microalgae *Chlorella* to sawdust resulted in a decrease in densification energy and improvement in pellets' properties, i.e. higher durability, density, and heating value, lower porosity, moisture adsorption, and pellets' expansion. The results indicated that adding microalgae to sawdust eliminates the need for high pelletization temperature and force. The temperature of 75° C and maximum force of 2500 N, which are considered as moderate conditions, were adequate for making pellets containing microalgae with desirable characteristics because of the presence of natural binders in microalgae. Working at a low/moderate temperature and force improves the process economics by decreasing energy consumption.

Lay Summary

Thin-layer drying of microalgae *Chlorella* from an initial moisture content of 65% wet basis in the temperature range of 40-140° C was studied. Microalgae drying rate decreased by time and there was no period in which the rate remains constant. The results showed that diffusion controlled moisture evaporation from microalgae *Chlorella*. It was observed that both low and high drying temperatures were destructive to microalgae characteristics, and microalgae properties were best preserved at 60 and 80° C.

The pelletization experiments revealed that mixing microalgae with sawdust improved pellets' quality including durability, density, moisture adsorption, expansion, and heating value. It was also observed that due to moderate required force and temperature for making pellets containing microalgae, less energy is required. Namely, the temperature of 75° C and pressure of 2500 N were enough for making durable pellets composed of microalgae and sawdust.

Preface

This Ph.D. dissertation is divided into five chapters and one appendix. The author, Hasti Hosseinizand, has done all the literature review, designing and conducting the experiments, data processing and analysis, and preparation of manuscript and thesis under the supervision of Professor Shahab Sokhansanj and co-supervision of Professor C. Jim Lim., Chemical and Biological Engineering Department, University of British Columbia (UBC). The co-authors contributed to the scientific content of the manuscript. A version of chapters 2, 3, 4, and Appendix A is published in peer-reviewed journals and/or presented at conferences. The list of publications is presented as follows:

Journal Publications:

- Hosseinizand, H., Lim, C.J., Webb, E., Sokhansanj, S. "Economic analysis of drying microalgae *Chlorella* in a conveyor belt dryer with recycled heat from a power plant". Applied Thermal Engineering. 124 (2017) 525-532. doi:10.1016/j.applthermaleng.2017.06.047. (This paper is based on the data presented in Appendix A of this thesis.)
- Hosseinizand, H., Lim, C.J., Sokhansanj, S. "Studying the drying mechanism of microalgae *Chlorella vulgaris* and the optimum drying temperature to preserve quality characteristics". Drying Technology. 36:9 (2017) 049-1060. doi:10.1080/07373937.2017.1369986. (This paper is based on the data presented in chapter 2 of this thesis.)
- Hosseinizand, H., Lim, C.J., Sokhansanj, S. "Co-pelletization of microalgae *Chlorella vulgaris* and pine sawdust to produce solid fuels". Fuel Processing Technology. 177 (2018) 129-139. (This paper is based on the data presented in chapters 3 and 4.)

Table of Contents

Abstract ..... **iii**
Lay Summary ..... **iv**
Preface ..... **v**
Table of Contents ..... **vi**
List of Tables ..... **x**
List of Figures ..... **xii**
List of Symbols ..... **xvii**
List of Abbreviations ..... **xix**
Acknowledgment ..... **xx**
Dedication ..... **xxi**
Chapter 1: Introduction **1**
1.1 Microalgae Characteristics 1
1.2 Microalgae Cultivation and Harvesting 4
1.3 Microalgae Conversion 7
1.4 Microalgae Drying 9
1.4.1 Importance of Drying 9
1.4.2 Literature Review on Microalgae Drying 11
1.4.3 Industrial Dryers for Microalgae Drying 12
1.4.4 Waste Heat Recovery Coupled with Drying 13
1.5 Densification 14
1.5.1 Literature review on Microalgae Densification 17
1.5.2 Biomass Co- Pelletization Practices 17
1.5.3 Quality of Densified Biomass 18
1.5.3.1 Moisture Content 18
1.5.3.2 Unit Density 18
1.5.3.3 Durability Index 18
1.5.3.4 Calorific Value 20
1.6 Knowledge Gap 20

1.7 Research Objectives and Thesis Organization 21
Chapter 2: Thin-Layer Drying Mechanism of Microalgae *Chlorella vulgaris* 22
2.1 Materials and Methods 22
2.1.1 Microalgae Cultivation 22
2.1.2 Thin- Layer Drying Tests 23
2.1.3 Biomass Characterization 25
2.1.3.1 Ultimate and Proximate Analysis 25
2.1.3.2 Chemical Composition 26
2.1.3.3 Surface Color 27
2.1.3.4 Scanning Electron Microscopy (SEM) 28
2.1.4 Drying Kinetics Modeling 28
2.1.5 Statistical Analysis of Experimental Data 29
2.2 Results and Discussion 30
2.2.1 *Chlorella* Drying Behavior and Kinetics Parameters 30
2.2.2 Microalgae Characteristics 37
2.2.2.1 Surface Color 38
2.2.2.2 Ultimate and Proximate Analysis 40
2.2.2.3 Biochemical Composition 43
2.2.2.4 Biomass Surface Structure 44
2.3 Summary 45
Chapter 3: Co-Pelletization Mechanism of Microalgae *Chlorella vulgaris* and Pine Sawdust 46
3.1 Materials and Methods 46
3.1.1 Sample Preparation 46
3.1.2 Raw Biomass Characteristics 48
3.1.3 Pelletization 49
3.1.4 SEM Analysis 51
3.1.5 Statistics 51
3.2 Results and Discussion 51
3.2.1 Densification Mechanism 51

3.2.2 The Effect of Temperature on Densification Mechanism 59
3.2.3 Energy Consumption 64
3.3 Summary 67
Chapter 4: Characteristics of Microalgae *Chlorella vulgaris* and Pine Sawdust Pellets 69
4.1 Methods for Evaluation of Pellets Quality 69
4.1.1 Dimensions, Density, and Expansion 69
4.1.2 Particle Density 69
4.1.3 Moisture Adsorption 70
4.1.4 Mechanical Hardness: Durability 70
4.2 Pelletization Modeling 71
4.3 Results and Discussion 72
4.3.1 Mechanical Hardness 72
4.3.2 Density, Expansion, and Porosity 74
4.3.3 Moisture Adsorption 79
4.3.4 Thermochemical Parameters 80
4.3.5 Compaction Modeling 81
4.4 Summary 89
Chapter 5: Concluding Remarks and Recommendations 91
5.1 Discussion and conclusions 91
5.2 Recommendations 94
Bibliography 96
Appendices 108
Appendix A Economic Analysis of Drying Microalgae *Chlorella* in a Conveyor Belt Dryer with Recycled Heat from a Power Plant 108
A.1 Approach and Assumptions for Analysis: Description of the System 108
A.2 Approach and Assumptions for Analysis: Drying Mass Transfer Coefficient 109
A.3 Approach and Assumptions for Analysis: Dryer Design 110
A.4 Approach and Assumptions for Analysis: Heat Recovery System 113
A.5 Approach and Assumptions for Analysis: Economic Analysis 114
A.6 Design Results and Discussion 117

A.7 Economics Results and Discussion 119
A.8 Summary 122

List of Tables

Table 1.1 Comparisons of oil yields from biomass feedstock and microalgae [9] 2
Table 1.2 Methods of energy extraction from microalgal biomass [14] 7
Table 1.3 Some of the industrial waste heat resources and their temperatures [52] 14
Table 2.1 Equilibrium moisture content at different drying temperatures (40-140 °C). By increasing the drying temperature, equilibrium moisture content decreased. 32
Table 2.2 Kinetic parameters and statistical evaluation of thin layer drying models 35
Table 2.3 Biochemical composition, ultimate and proximate analysis of freeze-dried *Chlorella* as control sample 38
Table 2.4 The overall color difference of *Chlorella* dried at different temperatures compared to freeze-dried *Chlorella.* Drying temperatures of 60 and 80° C had the least color difference with the control sample. 39
Table 2.5 Ultimate and proximate analysis results of *Chlorella* dried at 40, 60, 80, 100, 120, and 140° C temperatures. There was no significant difference in elemental composition and calorific value of samples dried under different temperatures. 42
Table 3.1 Properties of raw samples of *Chlorella vulgaris* and pine sawdust 49
Table 3.2 The force to overcome friction for the expulsion of pellets from die. The results are based on at least 6 produced pellets. The force is significantly lower for pure microalgae compared to other fractions. 58
Table 4.1 Moisture adsorption kinetic data at 2500 N and 75° C. Conditions inside humidity chamber: 30° C and 90% relative humidity. Pure microalgae had the lowest moisture adsorption rate and equilibrium moisture content. 80
Table 4.2 Calorific value and ash content of pellets made at 2500N and 75° C*. Pure microalgae had a significant higher calorific value compared to pure sawdust. Note that adding microalgae to sawdust increased the ash content. 81
Table 4.3. The parameters of the empirical model showing the relation of pressure and density (Equation 18) during compression of biomass at pelletization temperature of 50° C, and maximum pelletization force of 3500 N for pellets composed of pure microalgae, 25%, 50%, and 75% sawdust fraction, and pure sawdust. 83

Table 4.4 Jones model parameters for densification temperatures of 50 and 100° C and different blends of biomass fractions (Pure *Chlorella*, 25%, 50%, 75% sawdust, and pure sawdust)..... 84
Table 4.5 Cooper-Eaton model parameters for densification temperatures of 50 and 100° C and fractions of biomass blends (Pure *Chlorella*, 25%, 50%, 75% sawdust, and pure sawdust)..... 86
Table 4.6 Kawakita- Ludde model parameters for densification temperatures of 50 and 100° C and fractions of biomass blends (Pure *Chlorella*, 25%, 50%, 75% sawdust, and pure sawdust) 88
Table A.1 List of process assumptions and input data for dryer and heat recovery system design 111
Table A.2 List of economic assumptions and cost data..... 114
Table 5.3 Design parameters of conveyor belt dryer coupled with waste heat recovery system at initial moisture contents of 35, 45, 55, 65, and 75% (w.b.)..... 118
Table A.4 Purchase cost of equipment to produce 1000 kg/h of microalgae at 10% moisture content from the initial moisture content of 55% (wet basis). The costs were converted to 2015 dollars..... 119

List of Figures

Figure 1.1 Microalgae photosynthesis using sunlight during the growth cycle 1
Figure 1.2 Microscopic images of microalgae species. (A) Scenedesmus; (B) Chlorella minutissima; (C) Phaeodactylum tricomutum; (D) Tetraselmis suecica [15] 3
Figure 1.3 Microalgae processing steps..... 5
Figure 1.4 Microalgae cultivation systems. (A) photobioreactor (Photo was taken at ATP^3 site); (B) open pond [20]..... 5
Figure 1.5 A schematic diagram of pellet mill. 16
Figure 2.1 Experimental setup of thin layer drying (parts are not to the scale) (a) dryer unit diagram (b) dryer unit photo (c) thin-layer of wet microalgae *Chlorella* on the pan at a moisture content of 66.4%. The drying pan was 12 cm in length and 6 cm in width..... 25
Figure 2.2. The graph from thermogravimetric analysis. The moisture content was calculated using the weight loss of the sample until heating to 112° C. The volatile content was estimated using the sample weight loss from 112 to 941° C. The remaining mass after 941° C was fixed carbon and ash..... 26
Figure 2.3 Moisture content curves of *Chlorella* with an initial moisture content of 66.4% (w.b.) at drying temperatures of 40, 60, 80, 100, 120, and 140° C. 31
Figure 2.4 Drying rate curves of *Chlorella* with an initial moisture content of 66.4% (w.b.) at drying temperatures of 40, 60, 80, 100, 120, and 140° C. No constant rate period was evident.. 31
Figure 2.5 The dependency of equilibrium moisture content on drying temperature in the range of 313-413 K. 32
Figure 2.6 Moisture ratio curves of *Chlorella* with an initial moisture content of 66.4% (w.b.) at drying temperatures of 40, 60, 80, 100, 120, and 140° C 34
Figure 2.7 (a) Temperature dependency of drying rate constant. (b) temperature dependency of diffusion coefficient. 37
Figure 2.8 Color coordinates of *Chlorella* dried at temperatures of 40, 60, 80, 100, 120, and 140 ° C. L, a, and b are indicators of whiteness/blackness, greenness/redness, and blueness/yellowness, respectively. Drying temperatures of 60 and 80° C best-preserved samples' color. 39

Figure 2.9 Biochemical composition (lipid, carbohydrate, and protein) of microalgae *Chlorella* dried at drying temperatures of 40, 60, 80, 100, 120, and 140° C and freeze-dried *Chlorella*. Drying temperatures of 60 and 80° C, best-preserved carbohydrate and lipid content of dried samples. 43
Figure 2.10 SEM images of microalgae *Chlorella* dried at different temperatures (a) 40° C (b) 80° C (c) 140° C. In the figure a and c, the cracks and shrinkage are evident in the biomass structure, respectively. Drying at 80° C, the best preserved microalgal cell structure. 45
Figure 3.1 Pine sawdust particles (left) and microalgae particles (right) at 10% wet basis moisture content. The average diameter of sawdust particles was almost 3 times larger than that of microalgae particles. 47
Figure 3.2 Particle size distribution of microalgae *Chlorella vulgaris* and sawdust measured using laser diffraction method. The sawdust surface average diameter was almost 3 times larger than microalgae particles. 47
Figure 3.3 The picture of piston-cylinder set up in the pelletizing machine 50
Figure 3.4 Force-displacement graph for compression at maximum pelletization force of 3500 N and temperature of 75° C for pure *Chlorella*, sawdust fraction of 25, 50, 75%, and pure sawdust. Complete rearrangement happened for pure microalgae and sawdust fractions of 25, and 50%. 53
Figure 3.5 Force-displacement graph for expulsion at maximum pelletization force of 3500 N and temperature of 75° C for pure *Chlorella* (0%), sawdust fraction of 25, 50, 75%, and pure sawdust. (a) The graph for the entire expulsion period (b) The graph until the maximum force to overcome friction between the pellet and die wall. 54
Figure 3.6 A conceptual representation of the particle arrangement in the die. (a) Microalgae and (b) sawdust particles in the die. It should be noted that the picture does not show the real particles' shape and particle size distribution. The figure shows a possible configuration of particles in the die. Microalgae particles had a smaller average diameter (0.191 mm) compared to sawdust particles (0.603 mm). The porosity of microalgae and sawdust particles was 55% and 86%, respectively. 56
Figure 3.7 SEM images of a cross-section of pellets. (a) pure *Chlorella* at x1500 magnification, (b) 25% at x500 magnification sawdust, (c) 50% sawdust at x1500 magnification, (d) pure sawdust at x250 magnification..... 57

Figure 3.8 Force-displacement graph for compression at maximum pelletization force of 3500 N and temperature of 50° C for pure *Chlorella* (0%), sawdust fraction of 25, 50, 75%, and pure sawdust. Complete rearrangement of particles only happened for pure microalgae. 59
Figure 3.9 Force-displacement graph for compression at maximum pelletization force of 3500 N and temperature of 100° C for pure *Chlorella* (0%), sawdust fraction of 25, 50, 75%, and pure sawdust. Complete rearrangement of particles happened for pure microalgae and sawdust fractions of 25, 50, and 75%. 60
Figure 3.10 Force-displacement graph for compression at maximum pelletization force of 3500 N and different temperatures of 50, 75, and 100° C for pure *Chlorella* (0%). At all three temperatures, pellets experienced complete rearrangement of particles. 62
Figure 3.11 Force-displacement graph for compression at maximum pelletization force of 3500 N and different temperatures of 50, 75, and 100° C for 25% sawdust fraction. Increasing the temperature to 75° C resulted in a complete rearrangement of particles. The mechanism at 75 and 100° C were similar. 62
Figure 3.12 Force-displacement graph for compression at maximum pelletization force of 3500 N and different temperatures of 50, 75, and 100° C for 50% sawdust fraction. Increasing the temperature to 75° C resulted in a complete rearrangement of particles. The mechanism at 75 and 100° C were similar. 63
Figure 3.13 Force-displacement graph for compression at maximum pelletization force of 3500 N and different temperatures of 50, 75, and 100° C for 75% sawdust fraction. Increasing the temperature to 100° C resulted in a complete rearrangement of particles. The mechanism at 50 and 75° C were similar..... 63
Figure 3.14 Force-displacement graph for compression at maximum pelletization force of 3500 N and different temperatures of 50, 75, and 100° C for pure sawdust. There was no significant difference between pelletization mechanism of sawdust at different temperatures. Increasing the temperature did not affect compaction mechanism. 64
Figure 3.15 Energy consumption for densification of microalgae *Chlorella*/pine wood particles at two different forces of 2500 and 3500 N, temperatures of 50, 75, and 100° C, and five fractions of sawdust: 0, 25, 50, 75, and 100%. (a) compression energy, (b) extrusion energy, (c) total energy. The compression energy increased by increasing the fraction of sawdust (a). Extrusion

energy of sawdust was significantly higher that other biomass blends and pure microalgae (b). The total densification energy increased by increasing the ratio of sawdust in the blend (c). 67
Figure 4.1 The single pellet durability tester 71
Figure 4.2 The durability of pellets made at two forces (2500 and 3500 N), three pelletization temperatures (50, 75, and 100° C), and five fractions of sawdust (0, 25, 50, 75, 100%). At the pelletization temperature of 50° C, increasing the ratio of sawdust resulted in decreasing the durability of pellets. At all pelletization conditions, the durability of pure microalgae pellets was significantly higher than that of pure sawdust pellets..... 73
Figure 4.3 The density of pellets at two forces (2500 and 3500 N), three pelletization temperature (50, 75, and 100° C), and five fractions of sawdust (0, 25, 50, 75, 100%). The density of pure microalgae pellets and pellets containing microalgae fraction (25%, 50%, and 75%) was higher than the density of pure sawdust pellets. 75
Figure 4.4 Pellets made at maximum force of 3500 N and temperature of 75° C. From left to right: pure *Chlorella*, 25%, 50%, and 75% sawdust, and pure sawdust, respectively..... 76
Figure 4.5 Expansion of pellets at two forces (2500 and 3500 N), three pelletization temperatures (50, 75, and 100° C), and five fractions of sawdust (0, 25, 50, 75, 100%). (a) diameter expansion, (b) length expansion, (c) percent density change. Increasing sawdust fraction in the blend resulted in more expansion in diameter and length directions, and overall density decrease of pellets. 78
Figure 4.6 Porosity of pellets at two forces (2500 and 3500 N), three pelletization temperatures (50, 75, and 100° C) and five fractions of sawdust (0, 25, 50, 75, 100%). The porosity of pure microalgae pellets and pellets containing microalgae (25%, 50%, and 75%) was lower than the porosity of pure sawdust pellets..... 79
Figure 4.7 Moisture adsorption curves of pellets at 2500 N and 75° C pelletization conditions for pure *Chlorella* 0%, and blended with sawdust at 25%, 50%, 75% and pure sawdust 100%. Conditions inside humidity chamber: 30° C and 90% relative humidity. 80
Figure 4.8 Density-pressure data during compression of biomass at pelletization temperature of 50° C, and maximum pelletization force of 3500 N for pure microalgae, 25%, 50%, and 75% sawdust fraction, and pure sawdust. For all fractions of biomass other than pure *Chlorella*, density increased by increasing the pressure in the entire compression phase..... 82

Figure 4.9 Representing the data with Jones model for different proportions of biomass (Pure *Chlorella*, 25%, 50%, 75% sawdust, and pure sawdust). (a) densification temperature of 50° C, (b) densification temperature of 100° C. 85
Figure 4.10 Representing the data with Cooper-Eaton model for different proportions of biomass (pure *Chlorella*, 25%, 50%, 75% sawdust, and pure sawdust). (a) densification temperature of 50° C, (b) densification temperature of 100° C. 87
Figure 4.11 Representing the data with Kawakita- Ludde model for different proportions of biomass (Pure *Chlorella*, 25%, 50%, 75% sawdust, and pure sawdust). (a) densification temperature of 50° C, (b) densification temperature of 100° C. 89
Figure A.1 Schematic diagram of the conveyor belt dryer with the heat exchanger coupled with a liquid thermal loop for recovering waste heat from the power plant. Components of the diagram are not to scale. 109
Figure A.2 Element of the wet solid on the belt 112
Figure A.3 The experimental internal mass transfer coefficient for microalgae dried at 80° C. 117
Figure A.4 Moisture profile along the bed for initial moisture content of 55% and final moisture content of 10% (w.b.)..... 118
Figure A.5 Annual capital, operating, and total cost per ton of dried product for different drying systems by considering Hand factor (HF) from Figure A.2 (three data set on the left) and HF=1 (three data set on the right). (input moisture content 55% w.b) 120
Figure A.6 Sensitivity of drying cost to initial (input) moisture content for the belt dryer with recycled heat (HF=1) 121

List of Symbols

a	Surface color parameter, an indicator of greenness/redness
a_0	Surface color parameter of control sample, indicator of greenness/redness
a_1	Cooper-Eaton model constant
a_2	Cooper-Eaton model constant
A_1	Henderson-Pabis model constant
A_2	Logarithmic model constant
b	Surface color parameter, an indicator of blueness/yellowness
b_0	Surface color parameter of control sample, indicator of blueness/yellowness
c	Logarithmic model constant
C	Kawakita and Ludde model constant
D	Effective moisture diffusivity (m^2/s)
D_0	Arrhenius factor (m^2/s)
E	Activation energy in Arrhenius equation (kJ/mol)
e	Kawakita and Ludde model constant
f	Kawakita and Ludde model constant
h^*	Half thickness of slab (m)
k_1	Henderson-Pabis model constant (min^{-1})
k_2	Newton model constant (min^{-1})
k_3	Page model constant (min^{-1})
k_4	Logarithmic model constant (min^{-1})
K_{abs}	Moisture adsorption constant (min^{-1})
L	Surface color parameter, indicator of whiteness/blackness
L_0	Surface color parameter of control sample, indicator of whiteness/blackness
MR	Moisture ratio
m	Mass of each pellet (kg)
M	Moisture content of biomass (kg/kg dry mass)
M_{eq}	Equilibrium moisture content (kg/kg dry mass)
M_0	Initial moisture content (kg/kg dry mass)

n	Page model constant
P	Pelletization pressure (MPa)
p_1	Cooper-Eaton model constant
P_2	Cooper-Eaton model constant
R	Universal gas constant (kJ/mol.K)
r	Jones model constant
s	Jones model constant
T	Temperature (K)
t	Time (min)
u	The constant for empirical model showing the pressure-density relation
v	The constant for empirical model showing the pressure-density relation
w	The constant for empirical model showing the pressure-density relation
V_b	Volume of each pellet (m^3)
V_p	Volume of particles in each pellet (m^3)
ΔE	Total color difference from control sample
ρ	Density of a single pellet in Jones model (kg/m^3)
ρ_0	The constant for empirical model showing the pressure-density relation
ρ_b	Single pellet density (kg/m^3)
ρ_p	Particle density of each pellet (kg/m^3)
ε_0	Porosity of a single pellet

List of Abbreviations

AFDW	Ash free dry weight
ANOVA	Analysis of variance
ATP^3	Algae Test-bed Public Private Partnership
CHP	Combined heat and power
D.B	Dry basis
D.W.	Dry weight
EMC	Equilibrium moisture content
FAME	Fatty acid methyl ester
GHG	Greenhouse gas emission
HHV	Higher heating value
HPLC	High performance liquid chromatography
LEA	Lipid extracted algae
MR	Moisture ratio
PBR	Photo bioreactor
SEM	Scanning electrom microscopy
SSE	Sum of squared error
TGA	Thermogravimetric analyzer
VOC	Volatile organic compound
w.b.	Wet basis

Acknowledgment

I would like to acknowledge my supervisors, Dr. Shahab Sokhansanj and Dr. Jim Lim for their guidance and never-ending support during my Ph.D. studies. Their encouragement motivated me and enabled me to develop an understanding of the subject. I would also like to express my gratitude to my committee members, Dr. Susan Baldwin and Dr. Timothy Durance for their helpful ideas and suggestions for improving the work presented in the dissertation.

I would also like to thank all my colleagues in Biomass and Bioenergy Research Group, especially Dr. Hamid Rezaei and Jun Sian Lee for helping me during my experiments. The financial support from Natural Science and Engineering Research Council of Canada (NSERC) is also appreciated.

My love and appreciation go to my parents, Farah and Parviz, and my brother Amir for their unconditional love and support in my whole life. Finally, thanks to my soulmate and husband, Majid who has been by my side throughout my Ph.D., living every single moment of it with me.

To my beloved husband, Majid

Chapter 1: Introduction

1.1 Microalgae Characteristics

As the demand for oil and gas resources rises with the growth of population, viable alternative fuels are required [1–4]. Over the past decades, many countries have committed to increasing their share of producing and using renewable energy. For example, the European Commission has an objective of at least 27% substitution of fossil fuel by 2030. Similarly, China, Australia, Canada, Russia, Korea, Egypt, and Chile have committed to reach a specific goal by 2020 [5].

Microalgae have recently received substantial attention as a renewable energy feedstock owing to their distinct characteristics [5]. Microalga is an autotrophic unicellular organism, which utilizes light energy and inorganic nutrients (CO_2, nitrogen, phosphorous) and synthesizes valuable biomass compounds, such as protein, starch, oil, and secondary metabolites like carotenoids (Figure 1.1) [6]. Microalgae are rich in lipid (10-30% of dry weight (DW)), protein (10-40% of DW), and carbohydrate (5-30% of DW) content [7]. They are among the first organisms that first came into existence about 3 billion years ago [8].

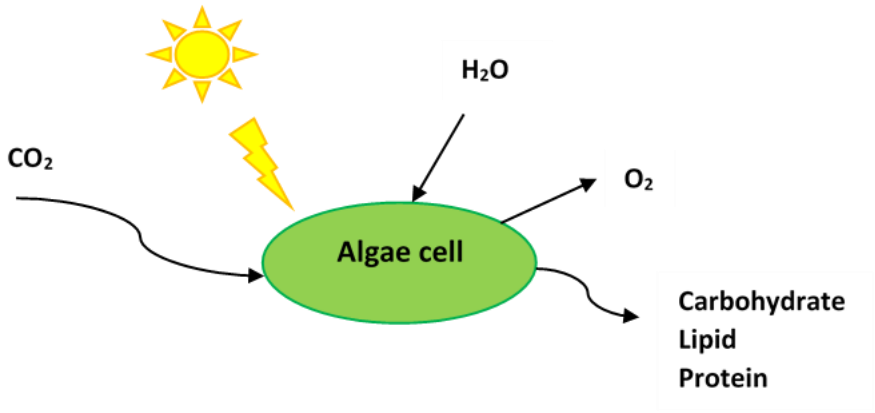

Figure 1.1 Microalgae photosynthesis using sunlight during the growth cycle

Microalgae have high productivity and do not compete with terrestrial food crops since microalgae do not need arable land for their growth [9–11]. They can grow in a wide range of climate and water conditions (freshwater, brackish water, and seawater) and they can capture CO_2 from different sources. Microalgae's carbon dioxide fixation ability is one to two orders of magnitude higher than terrestrial plants, and their associated environmental problems are much less than fossil fuels [1,10,12,13]. Many microalgae have a high growth rate, for example, doubling time of some C*hlamydomonas* species is reported as short as 6 hours [9]. Microalgae are potentially capable of producing 1000-4000 gal/acre-year biodiesel, which is dramatically higher than soybean and other oil crops [9]. Some microalgae species can produce high levels of lipids, so biodiesel productivity of some algae strains could be 100-fold higher than other oil crops [9]. Table 1.1 lists the oil productivity of some agricultural crops and microalgae.

Table 1.1 Comparisons of oil yields from biomass feedstock and microalgae [9]

Crop	Oil yield (gallon $acre^{-1}$. $year^{-1}$)
Soybean	48
Camelina	62
Sunflower	102
Jatropha	202
Oil palm	635
Microalgae	1000-4000

Microalgae can use several conversion pathways for energy production like direct combustion, pyrolysis, gasification, hydrothermal liquefaction, transesterification, anaerobic digestion, and fermentation [10,13,14]. Microalgae can also be processed to produceanimal feed and high-value products like cosmetics, supplements, and food colorants [5].

Microalgae are categorized into two main groups of prokaryotes and eukaryotes. Eukaryotic algae, which has a clear nuclear structure, is subdivided into 12 major classes. The groups with a broad range of applications are diatoms (*Bacillariophyceae*), green algae (*Chlorophyceae*), red algae (*Rhodophyceae*), yellow-green algae (*Xanthophyceae*), golden algae

(*Chrysophyceae*), brown algae (*Phaeophyceae*), and *Euglenoids* [9]. The microscopic images of some microalgae species are shown in Figure 1.2.

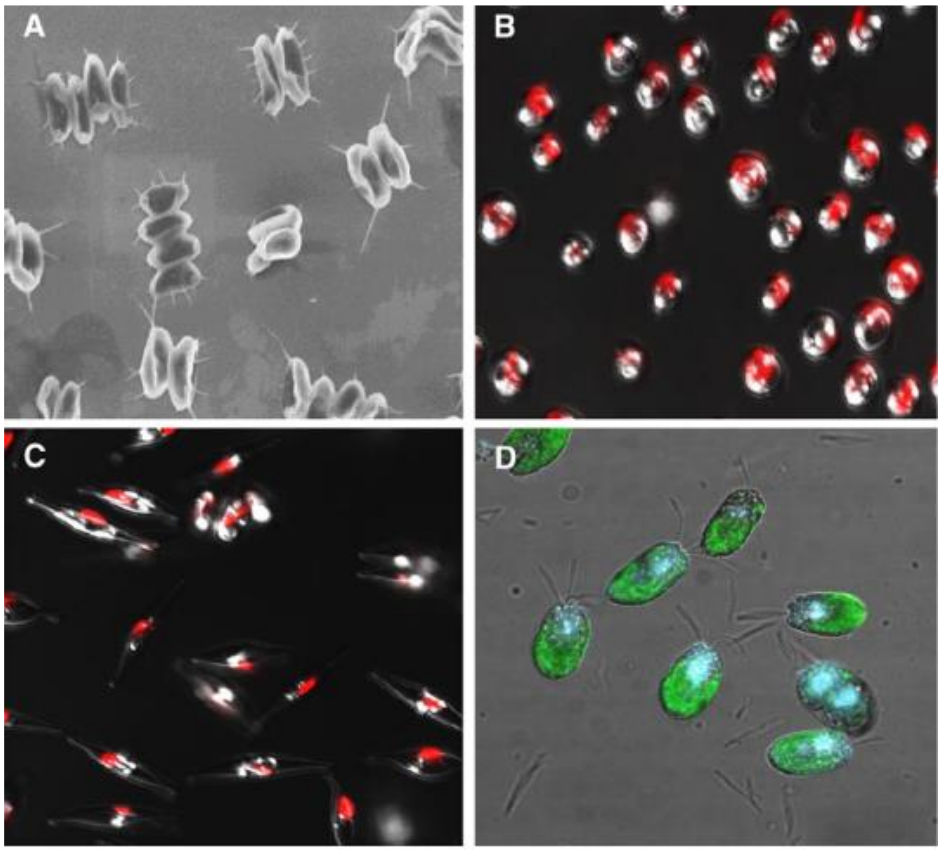

Figure 1.2 Microscopic images of microalgae species. (A) Scenedesmus; (B) Chlorella minutissima; (C) Phaeodactylum tricomutum; (D) Tetraselmis suecica [15]

Chlorella is green microalgae and a suitable biomass for both biofuel and high-value products. *Chlorella* is rich in protein, vitamins (group B, C, and E), and minerals (iron, calcium, phosphorous, potassium, etc.). They also contain 2-3% chlorophyll and carotenoids. In addition to their functional food and health applications, *Chlorella* is considered as biofuel feedstock owing to their fast growth rate, the ability to accumulate high concentration of oil under stress for biodiesel production, and the ability to accumulate starch under normal conditions for

bioethanol production. Furthermore, *Chlorella* can tolerate harsh culture conditions, mely a temperature as high as 40° C [7].

The production of algae-based products involves cultivation, harvesting, dewatering, stabilization for safe storage and conversion to usable products [15].

1.2 Microalgae Cultivation and Harvesting

The production of algae-based fuels involves cultivation, harvesting, dewatering and thickening, storage, and conversion to biofuel (Figure 1.3) [10,15]. Open ponds and closed photobioreactors (PBRs) are two major production systems that mainly differ in growth parameters control, contamination, water evaporation, and cost. Figure 1.4 demonstrates the two common microalgae cultivation systems. Open ponds are most widely used for large-scale outdoor cultivation and are economical and easy to build and operate [9,16–19]. There are different types of outdoor ponds which differ in shape, size, and agitation type, for instance, raceway ponds and circular ponds. Raceway ponds are commonly used. They are usually 15-25 cm deep and are agitated using a paddlewheel mixer to prevent sedimentation of culture. Although open systems are easy to operate, they suffer from some shortcomings, like high water loss due to evaporation, high possibility of contamination, and lower overall efficiency [9,16–18].

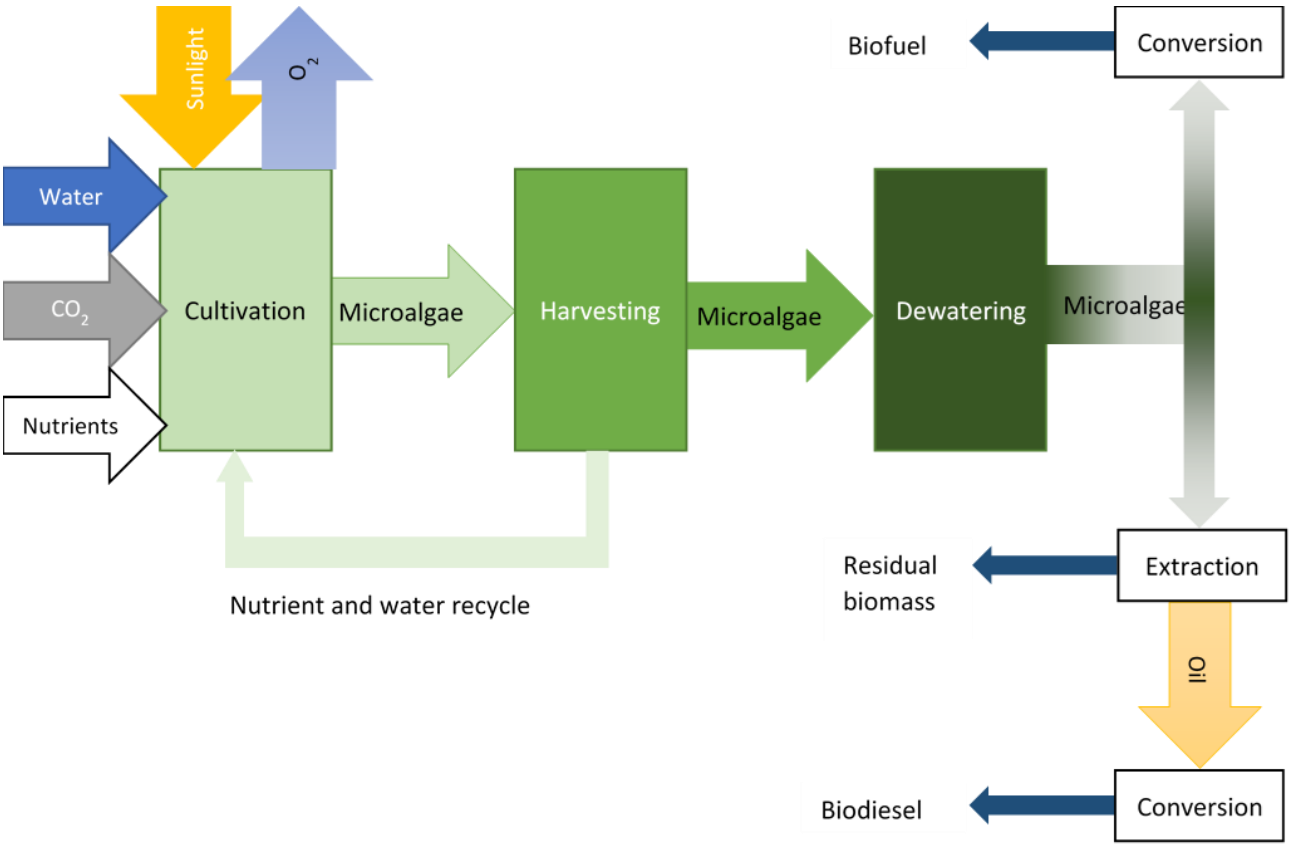

Figure 1.3 Microalgae processing steps

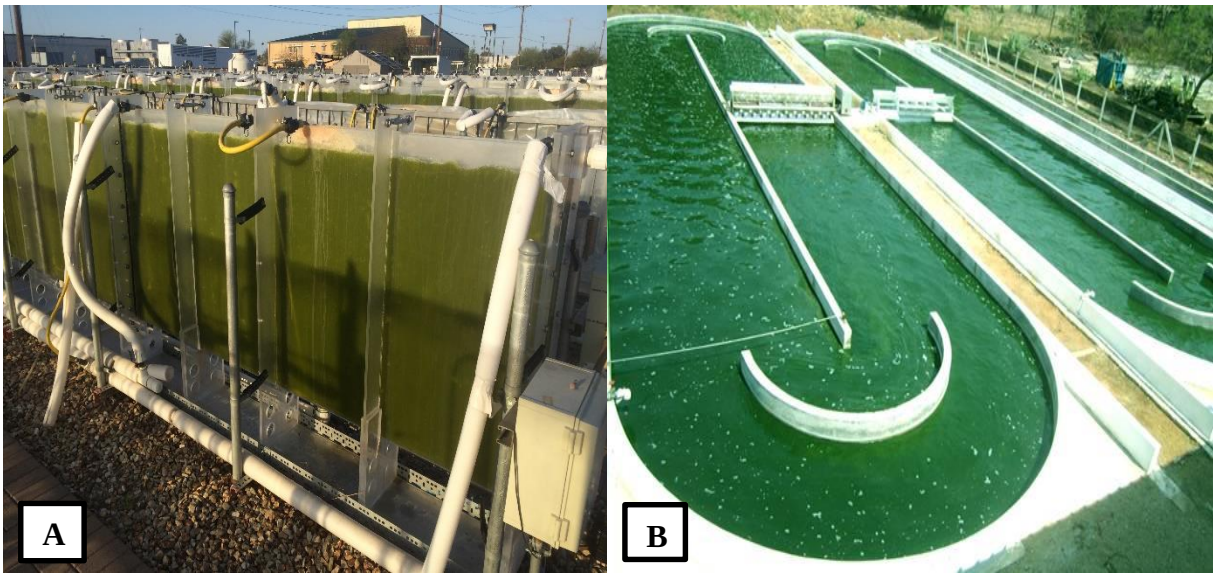

Figure 1.4 Microalgae cultivation systems. (A) photobioreactor (Photo was taken at ATP[3] site); (B) open pond [20].

To overcome the difficulties associated with open systems, closed photobioreactors (PBRs) are used. Tubular and plate PBRs are two major type of closed cultivation systems. PBRs can be installed vertical, horizontal, or inclined. Although PBRs are more appropriate to maintain a monoculture compared to open systems, they are expensive to scale up and operate [9,16–18].

Successful microalgae cultivation requires specific conditions, which vary from species to species. The major parameters that affect microalgae growth productivity are culture media, light, temperature, lack of contamination, CO_2 concentration, salinity, pH, and mixing conditions [9,17].

Microalgae are produced as dilute suspension of 0.06% (0.6 g L^{-1}) in growth media. When microalgae reach their maximum cell growth rate in cultivation ponds, they are harvested [15,21]. Harvesting of microalgae biomass from culture media is difficult because of low biomass concentration in culture broth, the small size of cells (<20 μm), the neutral buoyancy of cells in water (density is 1.08-1.13 g/ml vs. the density of water at 1.0), and strongly negative surface charge [21,22]. Dewatering processes are mostly carried out by mechanical, physical, and chemical techniques. Membrane filtration with the aid of a suction or vacuum pump is widely used for harvesting. Membrane fouling and clogging are problems associated with using membranes. Chemical coagulation is applied by adding a coagulant that neutralizes the negative surface charge of algal cells, resulting in settling of cells. Dissolved air flotation causes cells to float as foam at the top of the tank by pumping fine air bubbles that adhere to the cells. In centrifugation, algal cells are separated from culture media due to the density difference, and thus they deposit on the wall of the centrifuge as a thick paste [9,16–18]. Selection of an appropriate dewatering method for microalgae is highly dependent on the properties of microalgae suspension [21,22]. Harvesting can result in a 50-200-fold increase in the concentration of algal biomass, and the concentration would reach 15-20 % (200 g/L) of solids [21–23]. The remaining water in the biomass cannot be removed further by using mechanical methods [24].

1.3 Microalgae Conversion

After mechanical dewatering, the algal paste still contains a high amount of water. It is difficult and costly to produce microalgae-based products from wet biomass. For biodiesel production or non-polar target products such as carotenoids and omega-3 fatty acid compounds, dried microalgae are preferred. For most conversion processes, a concentration of 90% dry solids is targeted [25–27]. Knowledge of different conversion processes for microalgal biofuel production and the impact of water on the reactions further demonstrates the necessity of biomass drying.

Microalgae can be converted to a versatile range of products including, biodiesel via transesterification, bioethanol via fermentation, methane via anaerobic digestion, heat via combustion, bio-oil and biochar via thermochemical conversion, green diesel and gasoline replacements via direct hydrothermal liquefaction, and high protein animal feed. Table 1.2 lists the methods for energy extraction from microalgal biomass; this table also shows if the microalgae need drying prior to the conversion and if the process uses the whole microalgal biomass.

Table 1.2 Methods of energy extraction from microalgal biomass [14]

	Utilizes entire organic biomass	Requires biomass drying before conversion	Primary energy product
Direct combustion	Yes	Yes	Heat
Pyrolysis	Yes	Yes	Dominated by liquid in fast pyrolysis
Gasification	Yes	Yes	Dominated by gas
Liquefaction	Yes	No	Dominated by liquid
Bio-hydrogen production	Yes	No	Gas
Fuel cell	Yes	No	Electricity
Bioethanol production	No	No	Liquid
Biodiesel production (transesterification)	No	Yes	Liquid
Anaerobic digestion	Yes	No	Gas

In direct conversion methods, the whole biomass can be converted to biofuel. These techniques can be conducted via biological or thermochemical pathways. The major thermochemical conversion techniques are combustion, gasification, pyrolysis, and hydrothermal liquefaction. Direct combustion of microalgae is only practical when biomass has a moisture content less than 50% [28]. The co-firing of dried microalgae, which has been grown using the carbon dioxide emissions of the power plant, is an interesting method to reduce GHG emissions of the plant [14]. Gasification is partial oxidation of dry biomass at high temperature (700-1300 ˚C) to produce a low-value gas (syngas), which is then upgraded to liquid fuel. Similar to gasification, the biomass for pyrolysis should be dry. The products of pyrolysis are bio-oil, syngas, and charcoal in the absence of oxygen. The bio-oil produced in pyrolysis needs to be further upgraded to remove its excessive oxygen and water. In thermochemical (hydrothermal) liquefaction, the wet algal biomass is converted to crude bio-oil in the presence of superheated water (liquid water under pressure at temperatures between boiling point and the critical temperature) [19]. Although biomass with up to 90% moisture content can be processed via liquefaction, the commercial interest in liquefaction is low because of complex feeding system and high-pressure and temperature requirement. These problems have caused liquefaction to be an expensive process.

Another category of conversion reactions that convert the whole biomass to energy is biological processes. In anaerobic digestion, which is a biological method, the biomass is digested by bacteria to produce methane, which is used as a fuel for combined heat and power plants [14]. The growth of algae exclusively for methane production is not commercially viable, due to the high cost of algae digestion [19]. Hydrogen is produced from microalgae by using the enzyme hydrogenase. Hydrogen production from microalgae seems an attractive method since hydrogen combustion produces water vapor rather than greenhouse gases. However, hydrogen production from microalgae is not cost-effective due to low bio-hydrogen production yield from microalgae [14]. Microalgal fuel cells produce an electrical current based on oxidation-reduction reactions that occur within a living organism. The low energy production efficiency of this technique is its drawback [14].

Carbohydrates in microalgae can be converted to ethanol via fermentation. Research by Miranda et al. [29] showed that the fermentation efficiency of wet microalgae was 55% lower

than the dried biomass. Another technique for microalgal biofuel production is transesterification. The product of microalgae transesterification is liquid biodiesel which is suitable for storage and transportation. In transesterification, conventionally oil is extracted by using an organic solvent, mechanical cell disruption or a combination of both methods, then the oil is converted to biodiesel. Since transesterification is a costly and time-consuming process, recently in- situ transesterification is suggested to produce biodiesel from microalgae. In in-situ transesterification, simultaneous extraction and conversion of oil to fatty acid methyl esters (FAMEs) or biodiesel takes place. In this process, dry algae are mixed with an alcohol and an acidic catalyst with optional heating [30]. The most common alcohol and catalysts are methanol and sulfuric acid. The presence of water in this reaction causes many difficulties: 1- The FAME production reaction is reversible, and water may hydrolyze FAMEs back to free fatty acids. 2- Water can shield lipids from reacting with solvent. 3- Water can deactivate the acid catalyst. Sathish et al. [30] studied the effect of moisture on in-situ transesterification of a mixed population of microalgae dominated by *Chlorella* and S*cendesmus*. The results showed that moisture content of greater than 15- 20 % (w.b.) in algal biomass reduced the biodiesel production yield to 30-50% of maximum achievable yield. Other researchers also confirmed Sathish et al.'s observations [31,32]. Sathish et al. [30] investigated the effect of changing reaction conditions on biodiesel yield. It was observed that when biomass with 84% moisture content is used and methanol and sulfuric acid amount are increased, the biodiesel yield will rise to 80% of the maximum yield. Although the addition of alcohol and catalyst may improve the biodiesel yield, the production cost of biodiesel increases significantly. Therefore, more research should be conducted to compare the economics of microalgae drying and the addition of alcohol and catalyst in the transesterification process.

1.4 Microalgae Drying

1.4.1 Importance of Drying

Based on the following rationale, studying the drying of microalgae seems necessary. Primarily, the problems associated with conversion techniques, specifically transesterification and liquefaction (two most common conversion methods proposed for wet microalgae) indicate that microalgae drying is a key step. The efficiency of many conversion techniques in the

presence of water is as low as 30-50% of the maximum achievable yield [30–33]. The fluctuations in microalgae production rate between summer and winter (on average 5 to 1), supports the idea that part of the wet biomass during high season can be dried for use in low season [34]. Microalgae production solely for biofuel production on a large scale is not economically feasible and sustainable, at present [6]. Low-volume, high-value products such as antioxidants (astaxanthin and beta-carotene), polyunsaturated fatty acid supplements, pharmaceutical and cosmetic products could support biofuel production [5]. Therefore, the bio-refinery approach should be considered [12,35]. Commercialization of high-value products requires microalgae drying due to difficulties in storage, handling, and transportation of paste-like material. Therefore, it is suggested that part of harvested microalgae is dried for this application. Finally, after lipid extraction to produce biodiesel from microalgae, a protein or carbohydrate-rich by-product is left. This remnant has high nutritional value and can be used by ruminants which have the unique ability to use microbial fermentation to convert co-product into protein [36]. Using lipid extracted algae (LEA) for animal feed is specifically important in places where no local protein-rich feeding crops are available during the dry season [37]. Each liter of algae-based biodiesel would produce 2.4 kg of LEA [38]. Production of 3.8 billion L algae-based fuel (suggested by US Congress-2010) [38] would lead to almost 9.4 million ton of LEA, which is approximately 6% of US-feed demand for corn and soybean meal in 2011. Therefore, it is proposed that the remnant after lipid extraction is dried for animal feed application.

At a solid concentration of 15-20%, the microalgal suspension is not a fluid anymore which makes handling difficult [39]. Drying prevents microbial growth and reduces the costs of handling, transportation, packaging, and storage of microalgae [40]. By drying the biomass, the moisture content is decreased to a low level that causes an increase in product shelf life. In the food industry, water activity is mostly used as an indicator of safe water content in materials. Water activity is defined as the partial vapor pressure of water in the substance divided by the standard state partial vapor pressure of water [41,42]. High water activity tends to cause many problems like the growth of unwanted microorganisms and enzymatic and non-enzymatic reactions. Based on Raoult's law, for dilute ideal solutions, water activity is equal to material moisture content [41,42], so by using this assumption, moisture content was used in this study. The final moisture content of 10% wet basis was selected for drying experiments because beyond

this moisture content, the efficiency of conversion reactions decreases, significantly [30–33]. A 10% moisture content not only assures that no microbial growth, enzymatic and non-enzymatic reaction, and lipid oxidation occurs but also guarantees the efficient conversion of microalgae to biofuel via transesterification and other pathways [41,42]. 10% wet basis moisture content is called a safe moisture content because all unwanted reactions are prevented in the material. Therefore, thermal drying should be applied to decrease the moisture to 10%, which is regarded as safe for storage and handling [6,25,39].

Thin-layer drying is mostly used to study the drying behavior of different materials and its results can be applied to design convective dryers in which the material forms a thin layer. Although the thickness of the material in industrial dryers is larger than thin-layer experiments, the higher air velocity and mixing of the material assures that thin-layer drying is happening. In thin-layer drying, it is assumed that there is no spatial temperature or concentration distributions within a thin layer of the material studied [43].

1.4.2 Literature Review on Microalgae Drying

Leach et al. [44] studied spray drying of *Dunaliella salina* and the changes in beta-carotene under different inlet and outlet temperatures and feed solids content. Beta-carotene is an orange pigment and is a precursor of vitamin A. It is also a potent antioxidant and cancer-preventing nutraceutical [44]. For all combinations of solids levels and initial temperatures, a lower outlet temperature led to a better beta-carotene recovery.

After Leach's study, spray drying of microalgae *Spirulina* and the effect of drying on phycocynin, protein, and carbohydrate content was extensively investigated [45,46]. Morist et al. [46] conducted spray drying of *Spirilina platensis* with a rotary centrifuge atomizer with the inlet and outlet air temperatures of 200 and 90˚ C, respectively. Biomass initial moisture content was 70-80 % and the final moisture content was 3%. There was no significant difference in elemental composition (C, H, N, S, and O) of freeze-dried (control) and spray- dried product. The protein and carbohydrate content was lower in the spray-dried product in comparison to freeze-dried; this decrease may be related to the thermal treatment of samples. Similarly, Sarada et al. [45] observed approximately 55% loss of phycocyanin in a spray-dried sample of *Spirulina sp.* in comparison to fresh biomass.

In addition to spray drying research described above [45–47], there have been more recent studies (2008-2011) on using thin layer drying. Thin layer drying is mostly used to study drying kinetics of foodstuffs because of its simplicity and low equipment and operation cost [48]. Moreover, in the thin layer drying of the material the temperature and moisture distribution along the thickness is uniform. Therefore, it can be assumed that the temperature varies only with time not with position [43].

Oliveira et al. [43] studied thin-layer drying of *Spirulina platensis* in a convective oven with perpendicular airflow at temperatures of 50° and 60° C. No constant drying rate period was observed. The effect of material load on drying kinetics was studied. The results indicated that material load has an independent effect on drying kinetics. In another study, Vega Galvez et al. [49] studied thin-layer drying kinetics of brown algae *Macrocystis pyrifera* in the temperature range of 50°-90° C. Viswanathan et al. [26] analyzed thin-layer drying characteristics of a consortium of green algae consisting of *Scenedesmus bijuga*, *Chlamydomonas globose*, and *Chlorella minutissima* as a possible biofuel source. The drying rate curve showed that in the range of 30-70° C, drying occurred at a falling rate with no constant drying rate. This means that drying was limited by a diffusion mechanism, and this is because of the resistance of individual cell walls against diffusion of moisture to the surface of the product. Scanning electron microscopy (SEM) results showed shrinkage of algae cells without any cell rupture or disintegration of the cell surface. Total lipid content did not change with temperature at 30, 50, and 70˚ C. There was just a slight drop in total lipid content at a temperature of 90˚ C. Temperature did not have a significant effect on elemental composition (carbon, hydrogen, nitrogen, and sulfur).

1.4.3 Industrial Dryers for Microalgae Drying

A suitable dryer should meet the required evaporation rate while minimizing thermal damage to the microalgae [8,11]. The most common drying methods proposed for microalgae are solar drying, spray drying and freeze drying. In developing countries where spray and freeze dryers are not available, solar drying is preferred. Solar drying is a simple and inexpensive algae drying technique, but it has many drawbacks especially when used for large-scale production [21]. Some of the limitations are high labor costs, large area requirement, lack of control on

drying process, possible degradation because of biochemical and microbiological reactions especially when the drying period is long, and weather dependency. Long drying time at low temperature increases the bacterial count [21]. Because of the mentioned limitations, solar drying has not been recommended by many studies [25,50].

Spray drying is a widely used method for a broad range of materials. The most important advantage of spray dryers is that drying takes place in a few seconds. This short drying time is beneficial for heat-sensitive materials, especially when algae is used for high-value products like vitamins or anti-oxidants [51]. However, the high capital and operating costs (providing high-temperature air requires a large amount of energy) are the main drawbacks of spray dryers [51].

Freeze drying is applied to materials such as pharmaceuticals and hormones that cannot tolerate even moderate temperatures. Freeze- dried microalgae usually have high quality and can be stored for a very long time while maintaining their chemical, physical and biological characteristics. Freeze drying at a large scale is very expensive because creating a high vacuum requires a lot of energy [52].

To the best of the author's knowledge conveyor belt dryer has never been evaluated for microalgae drying. In this type of dryer, the material is spread on a horizontal moving belt in a continuous process. Airflow in a belt dryer is not as turbulent as in a rotary or a flash dryer and therefore cyclones to separate gas from particles may not be needed. The key characteristic of a conveyor belt dryer is that the dryer can be operated at low temperatures. The low operating temperature lowers the risk of fire and results in lower emissions of volatile organic compounds (VOC) [15,16]. Moreover, a drying temperature below 100° C could dramatically minimize damage to the algal cells. Finally, drying at low-temperature results in low energy consumption and provides opportunities for recycling heat and utilizing waste heat.

1.4.4 Waste Heat Recovery Coupled with Drying

In manufacturing industries, about 20-50% of energy is wasted in the form of hot exhaust gases and liquid and also through heat conduction, convection, and radiation from hot surfaces [53]. A practical approach to enhance the energy efficiency of equipment in the industrial sector is to re-use the waste heat from the equipment. In some cases, waste heat recovery can improve the energy efficiency of the system by as much as 50% [53].

There is a wide range of waste heat resources with different quality (temperature) and quantity. For example, the cooling water in industries has a low temperature around 40-90° C, and the gas exiting glass melting furnace has the temperature of 1320° C. Waste heat temperature is an important parameter that determines the feasibility of waste heat recovery [53]. Table 1.3 lists some examples of waste heat resources and their temperatures.

Table 1.3 Some of the industrial waste heat resources and their temperatures [52]

Waste heat source	Temperature (°C)
Nickel refining furnace	1370-1650
Steel heating furnace	930-1040
Steam boiler exhaust	230-480
Process steam condensate	50-90

The waste heat can be used through numerous methods. For instance, the heat exchanger can be used to transfer the waste heat to the air in a drying process. This heat substitutes fossil fuels and will reduce the drying costs. In addition, waste heat is a sustainable source of energy that will reduce GHG emissions. Excessive care must be taken to the dew point of flue gas components to avoid vapor condensation and the following corrosion due to NOx and SOx in the exhaust gas. Usually, the minimum allowable temperature to avoid gas condensation is 150° C [53]. In this case, only the sensible heat in the flue gas stream is utilized.

Efforts are underway to co-locate microalgae growth ponds near power plants to capture and recycle CO_2 [54,55]. Therefore, if the CO_2 in power plant flue gas is used for microalgae cultivation and its heat is recovered for microalgae drying, the economics of the whole system is significantly improved [54] because dryers consume a large amount of energy to provide the latent heat of evaporation for the moisture in the wet material [56,57].

1.5 Densification

Algal biomass has a density (around 600 kg/m^3) after drying and grinding. Storage, transportation, and thermochemical conversion of low-density dried biomass are challenging

[58,59]. In addition, handling of fine microalgal particles is challenging since significant electrostatic charges may build up when fine particles are fed into the equipment. Moreover, because of high surface per unit volume of fine particles, surface forces like Van der Waals' play an important role in creating bonds between particles. The formed bonds and charged particles lead to the blockage of storage and handling equipment like hoppers and poor handling characteristics. Pelleting increases the density of loose and bulky biomass. The high density of pellets compared to the density of raw biomass [60] makes pellets valuable fuel to be used in industrial and residential applications. Their elevated density will reduce handling, storage, and transportation costs [61–65]. Densification consists of multiple steps including raw material pre-treatment, which can be drying, grinding, and conditioning based on the biomass characteristics, the compaction, cooling and screening to remove small particles [66].

Pelletization is carried out by forcing particles together using a mechanical system to produce a homogeneous pellet [65]. There are many biomass densification systems like pellet mill, cuber, briquette press, screw extruder, and agglomerator. Pellet mill is the most common system for bioenergy production [58,67]. A pellet mill consists of a perforated die with one or two rollers. Rotation of die and rollers force the feedstock into the holes of the pellet mill to form pellets. Due to the friction between biomass and the die wall, a high back-pressure is built up and heat is generated during pelletization [66]. After densification, the knives mounted on the swing cover cut the pellets while they are extruding from the die [58]. Figure 1.5 shows how a pellet mill operates. Pellets have a cylindrical shape and are about 5.84-7.25 mm in diameter and less than 38.1 mm in length [66].

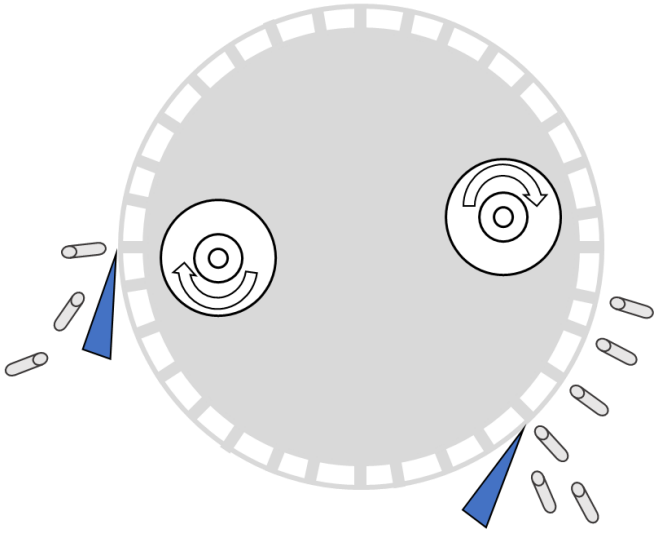

Figure 1.5 A schematic diagram of pellet mill.

One of the applications of densified biomass is co-firing them with coal in existing combined heat and power (CHP) plants. This is an inexpensive and simple method to cut down net CO_2 emissions in a power plant. Moreover, densification enhances the burning efficiency of biomass when co-firing with coal because pelleted biomass has a uniform particle size distribution, and conforms to supply system specifications [58].

In the animal feed industry, the pelleting process has gained much interest because of better animal growth (weight gain and feed efficiency) while taking pelleted feed rather than ground mash feeds. The weight gain of the animal may be due to increased digestion. High-quality pellets are able to tolerate harsh handling conditions without disintegrating and with a final product with the minimal amount of fines [68]. Furthermore, spillage and wind loss happen less frequently for pelleted feed [69].

Both process and feedstock variables affect pellets' quality and required energy for densification [58,65]. Temperature and pressure are two main process parameters and many studies have been conducted to investigate the effect of densification pressure and temperature on pellets' quality and densification behavior of woody and agricultural biomass [70–72]. Heat is generated during densification as a result of friction between biomass and wall of the press channel in a pellet mill. Tabil observed that increasing temperature to more than 90° C

significantly improved alfalfa pellets' durability [73]. Pressure plays an important role in the quality of pellets because it enhances bindings between particles. Li and Liu observed that increasing pressure from 0.24 to 5 MPa improved the density of sawdust pellets.

There are other parameters affecting the pelletization process that are not studied here like retention and relaxation time after pelletization, die geometry and speed, the moisture content of the raw material, and particle size distribution [58].

1.5.1 Literature review on Microalgae Densification

Thapa et al.'s research [74] is the only published study on mechanical densification of algae. They used dried fine powder *Rhizodonium spp.* algae, which was a waste product obtained from wastewater treatment system, as a natural binding agent for densification of Miscanthus (silvergrass). The results of compressing using a mounting press indicated that discs containing more than 20% algae had better strength than pure miscanthus discs.

1.5.2 Biomass Co- Pelletization Practices

At the current stage of technology, combustion of pure pelleted microalgae might not be economically viable [14]. Co-pelletization of microalgae with woody biomass, a commonly used biomass for energy production, is proposed as a potential approach to making energy production from microalgae feasible, as suggested by Thapa et al. [74]. Blending biomass having the high natural binding capacity with the base feed to improve the durability of densified fuel is a common practice, and many examples of this method are available in the literature [67]. Waelti and Dobie showed that mixing 15-20% of beet pulp or ground barley increased the durability of rice straw cubes from 30% (no added second material) to 80% [67]. Also, a durability of 75% was observed when 25% of ground almond hulls was mixed with rice straw [67]. In addition, in densification of water hyacinth (Eichhornia crassipes), increasing the ratio of rice husk from 25 to 75% in the blend, led to an increase in compressive strength of briquettes from 9.7 to 25.3 MPa [67]. Bradfield and Levi's study is another example of co-pelletization. They observed that it was impossible to produce pure wood pellets from hardwood species like white oak (Quercus alba), red oak (Quercus rubra), sweetgum (Liquidambar styraciflua), and red maple (Acer rubrum) [75]. However, blending 15-35% bark with pure wood resulted in pellets with

durabilities of 93-99% [75]. It appears the phenolic compounds in bark were responsible for the improved bonding.

1.5.3 Quality of Densified Biomass

The standards for solid densified fuels in the USA are given as PFI and in Europe as CEN and ISO. These standards list the required range of some parameters like density, diameter, length, moisture content, durability index, the percentage of ash and fines, and concentration of some chemicals. Some of the important factors related to pellets' quality are discussed in this section.

1.5.3.1 Moisture Content

It is important to produce pellets with the optimum final moisture content since both low and high moisture levels have adverse effects on pellets' quality [58,65]. Pellets with low moisture content (<5%) tend to break and create more fines during storage and transportation. On the other hand, pellets with high moisture content are prone to microbial decomposition and spoilage [56,68].

1.5.3.2 Unit Density

Density is an important parameter for storage and transportation and is affected by pelletization temperature and force. Tumuluru et al. [2] showed that in pelleting wheat-based distillers dried grains with soluble (DDGS, the byproduct of the distillation process), unit density was dependent on particle size and densification temperature, and maximum unit density of 1200 kg/m^3 was obtained at a temperature of 100 °C and feed moisture content of 5-7%. Generally increasing moisture content and particle size results in a decrease in density, and increasing temperature and force increases the density [58].

1.5.3.3 Durability Index

Biomass pellets are subject to mechanical loads and environmental stress during production, i.e. pellets are pumped into silos and are transported by trucks or ship. During these steps there is a risk of mechanical failure of pellets, resulting in fines and dust formation and

deterioration of pellets' quality [58]. This durability indicates the ability of densified biomass to remain intact during handling, storage, and transportation. In other words, durability is an indication of the mechanical strength and resistance of the pellets to being broken up. Material composition and moisture content affect the durability of pellets [58,65].

There are different methods to determine the pellets' quality. Some measure pellets' hardness (compression strength), some durability (abrasion resistance), impact resistance, and moisture uptake. Compressive resistance is the maximum amount of force a pellet can withstand before cracking and breaking. The test simulates the weight of top pellets on lower pellets during storage in bins and silos. To measure the compression strength, the pellet is placed between two parallel plates and is compressed at an increasing force with a constant rate. The force at the breakage of the pellet indicates the pellet hardness [58,65]. Impact resistance (drop-shattering) simulates the process of emptying pellets from trucks onto the ground. For this purpose, pellets are dropped from 1.85 m height onto a metal plate, four times [58,65].

Abrasion resistance is of great importance because it demonstrates the ability of pellets to withstand different mechanical forces when in contact with other pellets or with the wall of the container. The basis of this measurement is weighing a specific amount of pellets and exposing them to mechanical stress for a defined time interval and finally measuring the amount of fines and intact particles [58,67]. The three main standard test procedures for measurement of abrasion resistance are Holmen test, tumbling can, and Lingo test. In a Holmen durability tester, the pellets are exposed to pressurized air and are pneumatically circulated through a square pipe with right-angled bends; the pellets hit the surfaces many times [58,65]. In a tumbling can, pellets are rotated. For this test, 500 g of pellets is shaken for 10 min at 50 rpm rotational speed. Then the material is sieved using a sieve size of 0.8 times of pellet diameter. Some modified tumbling tests have been introduced by adding steel nuts and bolts to the can [58,65]. In a Lingo tester, pressurized air circulates pellets around a perforated chamber for 30 s. There is no need for screening after Lingo test because fines are removed constantly via the holes during experiment [58,65].

Pellets with poor hydrophobicity are prone to adsorb moisture and disintegrate into fines under humid conditions. Since the biomass will be lost as fines, transportation will be challenging. The high surface area of small fines will also increase the risk of microbial

degradation. Moreover, the high moisture content of pellets reduces burning efficiency in power plants. Therefore, hydrophobic pellets are desired for safe handling, storage, and transportation [76]. The moisture adsorption rates of pellets in a humidity chamber set at a specific temperature and humidity, for example, 30° C and 90% relative humidity is used as an indicator of moisture uptake of pellets.

1.5.3.4 Calorific Value

The calorific value indicates the combustion efficiency of a biomass. Some pre-treatments like steam- explosion and torrefaction prior to densification increase the calorific value of pellets. For example, wood and straw-based pellets have calorific values of 17-18 MJ/kg, and torrefaction increases this value to 20-22 MJ/kg [77].

1.6 Knowledge Gap

A dry and dense form of microalgae is stable during storage and can be handled and transported efficiently. My literature review shows that the integrated drying and pelletization of microalgae has not been investigated. To design a suitable dryer which meets required evaporation capacity while maintaining microalgae quality, a detailed study on microalgae drying behavior, kinetics and the effect of drying conditions on biomass properties are needed [25]. To best of author's knowledge, no report in the literature has addressed the drying characteristics of *Chlorella vulgaris* as a suitable biomass for biofuel or high-value products. In addition, the few available studies on algae drying, have observed microalgae drying behavior in the limited temperature range of 30-90˚ C [45–49].

On the other hand, to the best of author's knowledge, there is no study in the open literature on pelletization of microalgae *Chlorella vulgaris*. Data on the behavior of the microalgae under pressure and temperature during compression are missing. The wood pellet manufacturers are interested in developing a natural binder that would increase the durability of their pellets. It is an interesting and important question to find out if microalgae *Chlorella* improves the binding capacity of wood particles during pelletization. In addition, there is a lack of knowledge on the co-pelletization mechanism of microalgae *Chlorella vulgaris* with woody biomass. Thapa et al.'s research [74] is the only published study on mechanical densification of

algae. They used dried fine powder *Rhizodonium spp* algae, which was a waste product obtained from wastewater treatment system, as a natural binding agent for densification of miscanthus. The algae used in Thapa et al.'s study was a low-value waste biomass, and its low calorific value (11 MJ kg^{-1}) reveals that it might have been combined with some impurities. In addition, the densification mechanism has not been addressed in Thapa et al.'s paper.

1.7 Research Objectives and Thesis Organization

The central question in this thesis is whether it is feasible to pelletize dried microalgal biomass. To this end, the overall goal of the research is set to investigate the characteristics of microalgae *Chlorella vulgaris* during thermal drying and pelletization. The following objectives were set to achieve the main goal:

1. Study thin-layer drying of *Chlorella* over a wide temperature range of 40-140 ^{o} C.
2. Study the effect of drying temperature on the quality of dried microalgae.
3. Investigate pelletization characteristics of pure microalgae *Chlorella* and its blends with pine sawdust.

In Chapter 2 of this thesis, experimental data on thin-layer drying of *Chlorella vulgaris* in a convective dryer is presented. Chapters 3 and 4 describe densification experiments of microalgae *Chlorella* and its mixture with pine sawdust in a single pelletizer machine. Chapter 3 is focused on describing the densification mechanism. Chapter 4 discusses the pellets' characteristics. Chapter 5 describes the overall conclusions and recommendations for further studies. Appendix A presents the published paper on the economic analysis of microalgae drying in a conveyor belt dryer coupled with waste heat captured from the flue gas of a power plant.

Chapter 2: Thin-Layer Drying Mechanism of Microalgae *Chlorella vulgaris*

Drying of harvested microalgae from an average moisture content of 60-80% wet basis to 10% is challenging. Removing this high amount of water from microalgal biomass is time-consuming and is not as easy as drying agricultural crops. The long drying time results in high drying costs. Although drying is a suitable technique for algae-based fuel production, it has not been commercialized due to its high cost and detrimental effects that high-temperature drying or long-time exposure to heat has on the quality of dried microalgae. The research in this chapter was performed to fulfill the knowledge gap in the microalgae drying mechanism and to understand the reason for long drying times. For this purpose, the thin-layer drying of microalgae *Chlorella vulgaris* at the temperature range of 40 to 140° C is studied. The effect of drying air temperature and drying time on *Chlorella*, the elemental and chemical composition, surface color, and surface structure of the microalgae *Chlorella vulgaris* is presented and analyzed.

2.1 Materials and Methods

2.1.1 Microalgae Cultivation

Chlorella vulgaris was provided by Algae Test-bed Public-Private Partnership (ATP^3) (Arizona, U.S.). The microalgae were cultivated in flat panel photobioreactors (PBR) at their site. The seed culture coming from indoor cultivation in the lab under constant temperature, light, and nutrient conditions was inoculated in a 680 L reactor. The outdoor PBRs had the initial concentration of 0.5 g/L (AFDW ash-free dry weight basis) in BG-11 culture media.

After 4 days, the concentration reached 2 g/L and the culture was diluted. For this purpose, the culture in the main reactor was split into two 340 L portions and each portion was transferred to a 680 L capacity reactor. To perform the dilution, 340 L water containing nitrogen, phosphorous, and silica was added to each reactor. The outcome of dilution was two 680 L reactors containing culture at a concentration of 1 g/L. The two PBRs were operated for another 18 days until reaching 3 g/L concentration. The biomass was centrifuged and the resultant paste was kept frozen at -20° C until shipping to our lab in Vancouver, BC, Canada for the experiments. Upon receiving the sample, the algae mass was kept frozen at -4° C. The algae mass was thawed at 4° C prior to use.

2.1.2 Thin- Layer Drying Tests

Figure 2.1.a and Figure 2.1.b show a schematic diagram of the thin-layer dryer and a photo of the dryer system, respectively. A continuous air stream passed through a desiccant to absorb moisture. The dry air passed through an in-line electrical heater (AHP-7562 model, Omega Engineering, Canada). The hot air entered the dryer chamber and passed over and under the horizontal tray containing about 20 g of algae sample. An infrared heater (QC-061040-T model, Omega Engineering, Canada) installed on the upper part of the chamber provided additional heat to the dryer. A thermocouple inside the chamber recorded the temperature of air very close to the material.

An aliquot of microalgae paste was placed on parchment paper, and then the parchment paper covered by microalgae was placed on an aluminum pan (Figure 2.1.c). The thickness of the biomass in the pan was kept at 3 mm for all experiments. The thickness was measured by inserting a ruler in different areas of microalgae paste.

Before loading the biomass in the dryer, the airflow rate was set at 50 L/min and the heaters were turned on to maintain the temperature at the targeted value. Drying was performed at temperatures of 40, 60, 80, 100, 120 and 140 °C. The drying was continued until the wet sample reached a constant mass. During drying, the mass of biomass and the corresponding time were logged and saved. The moisture at the material surface was assumed to be the same as equilibrium moisture content at the corresponding temperature. After cooling in ambient conditions, the dried biomass was ground, vacuum packed and stored at 4° C for further analysis.

(a)

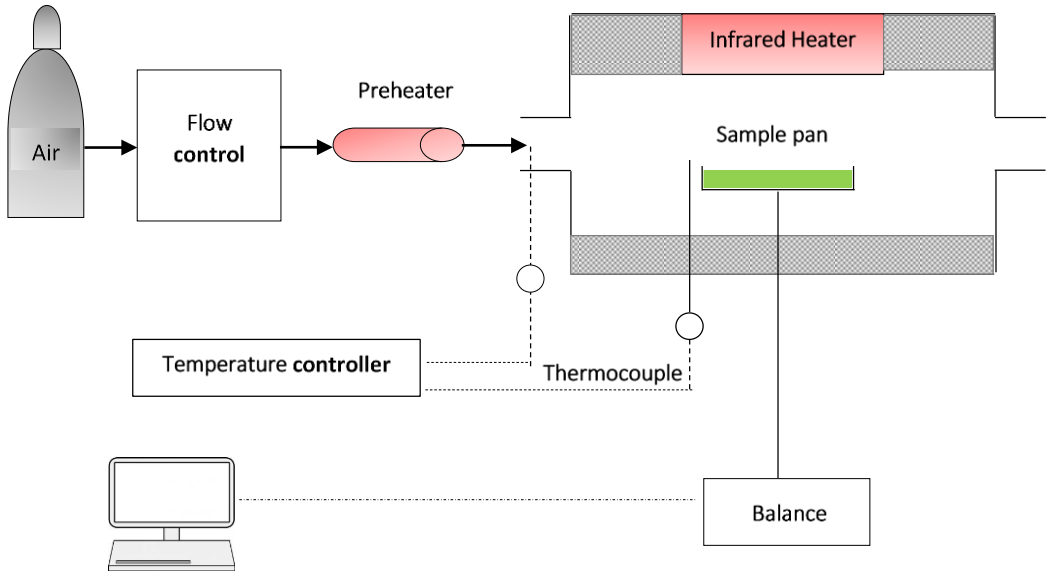
Air
Flow control
Preheater
Infrared Heater
Sample pan
Temperature controller
Thermocouple
Balance

(b)

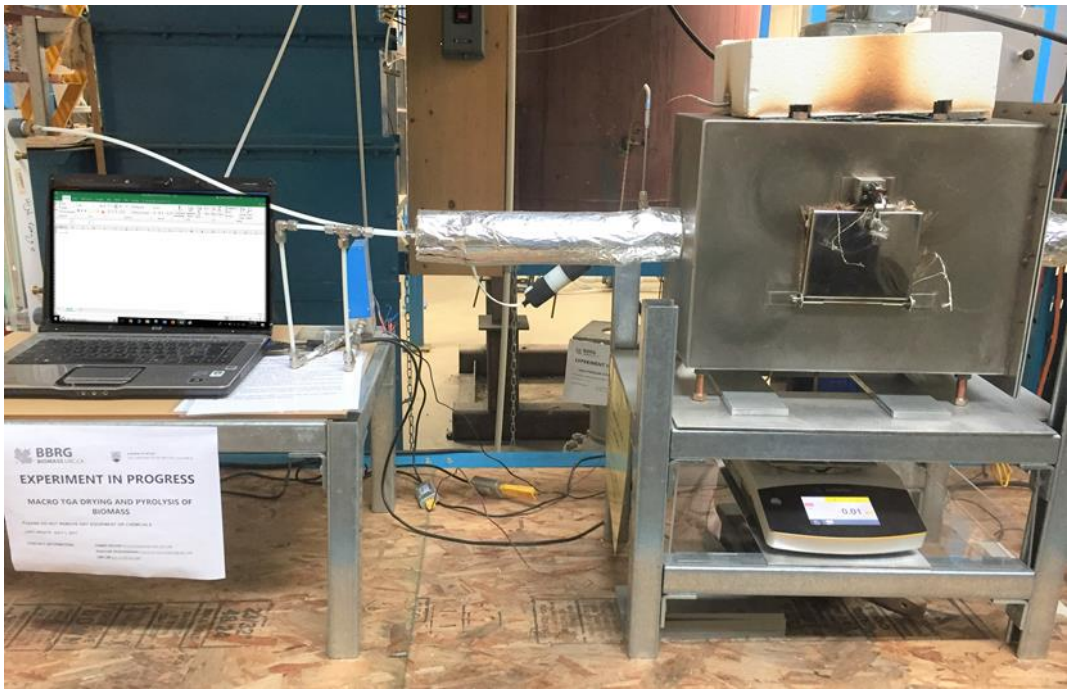
BBRG
EXPERIMENT IN PROGRESS
MACRO TGA DRYING AND PYROLYSIS OF BIOMASS

(c)

Figure 2.1 Experimental setup of thin layer drying (parts are not to the scale) (a) dryer unit diagram (b) dryer unit photo (c) thin-layer of wet microalgae *Chlorella* on the pan at a moisture content of 66.4%. The drying pan was 12 cm in length and 6 cm in width.

2.1.3 Biomass Characterization

2.1.3.1 Ultimate and Proximate Analysis

Moisture and ash content of the biomass was measured using the method of Wychen [78]. Briefly, the moisture content was determined by placing the sample in a convective oven at 60 °C for at least 18 h. The ash content of a sample was determined by its oxidation in a muffle furnace under a ramping program up to a temperature of 575 °C. The volatile and fixed carbon measurements were performed in a proximate analyzer (Model SDT-Q600, TA Instruments, DE, USA). Ultra-pure nitrogen (99.999%) with a flow rate of 50 ml/min was used as the carrier gas to protect the samples from oxidation. Microalgae samples were heated to 900° C at a rate of 5° C min^{-1} and the resulting graph was analyzed. From the peaks of the gravimetric graph, moisture content and volatile matter were determined (Figure 2.2). In the oxygen-free environment, the solid matter that is left at the end of TGA is the combination of fixed carbon and ash. The fixed carbon was calculated from the difference between 100 and sum of moisture, ash, and volatile percentage from other experiments [26,79,80]. Average moisture, volatile, and ash content were calculated from three replicates of the experiment per sample.

The elemental analysis was performed using Flash 2000 elemental analyzer (Thermo Scientific, MA, USA).

Calorific value was measured using a bomb calorimeter (Model 6600, Parr Instrument Company, Moline, IL). 1 g of dried biomass was combusted in a combustion bomb filled with 2.7 MPa of pure oxygen. After the ignition, the gross calorific value of the as-received sample (wet basis) was calculated. Then, the higher heating value (HHV) of the sample was calculated based on its moisture content.

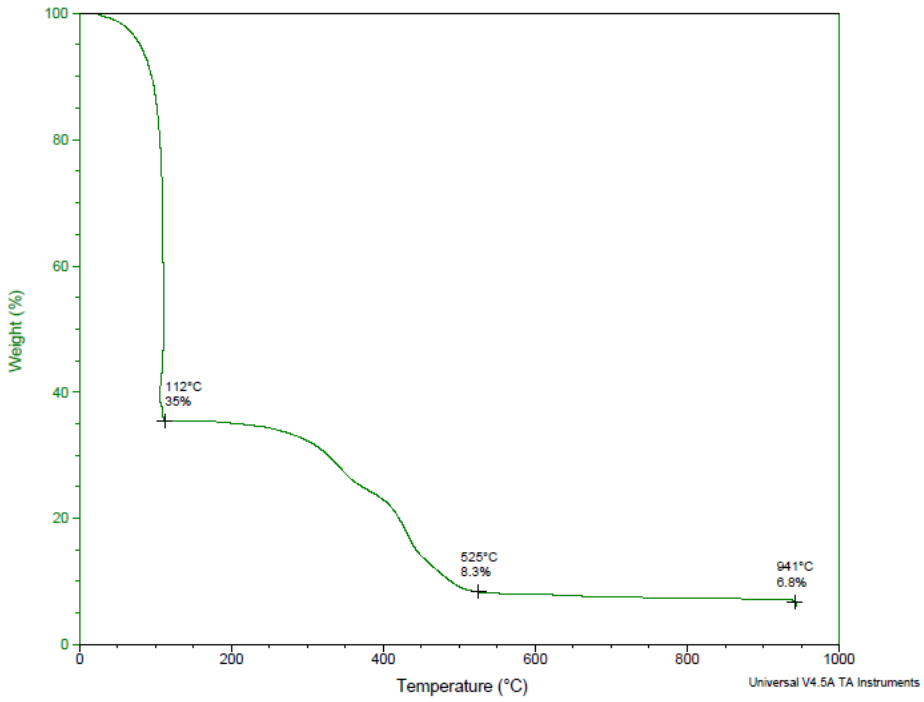

Figure 2.2. The graph from thermogravimetric analysis. The moisture content was calculated using the weight loss of the sample until heating to 112° C. The volatile content was estimated using the sample weight loss from 112 to 941° C. The remaining mass after 941° C was fixed carbon and ash.

2.1.3.2 Chemical Composition

The total non-polar lipid content, the key lipid compounds for biodiesel production, of *Chlorella* was estimated according to Soxhlet extraction method using petroleum ether solvent (Sigma-Aldrich, U.S.) based on the United States Department of Agriculture (USDA) standard method [81]. Briefly, a boiling flask containing small pieces of boiling chips was weighed and filled with 200 ml of anhydrous petroleum ether (Sigma-Aldrich, U.S.) as the solvent. The boiling flask, soxhlet flask, and condenser were assembled. Two grams of the sample which was

placed in a filter paper (Whatman, UK) and protected tightly with a string was placed in the soxhlet tube. The extraction was performed by heating the solvent for 16 hours. After extraction, the solvent in the boiling flask was evaporated using a rotary evaporator and the boiling flask containing the extracted lipid was dried in an air oven at 100° C for 30 minutes. Finally, the flask was cooled in a desiccator and weighed.

The carbohydrate content of the biomass was determined by the phenol-sulfuric acid method [81,82]. The composition of all classes of carbohydrates is measured by this method, namely, mono-, di-, oligo-, and polysaccharides [81,83]. Briefly, a 1000-time diluted solution of the sample in deionized water was prepared. Two milliliters of diluted sample was collected and mixed with 0.05 ml of 80% phenol solution (Sigma-Aldrich, U.S.) and 5 ml of 98% sulfuric acid (Sigma-Aldrich, U.S.). The mixture was placed in a water bath at 40° C for 30 minutes and was then cooled in cold water. The absorbance of the sample was measured by a spectrophotometer (infinite M200 pro model, TECAN, Switzerland). The sample concentration was determined by using the standard curve obtained by measuring the absorbance of standard solutions.

To obtain the protein content, the percentage of nitrogen content obtained from elemental analysis was multiplied by the factor 6.25 because protein contains about 16% nitrogen (1/0.16=6.25) [83].

2.1.3.3 Surface Color

The surface color of the samples was measured using a colorimeter (CM-5 model, Konica Minolta, Japan). The results were reported in Hunter *L*, *a*, *b* scale. *L* scale ranges from 0 for black to 100 for white, *a* scale ranges from -50 for green to +50 for red, and *b* scale from -50 for blue to +50 for yellow. The total color difference (ΔE) was calculated using Equation 1, where l_0, a_0, and b_0 are the control values for freeze-dried *Chlorella* [48,84].

$$\Delta E = \sqrt{((L - L_0)^2 + (a - a_0)^2 + (b - b_0)^2)} \quad (1)$$

where *L*, *a*, and *b* are Hunter parameters indicating the black/white, green/red, and blue/yellow color elements of the samples, respectively. Similarly, L_0, a_0, and b_0 are the same color parameters for the control sample. ΔE is the total color difference of sample compared to the control.

2.1.3.4 Scanning Electron Microscopy (SEM)

For SEM tests, the sample was placed on double-sided adhesive tape, mounted on an aluminum stub, and coated with gold under vacuum using a cathodic pulverizer (Hummer II Technics). All the images were taken at 2.5 to 5 kV accelerating voltage by using a field emission scanning electron microscope (Model S4700, Hitachi, Japan).

2.1.4 Drying Kinetics Modeling

Thin-layer drying experimental data (moisture ratio vs time) were fitted with the following semi-theoretical drying models: Henderson and Pabis (Equation 2), Newton (Equation 3), Page (Equation 4), and logarithmic model (Equation 5). Semi- theoretical models are all approximate analytical solutions to Fick's second law of diffusion [85,86].

$$\mathrm{MR} = \frac{M(t)-Meq}{M0-Meq} = A_1 \exp(-k_1 t) \quad (2)$$

$$\mathrm{MR} = \frac{M(t)-Meq}{M0-Meq} = \exp(-k_2 t) \quad (3)$$

$$\mathrm{MR} = \frac{M(t)-Meq}{M0-Meq} = \exp(-k_3 t^n) \quad (4)$$

$$\mathrm{MR} = \frac{M(t)-Meq}{M0-Meq} = A_2 \exp(-k_4 t) + c \quad (5)$$

where MR is the moisture ratio (dimensionless) defined as the ratio of water still to be removed at any time t (min) to the total water initially available, *M(t)* is moisture content (kg water/kg dry matter, dry basis (d.b.)) at each time, M_0 is the initial moisture content (d.b.), M_{eq} is the equilibrium moisture content (d.b.), k_1, k_2, and k_4 are drying constants (min^{-1}), k_3 is also the drying rate constant, but its unit might vary based on the value of parameter *n*. A_1 and A_2 are constants related to the shape of biomass spread, and *n* is the page constant which is related to the physical properties of the sample [48].

Drying rate curve was also derived by applying the finite difference method to drying data. During the falling drying rate period, the internal diffusion is the controlling mass transfer mechanism, and it can be explained by Fick's second law of diffusion (Equation 6).

$$\frac{\partial M}{\partial t} = D \frac{\partial^2 M}{\partial x^2} \quad (6)$$

Where M is moisture content (d.b.), t is the drying time (s), and D is the moisture diffusion coefficient (m^2/s) in the thin layer. The analytical solution for Fick's equation in the Cartesian coordinate is Equation 7.

$$MR = \frac{8}{\pi^2} + \sum_{n=0}^{\infty} \frac{1}{(2n+1)^2}\ exp\left(-(2n+1)^2\ \pi^2 D \frac{t}{4\ (h^*)^2}\right) \quad (7)$$

where h^* is the half thickness of the slab (m). In practice, for a long period of time, only the first term of the series is often considered. Further simplification of the solution leads to Equation 8 [85].

$$\ln(MR) = \ln\left(\frac{8}{\pi^2}\right) - (\pi^2 D\ t/4(h^*)^2) \quad (8)$$

Moisture diffusion coefficient was calculated by fitting the drying data to the analytical solution of Fick's second law (Equation 6). Temperature dependence of diffusion coefficient (*D)* is expressed by the Arrhenius equation (Equation 9):

$$D = D_0 \exp(-\frac{E}{RT}) \quad (9)$$

where *D* is the effective diffusivity, *E* is the activation energy (kJ/mol), R is the universal gas constant (kJ mol^{-1} K^{-1}), D_0 is the Arrhenius factor, and *T* is the absolute temperature (K). The general form of Equation 9 can be used to evaluate drying constants by replacing D with k_1, k_2, k_3, or k_4.

2.1.5 Statistical Analysis of Experimental Data

Drying tests and material characterizations were repeated at least three times. The repetitions were performed independently over several days to make sure that data are reproducible. The data were presented as mean values and their dispersion in terms of standard deviation. The calculated standard deviation indicates the level of confidence in the experiments.

The results were statistically evaluated using analysis of variance (ANOVA) with $\alpha = 0.05$. The models were fitted to the drying data using MATLAB 2008Ra, and the goodness of fit was evaluated based on the coefficient of determination (R^2) and the sum of squared errors of prediction (SSE) values.

2.2 Results and Discussion

2.2.1 *Chlorella* Drying Behavior and Kinetics Parameters

Thin-layer drying is widely applied to study the drying kinetics of biomass, fruits, vegetables, and many other materials [87,88]. In order to guarantee thin-layer drying conditions, the thickness of material should be small such that there is no temperature or moisture gradient along the thickness of the material layer on the tray. Under these conditions, a lumped model can replace the complex distributed models. In their extensive literature review on thin-layer drying, Guedes et al. [35] showed that a 3 mm thickness ensures that drying occurs in the thin-layer mode.

Microalgae drying was studied under a wide range of temperatures (40 to 140 ° C) to understand the impact of temperature and drying time on biomass characteristics. The drying curve of biomass with an average initial moisture content of 66.4% (w.b.) at different temperatures is shown in Figure 2.3. At all drying temperatures, the material moisture content decreased exponentially with time. The drying proceeded faster as the drying temperature increased because of higher drying rate (Figure 2.4). The drying time required to achieve equilibrium moisture content (EMC) at drying temperatures of 40, 60, 80, 100, 120, and 140° C were 555±10, 420 ±6, 360±13, 207±15, 124±13, and 82±6 min, respectively. The equilibrium moisture content (EMC) achieved at temperatures of 40, 60, 80, 100, 120, and 140° C is listed in Table 2.1. The suitable moisture content for long-term stable storage of microalgae is less than 10% (w.b.) [25–27]. The EMC of dried *Chlorella* at all temperatures except 40° C in this study was less than 10%, which guarantees safe storage of *Chlorella*. Similarly, other studies have reported EMC less than 10% for *Aphanothece microscopica Nageli* [84], brown algae *Macrocystis pyrifera* [49], *Spirulina* [89], and green algae consortium [26]. Figure 2.5 shows the dependency of equilibrium moisture content on drying temperature. An exponential equation (dotted line) of the following form M_{eq}=46570 exp(-0.026T) fitted the data well (R^2=0.99).

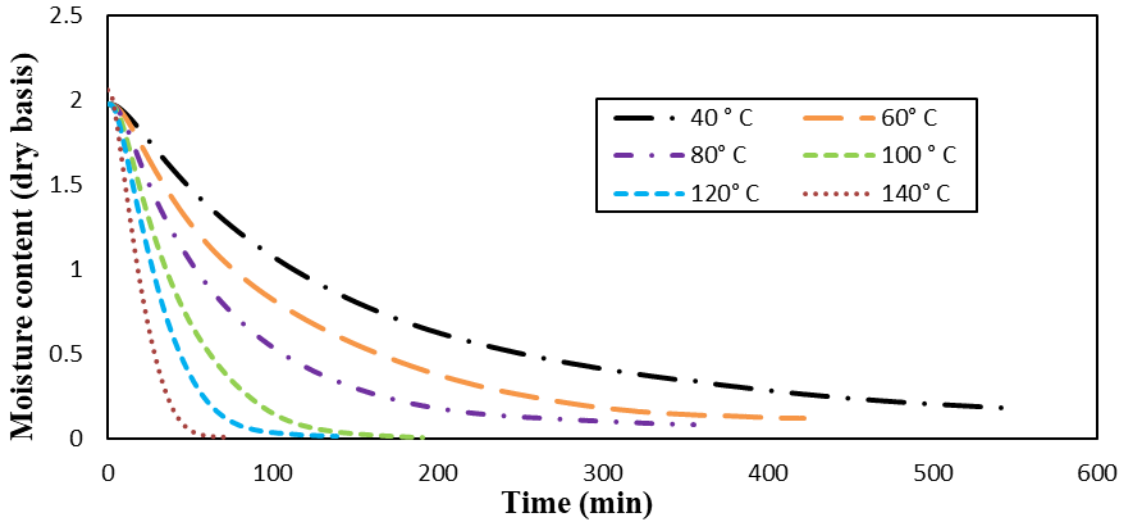

Figure 2.3 Moisture content curves of *Chlorella* with an initial moisture content of 66.4% (w.b.) at drying temperatures of 40, 60, 80, 100, 120, and 140° C.

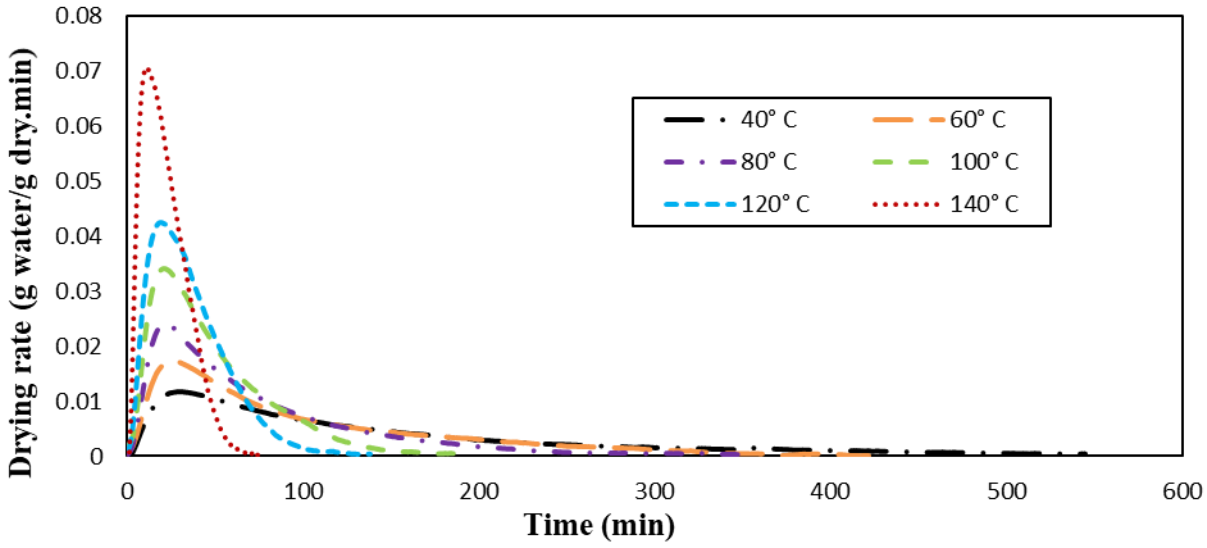

Figure 2.4 Drying rate curves of *Chlorella* with an initial moisture content of 66.4% (w.b.) at drying temperatures of 40, 60, 80, 100, 120, and 140° C. No constant rate period was evident.

Table 2.1 Equilibrium moisture content at different drying temperatures (40-140 °C). By increasing the drying temperature, equilibrium moisture content decreased.

Temperature (° C)	Equilibrium moisture content (% wet basis)
40	16.9±2.0
60	9.9±0.8
80	5.1±1.4
100	3.0±1.1
120	2.2±0.9
140	1.3±0.3

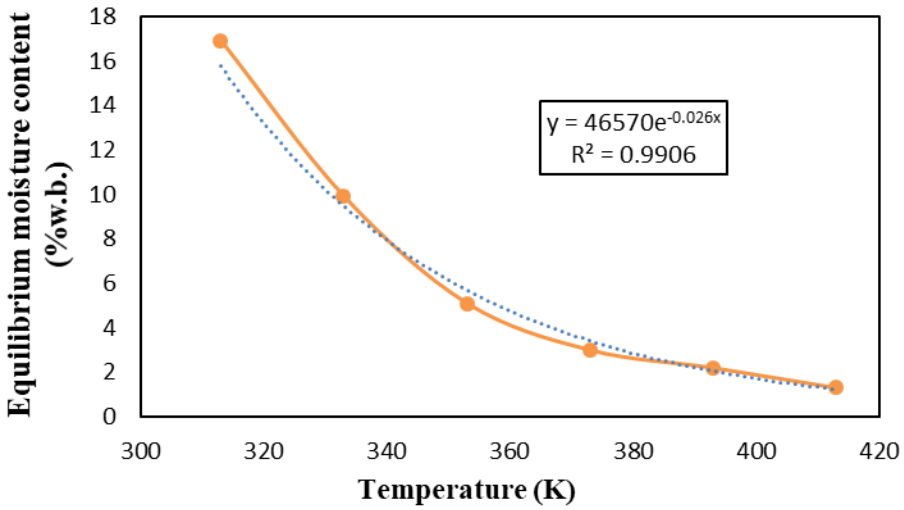

Figure 2.5 The dependency of equilibrium moisture content on drying temperature in the range of 313-413 K.

An initial rising period was observed in drying rate-time curve (Figure 2.4), which seems to be a warm-up period. During this initial period, the biomass temperature increased from room temperature to drying temperature. At the same time, the free water on the surface of cells evaporated. Since during this period, the temperature increased with time, the drying rate had a rising trend. As soon as the biomass temperature reached the corresponding drying temperature and all the surface free water was evaporated, the falling rate period started with no constant drying rate period [90].

The lack of constant rate period showed that diffusion was the dominant mechanism in microalgae drying. Decreasing the drying rate with time might be due to the resistance inside the cell walls to the free movement of water molecules. In fact, the moisture entrapped in the cell

should migrate to the cell surface and then evaporate. Case hardening during drying might be another reason for slowing down the rate of drying. Lack of constant rate drying period has been observed in the drying of many other algae biomass like *Aphanothece microscopica Nageli* [84], *Gelidum sesquipedale* [91], brown algae *Macrocystis pyrifera* [49], *Spirulina* [43,89], and green algae consortium [26]. The absence of constant rate drying period is a common behavior in drying organic and biological material [49].

The water content that has remained in the biomass after all mechanical dewatering methods is called bound moisture content. In contrast to the unbound moisture in the biomass that can be removed by mechanical means like centrifuge or compression, bound moisture is removed by drying. The unbound moisture content is either the water on the surface of the biomass or the water trapped between capillaries without any chemical bonds to the cells [92]. The bound water content of wet material limits to what extent the material can be mechanically dewatered [90]. The samples received and tested in our laboratory were already mechanically dewatered (centrifuge). The removal of the remaining bound moisture entrapped in the cell structure was controlled by diffusion, resulting in a long time for the material to dry. Cell disruption before drying could facilitate the drying of microalgae biomass by shifting the dominant drying mechanism from diffusion to convection.

In order to understand the thin-layer drying behavior of biomass, finding the theoretical model that best fits experimental drying data is very important [86]. Experimental drying data used for fitting with different thin layer drying models are presented in Figure 2.6. Table 2.2 lists the fitting results including drying constants and statistical parameters indicating goodness of fit for all drying temperatures and all studied drying models. The results showed that at 100° C, the Page model was a better fit than the Newton model ($p \leq 0.05$), however, no significant difference between the Page model and other models was observed ($p > 0.05$). At 120 and 140° C, the Page model was a better fit than other models ($p \leq 0.05$). However, there was no significant difference between different models at other drying temperatures ($p > 0.05$). Zepka et al. [83] and Viswanthan et al. [26] also observed that the Page model could predict the drying behavior of *Aphanothece microscopica Nageli* and green algae consortium better than other models.

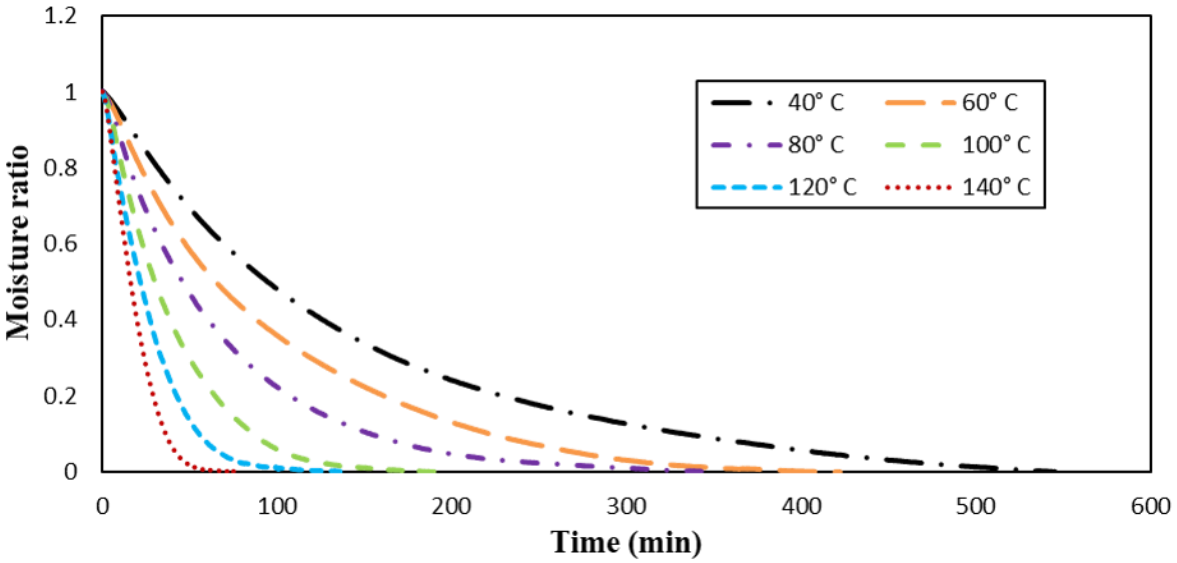

Figure 2.6 Moisture ratio curves of *Chlorella* with an initial moisture content of 66.4% (w.b.) at drying temperatures of 40, 60, 80, 100, 120, and 140° C

Table 2.2 Kinetic parameters and statistical evaluation of thin layer drying models

Model	Parameters	40° C	60° C	80° C	100° C	120° C	140° C
Henderon-	A1	1.014±0.014	1.005±0.007	1.037±0.018	1.063±0.012	1.098±0.018	1.147±0.012
Pabis	k1	0.006±0.002	0.011±0.001	0.014±0.001	0.024±0.002	0.041±0.003	0.059±0.004
	SSE	0.22	0.15	0.05	0.06	0.11	0.50
	R-square	0.996	0.997	0.999	0.998	0.994	0.985
Newton	k2	0.006±0.002	0.011±0.001	0.013±0.002	0.023±0.001	0.037±0.003	0.0525±0.004
	SSE	0.23	0.15	0.11	0.15	0.32	0.99
	R-square	0.995	0.997	0.998	0.995	0.985	0.970
Page	k3	0.005±0.003	0.009±0.003	0.010±0.003	0.014±0.002	0.015±0.004	0.017±0.003
	n	1.045±0.068	0.987±0.0430	1.064±0.044	1.133±0.028	1.280±0.057	1.424±0.037
	SSE	0.17	0.13	0.04	0.02	0.00	0.02
	R-square	0.997	0.998	0.999	0.999	0.999	0.999
Logarithm	A2	1.049±0.060	1.007±0.009	1.041±0.019	1.067±0.013	1.117±0.022	1.167±0.021
	k4	0.005±0.003	0.009±0.000	0.013±0.002	0.023±0.002	0.037±0.003	0.051±0.005
	C	-0.059± 0.072	-0.018± 0.001	-0.013± 0.006	-0.018± 0.008	-0.030± 0.009	-0.052± 0.017
	SSE	0.05	0.10	0.78	0.03	0.08	0.28
	R-square	0.999	0.998	0.983	0.999	0.996	0.992

The drying rate constant depends on air conditions and the thickness of material [84]. The dependency of Newton model constant (k_2) and diffusion coefficient with temperature is shown in Figure 2.7.a and Figure 2.7.b and are defined by Equation 10 and Equation 11. The Page model predicted the drying behavior best in most cases, but due to the random variation of parameter *n* with changing temperature and the inconsistency in Page model's constant unit, the dependency of Newton model constant on temperature was preferred.

$$D = 4.27 \times 10^{-6} \exp\left(-\frac{2984.4}{T}\right) \quad (10)$$

$$k_2 = 40.85 \exp\left(-\frac{2773}{T}\right) \quad (11)$$

Temperature T in Equations 10 and 11 is in K (Kelvin). The diffusion coefficient (D) is in m^2/s. Drying constant k_2 is in min^{-1}. Based on Eq. 10, the value for the Arrhenius factor (D_0) was 4.27×10^{-6} m^2/s and the required activation energy was 24.81 kJ/mol. The Newton model constant (k_2) for microalgae ranged from 0.006 to 0.0525 1/min. The k_2 value increased by raising the drying temperature, which meant the drying rate was higher at higher temperatures. For comparison, the drying rate for corn grain published by Brooker et al. [93] at 40^o C was 0.004 min^{-1} and at 140^o C was 0.038 min^{-1}. The drying constant for microalgae was slightly higher than the published data for grain corn, and this difference increased with drying temperature

Similarly, by increasing the drying temperature from 40 to 140° C, the diffusion coefficient increased 10 times higher at 3.61×10^{-9} m^2/s. The range of calculated diffusion coefficient for *Chlorella* was in the similar range to those obtained in other studies. The diffusion coefficient for brown algae *Macrocystis pyrifera* at 80° C was 10.216×10^{-9} m^2/s [49] and the diffusion coefficient for green algae consortium at 90° C was 1.74×10^{-9} m^2/s [26].

(a)

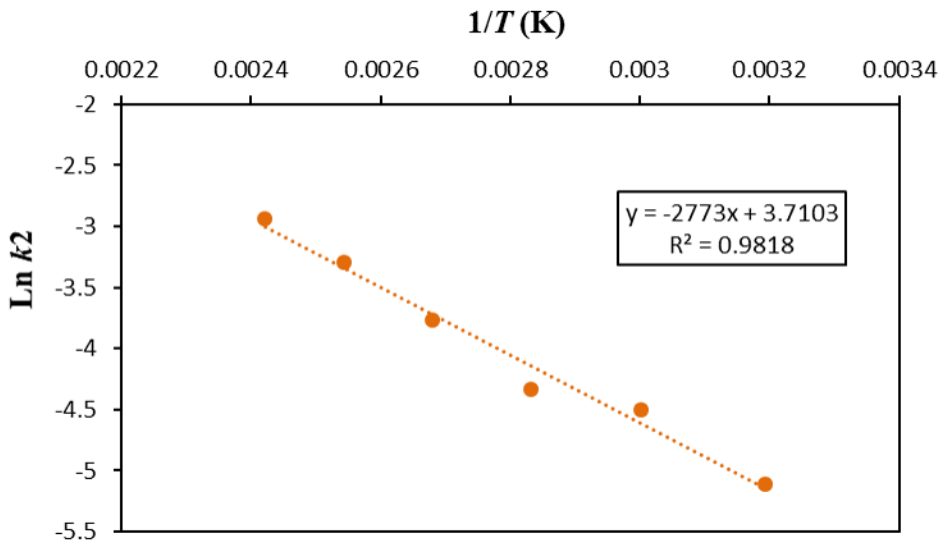

(b)

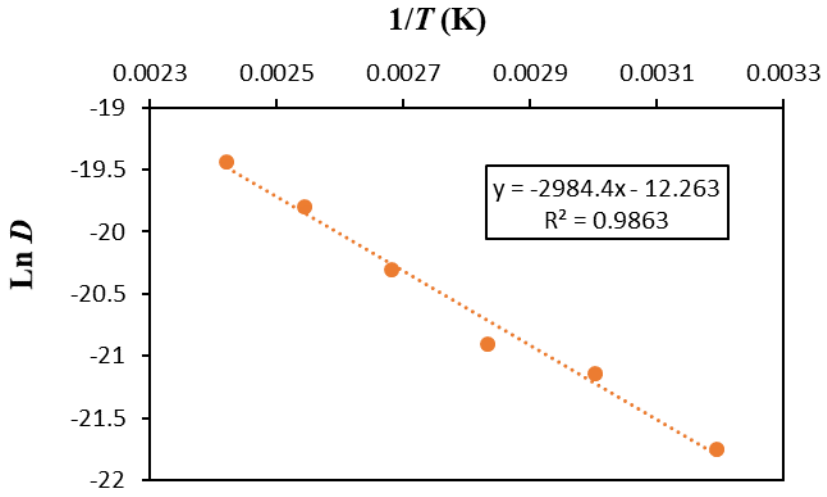

Figure 2.7 (a) Temperature dependency of drying rate constant. (b) temperature dependency of diffusion coefficient.

2.2.2 Microalgae Characteristics

Table 2.3 presents properties of freeze-dried *Chlorella*. In all characterization tests, freeze-dried *Chlorella* is taken as the control. In many studies, it is stated that freeze-drying

preserves microalgae characteristics [94], so biomass dried at other temperatures were compared to freeze-dried sample.

Table 2.3 Biochemical composition, ultimate and proximate analysis of freeze-dried *Chlorella* as control sample

Analysis		*Chlorella vulgaris*
Biochemical composition	Lipid (% D.W.)	10.63± 0.36
	Protein (% D.W.)	11.56± 0.06
	Carbohydrate (% D.W.)	26.18± 0.24
Ultimate analysis	Carbon (% D.W.)	59.17± 0.33
	Oxygen (%D.W.)	28.44±0.31
	Hydrogen (% D.W.)	8.20± 0.03
	Nitrogen (% D.W.)	1.85±0.01
	Sulfur (% D.W.)	0.26±0.01
Proximate analysis	Ash (% D.W.)	2.19±0.16
	Volatile matter (% D.W.)	83.08±3.02
	Fixed carbon (%D.W.)	14.73±1.84
	Higher heating value (MJ/kg)	27.29±0.69

2.2.2.1 Surface Color

The color of freeze-dried microalgae as the control and microalgae dried at different temperatures was monitored. Figure 2.8 presents the color coordinates for the samples.

The trend of results for *L* coordinate (brightness/darkness) and *b* coordinate (yellowness/blueness) were similar. The freeze-dried sample had the largest *L* value in comparison to all other temperatures ($p \leq 0.05$). Among other temperatures, 60 and 80° C drying temperatures preserved the brightness of the sample significantly more than other temperatures (40, 100, 120, and 140° C) ($p \leq 0.05$). Similar to the *L* coordinate, the freeze-dried *Chlorella* significantly had the largest *b* value ($p \leq 0.05$). Moreover, samples dried at 60 and 80° C were significantly yellower than those dried at 40, 100, 120, and 140° C ($p \leq 0.05$).

The freeze-dried sample had a significantly smaller *a* value in comparison to other samples (i.e., increased green pigmentation). By increasing the drying temperature from 40 to 140° C, the *a* value significantly increased, which means the greenness of the samples became smaller and the samples turned to red. There was no clear trend between drying temperatures of 40, 100, 120, and 140° C and changing *L, a, b*, and ΔE (Table 2.4).

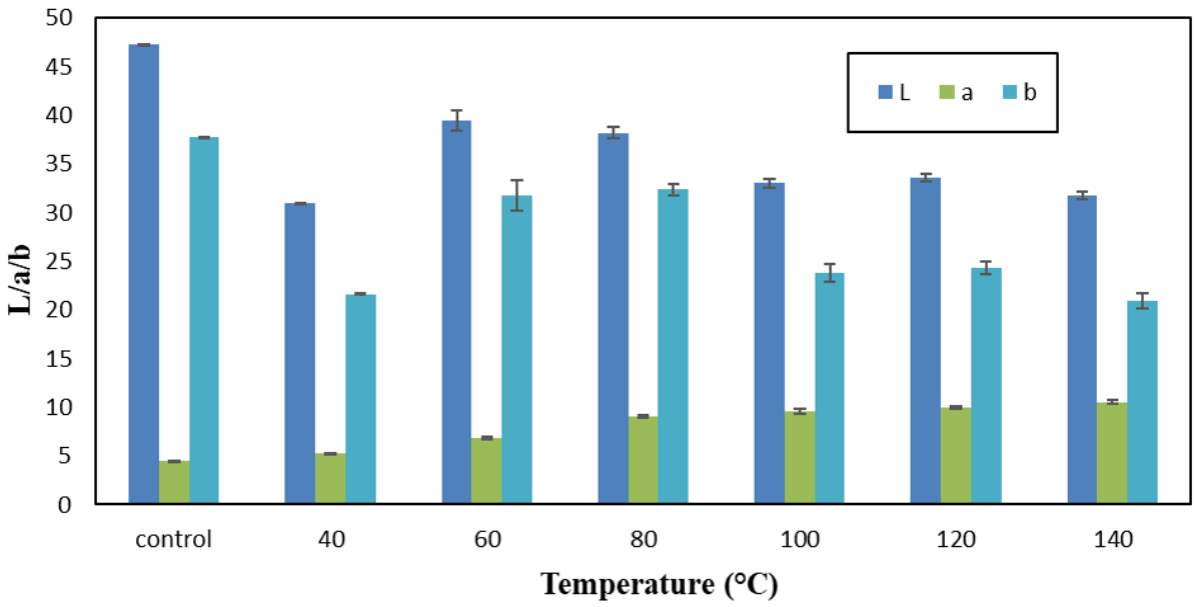

Figure 2.8 Color coordinates of *Chlorella* dried at temperatures of 40, 60, 80, 100, 120, and 140 ° C. L, a, and b are indicators of whiteness/blackness, greenness/redness, and blueness/yellowness, respectively. Drying temperatures of 60 and 80° C best-preserved samples' color.

Table 2.4 The overall color difference of *Chlorella* dried at different temperatures compared to freeze-dried *Chlorella.* Drying temperatures of 60 and 80° C had the least color difference with the control sample.

Temperature (° C)	*ΔE*
40	23.02±0.01
60	10.19±1.72
80	11.59±0.63
100	20.63±0.93
120	20.00±0.63
140	23.71±0.85

The total color difference of samples from the control sample (freeze-dried *Chlorella*) is indicated by *ΔE*, which is a function of *L, a, and b* coordinates. When analyzing *ΔE* values, 60 and 80° C drying temperatures showed significantly lowest differences compared to freeze-dried *Chlorella*. However, 40, 100, 120, and 140° C drying temperatures had significantly greater difference compared to the control sample ($p \leq 0.05$).

Chlorella contains 2-3% chlorophyll a and b giving them a bright green color. They also have accessory pigments including 0.1 to 0.25% (d.w.) beta-carotene (orange pigment) and xanthophylls (yellow pigments). It seems that deterioration of pigments because of drying contributes to changes in the color of *Chlorella*.

Tello-Ireland et al. [48] also observed a decrease in the greenness of algae *Gracilaria chilensis* when dried at 50, 60, and 70° C. Similarly, Lopes et al. [84] reported a change from bright green to dull olive green when drying cyanobacterium *Aphanothece microscopica Nageli* at 40, 50, and 60° C. Tello-Ireland et al. and Lopes et al. explained the color change by pigment deterioration because of thermal degradation.

Based on all the color results, it seems that brightness and yellowness of *Chlorella* are best preserved at 60 and 80° C drying temperatures and no significant difference was observed between these two temperatures ($p>0.05$). The ΔE results also confirmed the latter conclusion. The results showed that low and very high drying temperatures had the same impact on brightness, yellowness, and ΔE of *Chlorella*. In other words, drying at low temperature for a long time could be as harmful to pigments as drying at high temperature for a short time. The greenness results showed that by increasing temperature, the greenness of *Chlorella* decreases. Neoh et al.'s study [95] confirms the adverse effects of extremely low drying temperature on microalgae properties. They observed the lowest antioxidant activity when algae *Kappaphycus alvarezii* was sun-dried. The low seaweed quality was associated with long drying time in solar drying technique. Therefore, choosing an optimum drying temperature could guarantee to preserve green and yellow pigments and brightness of the biomass at the same time. The drying temperature of 60° C seems a good choice for preserving the pigments.

2.2.2.2 Ultimate and Proximate Analysis

No difference was observed between carbon, hydrogen, oxygen, nitrogen, sulfur, and heating value of freeze-dried *Chlorella* and biomass dried under different drying temperatures (Table 2.5). These results were similar to Viswanathan et al.'s results, where [26], drying tests in a convective oven with a constant parallel airflow velocity of 0.3 ms^{-1} at drying temperatures of 30, 50, 70 and 90˚ C were performed. They reported that drying temperature (30 to 90° C) had

no effect on the elemental composition (CHNS) of the green microalgae consortium consisting of *Scenedesmus bijuga, Chlamydomonas globose, and Chlorella minutissim*

Table 2.5 Ultimate and proximate analysis results of *Chlorella* dried at 40, 60, 80, 100, 120, and 140° C temperatures. There was no significant difference in elemental composition and calorific value of samples dried under different temperatures.

	C (% d.b.)	H (% d.b.)	N (% d.b.)	S (% d.b.)	O (% d.b.)	Higher Heating value (MJ/kg)
Freeze-dried	59.17±0.33	8.20±0.03	1.85±0.01	0.26±0.01	28.44± 0.31	27.29± 0.69
40 ° C	59.02±0.87	8.29±0.20	1.82±0.04	0.31±0.03	29.4±0.18	27.25±0.18
60° C	59.89±0.22	8.13±0.10	1.86±0.01	0.31±0.01	29.52±0.37	27.27±0.14
80° C	58.59±0.83	8.42±0.03	1.82±0.02	0.29±0.02	28.12±0.78	27.11±0.49
100° C	58.96±0.092	8.44±0.02	1.83±0.02	0.33±0.04	28.73±0.18	27.16±0.08
120° C	59.02±0.59	8.46±0.05	1.82±0.02	0.30±0.03	28.49±0.79	26.70±0.15
140° C	59.30±0.46	8.48±0.08	1.85±0	0.33±0.05	27.48±0.55	27.61±0.06

2.2.2.3 Biochemical Composition

The carbohydrate content of microalgae samples dried at 60° C was significantly higher than that of other samples dried at lower or higher temperatures ($p \leq 0.05$) with an average loss of 6.6 % in comparison to freeze-dried biomass (Figure 2.9). Drying at 60 and 80° C caused an average loss of 4.0 and 4.8 % lipid content in microalgae in comparison to freeze-dried biomass (Figure 2.9). However, lipid was best preserved at 60 and 80° C drying temperatures ($p \leq 0.05$). Also, there has been no significant difference between lipid content at 60 and 80° C. Results in Figure 2.9 showed that there was no significant difference in protein content between samples dried under different temperatures ($p > 0.5$).

Based on the results, it seems that 60 and 80° C drying temperatures best-preserved lipid and carbohydrate content of the microalgae. Viswanathan et al. noticed a slight drop in total lipid content by increasing the drying temperature of the green microalgae consortium to 90° C [26].

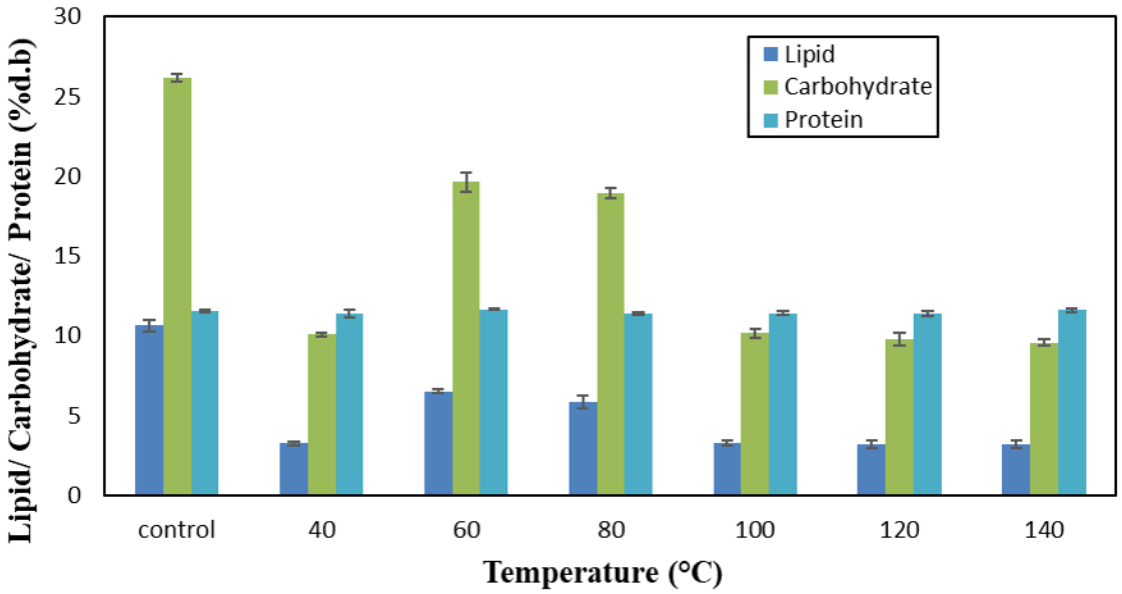

Figure 2.9 Biochemical composition (lipid, carbohydrate, and protein) of microalgae *Chlorella* dried at drying temperatures of 40, 60, 80, 100, 120, and 140° C and freeze-dried *Chlorella*. Drying temperatures of 60 and 80° C, best-preserved carbohydrate and lipid content of dried samples.

2.2.2.4 Biomass Surface Structure

Figure 2.10 shows the SEM images of microalgae dried at 40, 80, and 100° C drying temperatures. It seems that at 80° C cells have remained intact. However, at 140° C, more shrinkage has occurred in the cells. On the other hand, drying at 40° C resulted in more cracks at the material surface. Based on the SEM results, it seems that both very low and high temperatures adversely affect the cell structure. It seems that drying at medium temperatures (80° C) maintains the cell structure.

(a)

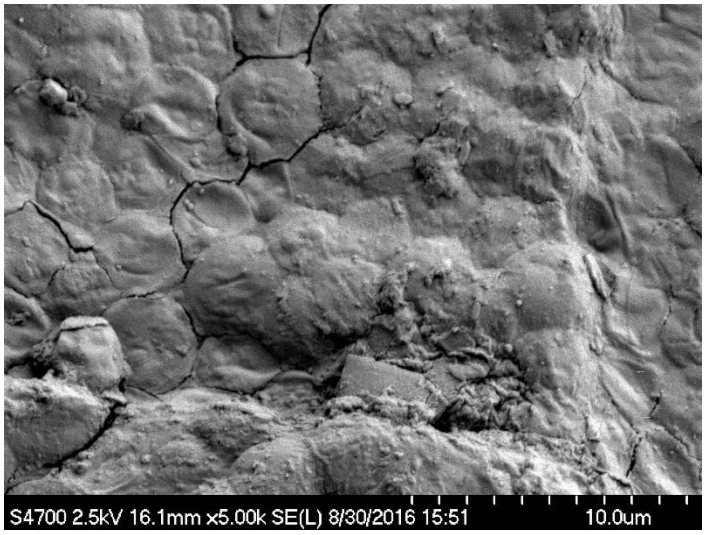

(b)

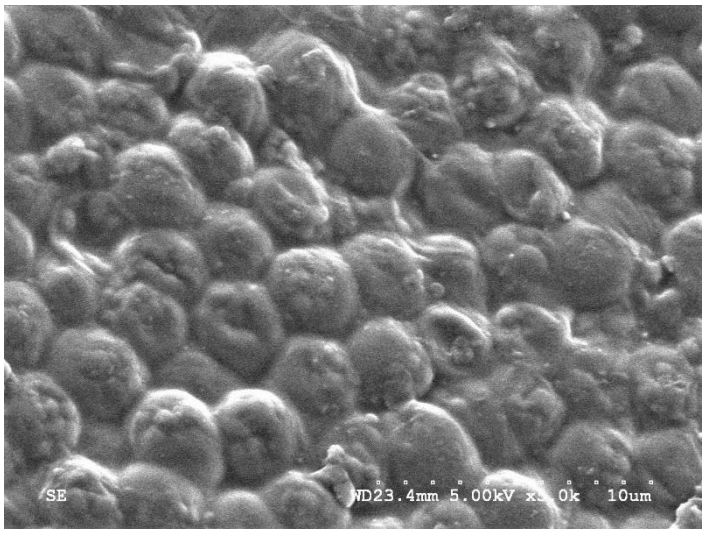

(c)

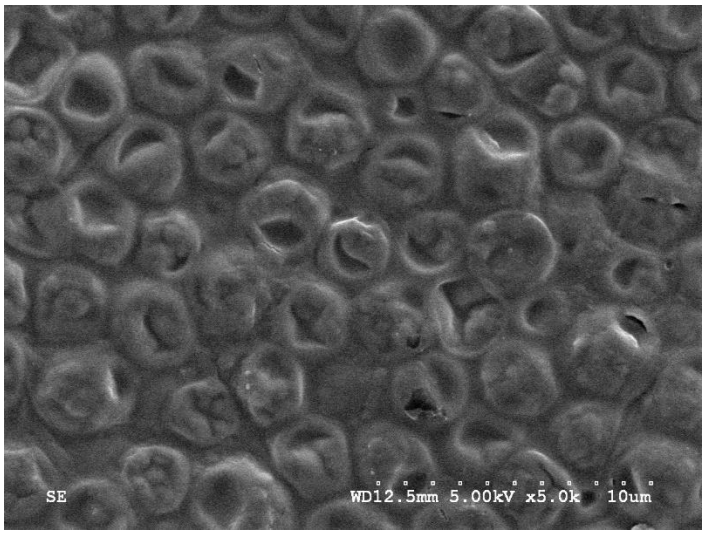

Figure 2.10 SEM images of microalgae *Chlorella* dried at different temperatures (a) 40° C (b) 80° C (c) 140° C. In the figure a and c, the cracks and shrinkage are evident in the biomass structure, respectively. Drying at 80° C, the best preserved microalgal cell structure.

2.3 Summary

At all drying temperatures in the range of 40-140^{o} C, *Chlorella* drying happened at a falling rate, with no constant rate period observed. This suggests that diffusion was the controlling mechanism during drying. The small values obtained for the effective diffusivity in this chapter corroborated the slow drying rates. Page equation best fitted to the drying rate data among other empirical models. The surface color measurement and biochemical composition showed that drying at medium temperatures (60-80^{o} C) preserved microalgae characteristics best, compared to drying at low temperature (40^{o} C) or at a higher temperature (100-140^{o} C). Both low and high drying temperatures had adverse effects on lipid, carbohydrate, and surface color (darkness, yellowness) of *Chlorella*. SEM results also confirmed that medium temperatures are suitable for *Chlorella* drying. The structure of the cells, when dried at 80^{o} C, was best preserved. The long drying time at 40^{o} C might result in enzymatic and non-enzymatic reactions, which in turn cause dark pigment formation and loss of essential nutrients such as amino acids [42].

Chapter 3: Co-Pelletization Mechanism of Microalgae *Chlorella vulgaris* and Pine Sawdust

Handling, storage, and transportation of dried microalgae are challenging due to its low bulk density. In this chapter, the pelletization of pure and blends of microalgae *Chlorella vulgaris* and sawdust is studied. The blends of *Chlorella vulgaris* and pine sawdust at 10% moisture content and blending proportions of 0, 25, 50, 75%, and 100% are subjected to compaction forces. The impact of densification temperature at three levels of 50, 75, and 100° C on the compression mechanism is analyzed. The chapter presents experimental data on the required energy for forming pellets in the die followed by expelling the pellet from the die.

3.1 Materials and Methods

3.1.1 Sample Preparation

Experiments in Chapter 2 indicated that drying at 80° C preserves microalgae quality to the greatest extent. Microalgae *Chlorella vulgaris* provided by Algae Testbed Public-Private Partnership (ATP^3) (Arizona, U.S.) were dried in a convective air dryer at 80° C in thin-layer drying mode to a final moisture content (w.b.) of 10% (drying experiment was described in detail in Chapter 2). After cooling in lab air, the dried biomass was ground to fine powder, vacuum packed and stored at 4° C until pelletization.

Pine sawdust was supplied by Fiberco Inc. (North Vancouver, BC, Canada). The material was reduced in size by a hammer mill (Glen mills Inc., USA; Model 10HMBL) using a screen opening of 3.2 mm (1/8 in). The ground sawdust was remoistened to 10% by adding the required amount of distilled water. The prepared sample was stored in plastic bags at 4˚ C until use [76].

Sawdust was blended with dried microalgae at the mass proportions of 0, 25, 50, 75, and 100%. Zero percent was pure microalgae, 100% was pure sawdust. The mixed samples were stored in glass containers at 4° C until pelletization. Figure 3.1 shows sawdust and microalgae particles at 10% moisture content.

The average surface-weighted diameter of pine sawdust and microalgae particles in this study was measured using the laser diffraction method and were 603±38 and 191±7 μm, respectively [96]. Sawdust particles were almost 3 times larger than microalgae particles. The particle size distribution of sawdust and microalgae are shown in Figure 3.2. In addition, the

porosity between microalgae particles and sawdust particles was measured using pycnometer and was 55% and 86%, respectively.

Figure 3.1 Pine sawdust particles (left) and microalgae particles (right) at 10% wet basis moisture content. The average diameter of sawdust particles was almost 3 times larger than that of microalgae particles.

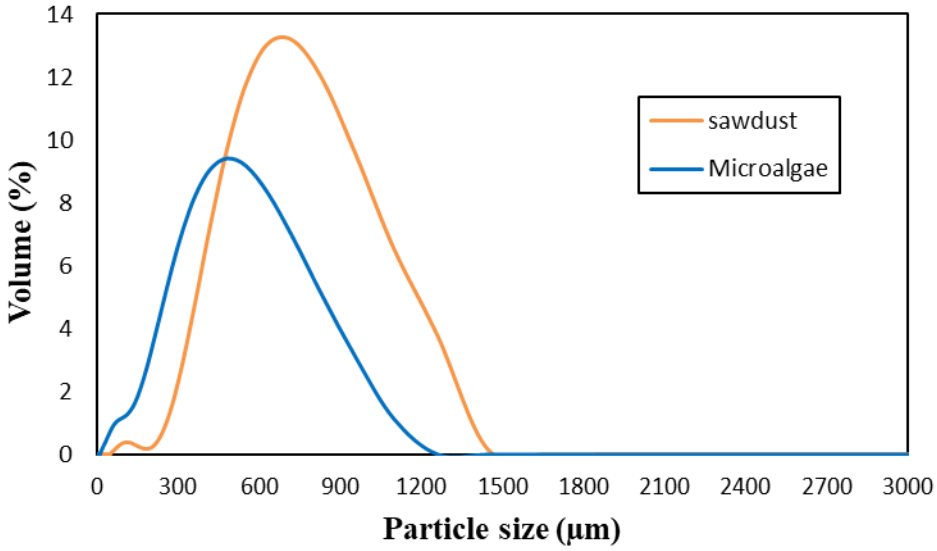

Figure 3.2 Particle size distribution of microalgae *Chlorella vulgaris* and sawdust measured using laser diffraction method. The sawdust surface average diameter was almost 3 times larger than microalgae particles.

3.1.2 Raw Biomass Characteristics

The characteristics of the two raw materials are presented in Table 3.1. Chemical composition of microalgae *Chlorella vulgaris*, proximate and ultimate analysis and calorific values of both materials were determined based on the methods described in Chapter 2.

For pine sawdust samples, chemical analysis was carried out according to Klason method in the Forestry Department [63]. In Klason analysis, acid breaks the biomass into sugar monomers and lignin, then the hydrolysate is analyzed to determine, cellulose, hemicellulose, and lignin content. The glucose is accounted for cellulose, other sugars indicate hemicellulose, and lignin consists of soluble and insoluble lignin, which can be measured separately. In the first step, the sawdust sample was ground using a 40-mesh screen (0.42 mm). Then the sample was oven dried. 0.2 g of dry biomass was poured into a clean Klason cup, the weight of cup was also recorded. To start the hydrolysis, 3 mL of 72% (w/w) sulfuric acid was added to the cup and the contents were stirred every 10 min for 2 hours of reaction time. The 113 mL of distilled water was added to the cup and the solution was filtered several times. Then, the bottle containing the hydrolyzed sample was sealed and autoclaved at 121° C for 60 min. The autoclaved sample was cooled at room temperature and was filtered to separate acid-insoluble lignin from acid soluble lignin and sugars. The residue left from filtration was dried in an oven for 2 hours, cooled in a desiccator, and weighed to determine acid-insoluble lignin. 10 mL of filtrate was used for sugar and acid-soluble lignin analysis. The absorbance of the solution was measured using a spectrophotometer at 280 nm, and the acid-soluble lignin was calculated by applying a dilution factor. Sugars were analyzed using HPLC and by having the data for standard solutions [63].

To determine the tapped bulk density of samples, a measured mass of the sample was poured into a 10 mL graduated cylinder. After dropping the cylinder from a height of 100 mm twenty times the tapped volume was recorded. The tapped density was calculated as the ratio of mass over volume [96].

Table 3.1 Properties of raw samples of *Chlorella vulgaris* and pine sawdust

Analysis		*Chlorella vulgaris*	Pine sawdust
Elemental analysis (% dry basis)	C	59.17±0.33	48.02±0.03
	O	28.44±0.31	45.85±0.05
	H	8.20±0.03	6.14±0.07
	N	1.85±0.01	--- [(a)]
	S	0.26±0.01	---[(a)]
Proximate analysis (% dry basis)	Moisture (%wet basis)	10.15±0.58	9.85±0.36
	Ash	2.19±0.16	0.086±0.01
	Volatile matter	83.08±3.02	87.68±0.25
	Fixed carbon	14.73±1.84	11.93±0.45
Chemical analysis (% dry basis)	Lipid	10.63±0.36	---[(a)]
	Protein	11.56±0.06	---[(a)]
	Carbohydrate	26.18±0.24	---[(a)]
	Cellulose	---[(a)]	41.81±0.43
	Hemicellulose	---[(a)]	27.48±0.87
	Lignin	---[(a)]	25.12±0.36
HHV (MJ kg^{-1})		27.29±0.69	19.46±0.04
Tapped bulk density (kg/m^3)		646.83±12.34	180.78±2.35

(a) Not measured

3.1.3 Pelletization

A single pelletizer machine was used to produce single pellets. The equipment (Figure 3.3) consisted of a piston 6.30 mm in diameter and 120 mm in length and a cylinder with 6.35 mm internal diameter and 90 mm in length. The assembly was placed under the crosshead of a mechanical testing machine (Measurement Technology Inc. (MTI) model, Rosewell, GA). The crosshead was equipped with strain gages to measure the force and the piston was pushed down in the cylinder [63]. The cylinder was wrapped with a heating element covered by an insulating tape. Two T-type thermocouples were placed on the cylinder wall and were connected to a temperature controller [97]. During the compression, the bottom of the cylinder was blocked by a removable block, and the block was removed after the completion of compression cycle and the start of the expulsion of the pellet from the cylinder.

Prior to each test, the cylinder was heated to the desired temperature (50, 75, or 100° C) and the crosshead of the MTI was moved manually to align the piston and the cylinder. The pre-

heated cylinder was loaded with the prepared sample so that the cylinder hole was full. The biomass was compressed up to the pre-set force load (2500 or 3500 N corresponding to 79.73 and 111.62 MPa compression pressure) with the downward displacement speed of 6.67 mm/min. The pellet was held for 30 s (relaxation time) to minimize the spring-back effect [98]. The pelleted biomass was removed from the cylinder by moving crosshead downward at a speed of 12 mm/min. During this expulsion phase, the spacer was removed. The resulting pellet was cooled at room temperature and was stored in a sealed glass bottle for further analysis.

A full factorial design experiment was designed for three levels of temperature, two levels of force, and five levels of sawdust and microalgae blends. At least six replicates of pellets were produced at each condition.

The force-displacement data was recorded during the entire compression and expulsion of the pellet. The energy consumption was obtained by integrating the area under the force-displacement curves. The total energy required to produce pellets was energy required to compress biomass plus the energy required to extrude the pellet from the die. The specific energy is the total energy divided by the mass of the pellet.

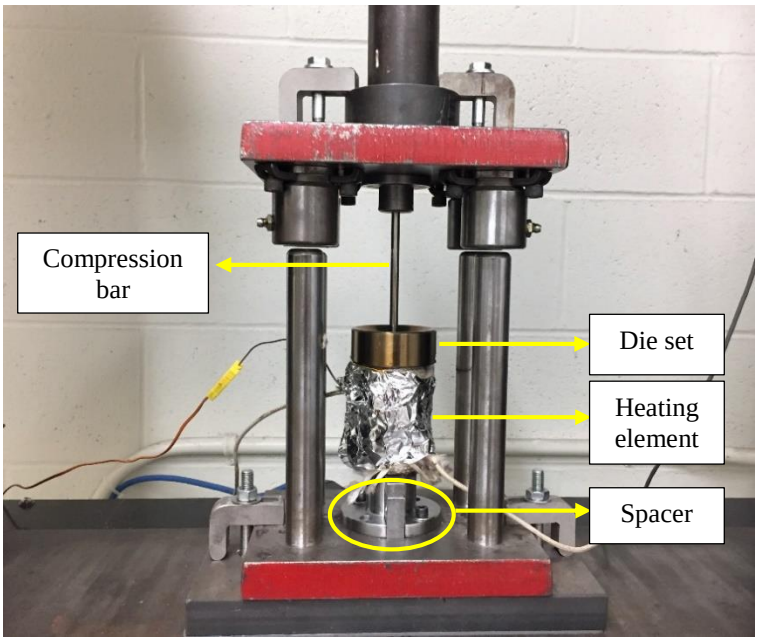

Figure 3.3 The picture of piston-cylinder set up in the pelletizing machine

3.1.4 SEM Analysis

Scanning electron microscopy (SEM) was used to understand the binding mechanism of the pellets by analyzing the cross-section of each pellet. For SEM tests, the sample was mounted on an aluminum stub using a double-sided tape. The sample was then coated with gold under vacuum. All the images were taken at 2.5 to 5 kV accelerating voltage by using a field emission scanning electron microscope (Model S4700, Hitachi, Japan).

3.1.5 Statistics

Pelletization tests and material characterizations were repeated at least three times. The repetitions were performed independently over several days to make sure that data are reproducible. The data were presented as mean values and their dispersion in terms of standard deviation. The calculated standard deviation indicated the level of uncertainty in the experiments. The results were statistically evaluated using analysis of variance (ANOVA) with $\alpha = 0.05$.

3.2 Results and Discussion

3.2.1 Densification Mechanism

Figure 3.4 and Figure 3.5 show the compression and expulsion graph at 3500 N maximum force and 75° C densification temperature, respectively. Based on Figure 3.4, the compression of pure *Chlorella* consisted of two regions, particles' rearrangement and elastic-plastic deformation. By applying force until about 200 N microalgae particles completed their rearrangement phase (0-27 mm, first stage). By applying further force, the particles experienced a plastic-elastic deformation (second stage), and finally, by further increasing the force to the maximum set point of 3500 N the pellet density was increased [62,99,100].

The major pore volume reduction happens without a change in particles' properties during the initial rearrangement of particles. The particle packing in the first stage is due to small and large particle rearrangements [62]. As the applied force increases, the particles are forced against each other to increase inter-particle contact. Physical factors such as capillary forces in movable liquid phase, solid bridges, and mechanical interlocking are identified as possible effective forces for a pellet formation [100]. Although these mechanisms contribute to initiating

the bonding, solid bridges have been proposed responsible for the final strength of the pellets [65]. The solid bridges are developed by chemical reactions, solidification, hardening of binders, hardening of melted substances, and crystallization of dissolved materials. The attraction between particles due to Van der Waals, electrostatic, and magnetic forces are also effective in forming pellets.

It seems that denatured proteins and gelatinized starch have improved bonding among particles. When protein is exposed to heat during pelletization, it loses its 3-D folded structure due to breakage of weak hydrogen bonds present in its molecule. As a result of unfolding (denaturation), functional groups of proteins like hydroxyl, carboxyl, and amine were more available to form new hydrogen bonds with wood and water molecules present as moisture. Moreover, heating during pelletization resulted in the loss of semi-crystalline starch granules' structure in the presence of moisture. The gelatinized starch formed a new network that held water through strong hydrogen bonds [62,65,99,100].

At 25 and 50% sawdust blend, particles reached to the end of rearrangement region and experienced plastic-elastic deformation. As shown in Figure 3.4, the rearrangement phase for 25 and 50% sawdust fraction continued until 1100 and 1300 N forces, respectively. However, it seems that at higher sawdust fraction, rearrangement of particles happened during the entire compression phase.

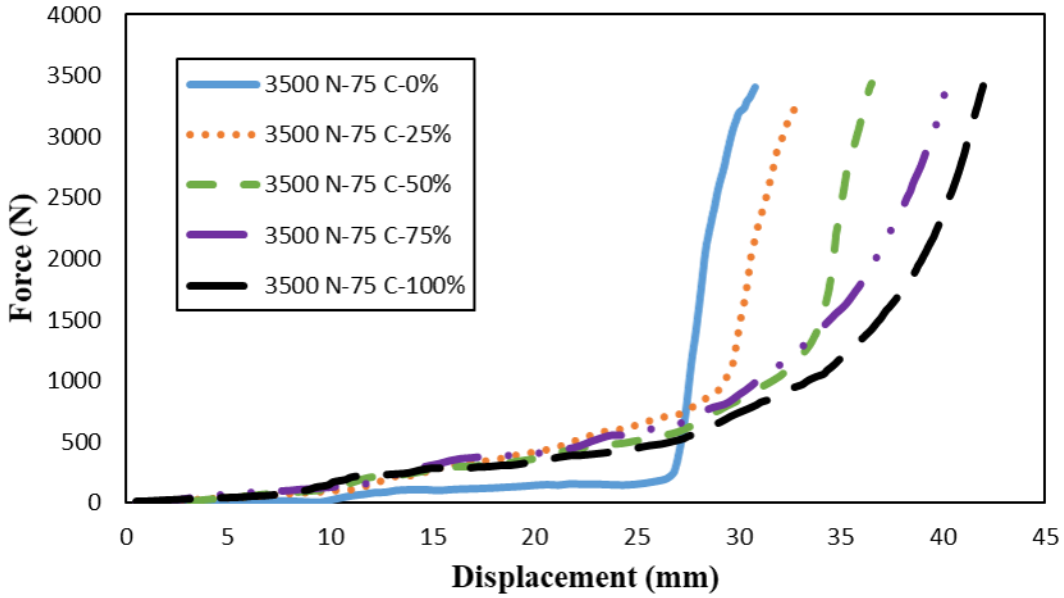

Figure 3.4 Force-displacement graph for compression at maximum pelletization force of 3500 N and temperature of 75° C for pure *Chlorella*, sawdust fraction of 25, 50, 75%, and pure sawdust. Complete rearrangement happened for pure microalgae and sawdust fractions of 25, and 50%.

(a)

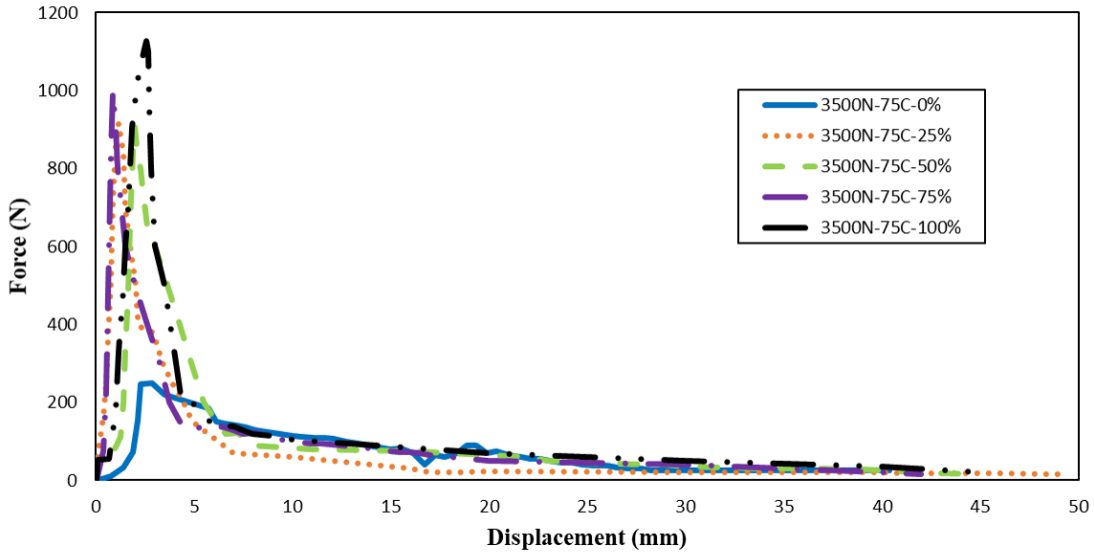

(b)

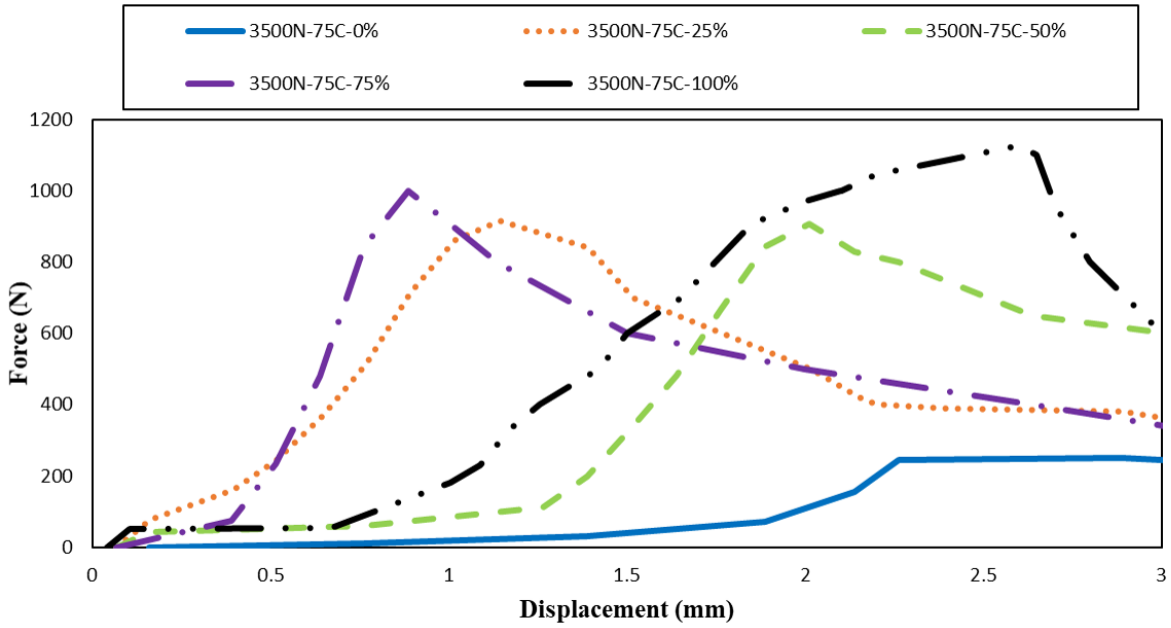

Figure 3.5 Force-displacement graph for expulsion at maximum pelletization force of 3500 N and temperature of 75° C for pure *Chlorella* (0%), sawdust fraction of 25, 50, 75%, and pure sawdust. (a) The graph for the entire expulsion period (b) The graph until the maximum force to overcome friction between the pellet and die wall.

Figure 3.4 shows that microalgae had the shortest displacement in rearrangement period compared to other biomass blends and pure sawdust. In addition, in the rearrangement region, the slope of the pure microalgae curve was smaller than other biomass.

The difference in pelletization behavior of microalgae and sawdust arises from the difference in both the physical and chemical properties of the two biomass. The small microalgae particles, which had a more homogenous structure, showed no resistance to rearrangement. In the rearrangement phase, the particles were packed closely toward each other while the force was increased by just a small amount. Further compression of microalgae particles resisted displacement since there was no more void volume for rearrangement. The fibrous structure of sawdust and its high void volume (86% porosity) led to a gradual resistance against packing and rearrangement of particles. In other words, the more homogenous particle shape of microalgae and their small diameter were the cause for a smoother movement toward each other in

rearrangement phase. Since most of the void space between microalgae particles have been filled in the first compression phase, in the second stage microalgae particles experienced compression without significant displacement. It seems that in the second compression phase, the particles' shape has changed under pressure (circled in Figure 3.7.a) and chemical bonds have been formed. In contrary, the irregular shape of sawdust particles, their higher roughness, and larger particle size was the reason for not having a complete particles' rearrangement in the first phase. Alternatively, sawdust particles were moving toward each other for the entire compression phase. The difference between the particles' structure of microalgae and sawdust is understood in Figure 3.6.

Hemicellulose, lignin, and the disordered part of cellulose in sawdust absorb water, soften, and experience glass transition [101]. Glass transition is of great importance because it affects the strength of structures containing wood. Glass transition usually occurs over a temperature range and reporting a sharp temperature for this phenomenon is not correct [101]. At 10% moisture content (used in this research), the glass transition of cellulose started at temperatures >50° C. The glass transition of hemicellulose and lignin at 10% moisture content starts at 100° C and 110° C, respectively [101]. It seems that at the temperature range of this study, glass transition of cellulose and hemicellulose have affected pelletization of sawdust. However, in the studied temperature range, lignin softening did not occur. It seems that the pelletization pressure and heat have been adequate for activating natural binders in microalgae (protein and starch) but not for activating lignin in sawdust. Since lignin has the major role in making strong bonds during pelletization of woody biomass [58], it is expected that sawdust pellets show weaker properties compared to microalgae-dominant pellets.

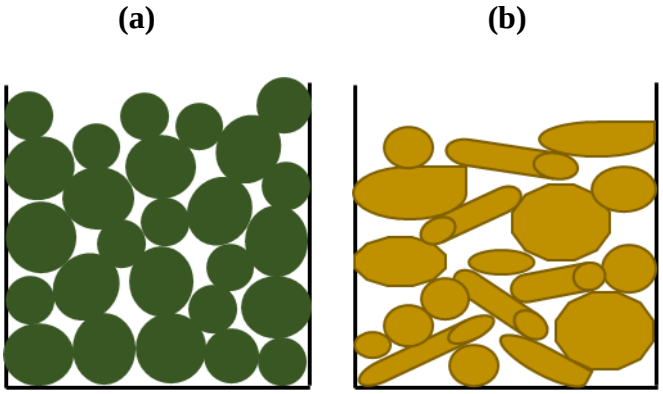

Figure 3.6 A conceptual representation of the particle arrangement in the die. (a) Microalgae and (b) sawdust particles in the die. It should be noted that the picture does not show the real particles' shape and particle size distribution. The figure shows a possible configuration of particles in the die. Microalgae particles had a smaller average diameter (0.191 mm) compared to sawdust particles (0.603 mm). The porosity of microalgae and sawdust particles was 55% and 86%, respectively.

The difference between pellets' structure was confirmed by SEM images. Figure 3.7 shows the SEM images of pellets' cross-section consisting of the different fraction of *Chlorella* and sawdust. In pure sawdust pellet, the more fibrous structure was evident (Figure 3.7.d). As it is evident in Figure 3.7.a, some of the *Chlorella* cells have lost their round structure under pressure. This fact is more realized when Figure 3.7.a is compared with Figure 2.10.b, which demonstrates round shape of the microalgal cell after drying at 80° C. It seems that pressure has resulted in pressing the cells and squeezing the cells' ingredients.

(a) **(b)**

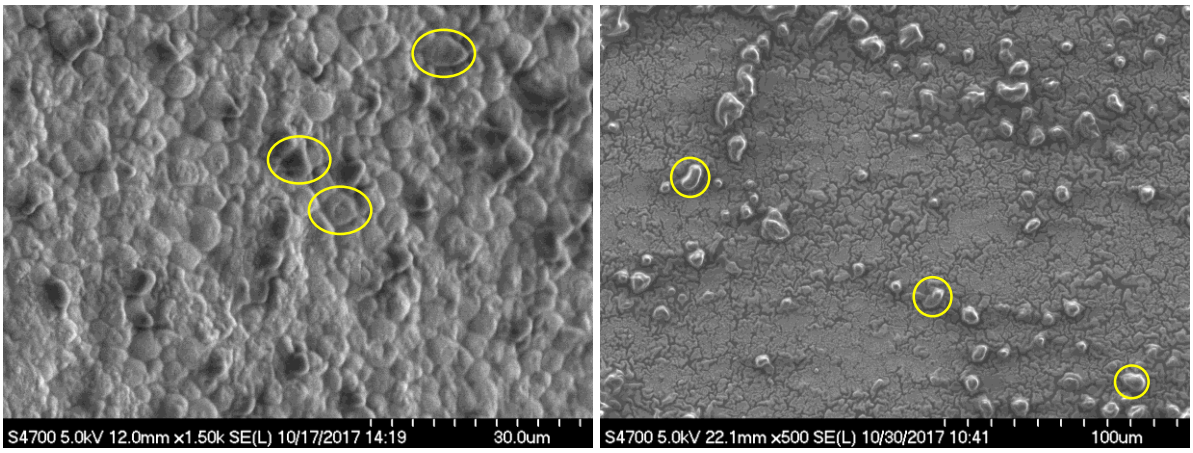

(c) **(d)**

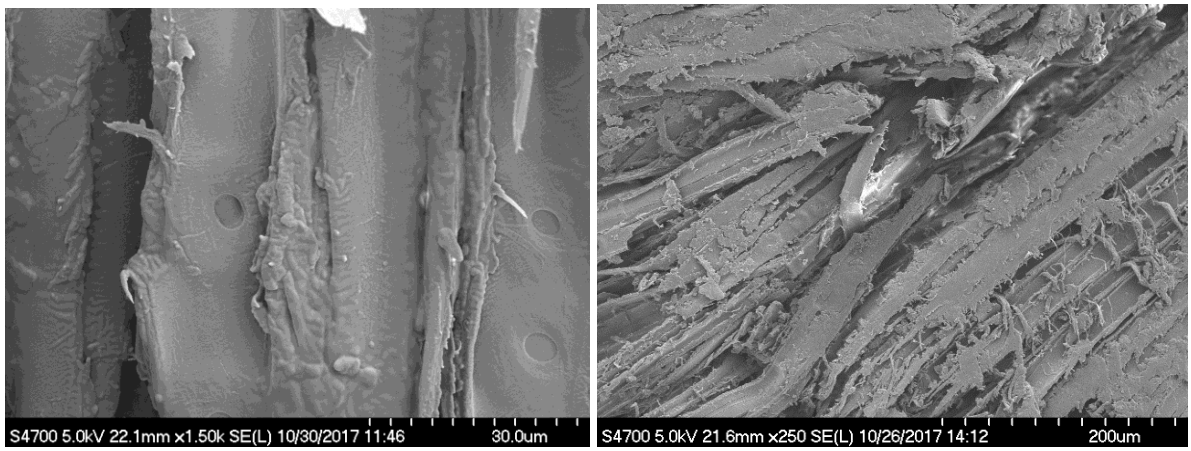

Figure 3.7 SEM images of a cross-section of pellets. (a) pure *Chlorella* at x1500 magnification, (b) 25% at x500 magnification sawdust, (c) 50% sawdust at x1500 magnification, (d) pure sawdust at x250 magnification.

The expulsion test was similar to the compression test with the only difference that the spacer was removed during the expulsion of the pellet from the die so that the pellet was easily pushed out from the die. Based on Figure 3.5.a, in expulsion tests, force increased to a maximum amount and then gradually decreased to the end of expulsion phase, where the whole length of the pellet was completely out of the die. It seems that the force gradually decreases when the pellets start to flow in the die during the expulsion.

There is a friction between the pellet and the die wall and the expulsion force applied by the machine should be high enough to overcome this friction and move the pellet forward in the die. Figure 3.5.b shows that the force of 250 N was required to overcome the static friction between the inner wall of the die and the pure *Chlorella* pellet in the expulsion experiments. The amount of this force for displacement of pellets for 25, 50, 75% sawdust fraction, and pure sawdust pellets were 915, 906, 1000, and 1126 N, respectively. The force for movement of pellets in the die in expulsion phase for pure *Chlorella* was significantly lower than other fractions of biomass ($p \leq 0.05$). The reason for the smaller amount of force to initiate the flow of pure microalgae pellet in the die might be the oil that has squeezed out of the cells during compaction. It is possible that oil lubricated the inner wall of the die that has been in contact with microalgae powder during compaction. The amount of force to overcome friction at other pelletization temperature and different fractions of biomass are listed in Table 3.2.

Table 3.2 The force to overcome friction for the expulsion of pellets from die. The results are based on at least 6 produced pellets. The force is significantly lower for pure microalgae compared to other fractions.

Pelletization force (N)	Pelletization temperature (°C)	Fraction of sawdust (%)	Expulsion force (N)
3500	50	0	387±35
		25	980±132
		50	914±76
		75	953±67
		100	995±105
	75	0	246±12
		25	969±54
		50	910±54
		75	973±71
		100	1024±103
	100	0	236±20
		25	970±77
		50	913±77
		75	970±73
		100	1022±95

3.2.2 The Effect of Temperature on Densification Mechanism

Figure 3.8 and Figure 3.9 show the compression graphs for the maximum pelletization force of 3500 N for two pelletization temperatures 50 and 100° C. From Figure 3.9, it is understood that at the lowest temperature studied (50° C) the complete rearrangement happened merely for pure microalgae. At the higher temperature of 75° C, a complete rearrangement was also observed for 25% and 50% fraction of sawdust (Figure 3.4). By comparing Figure 3.4 and Figure 3.8, the difference in behavior of 50% and 75% fraction at two temperatures of 50 and 75° C was evident. At 50° C neither of 50% and 75% fraction experienced a complete rearrangement, the curves were very close to each other. However, by increasing the temperature to 75° C, the compression behavior of 50% fraction varied and the space between 50% and 75% curves got bigger. Figure 3.9 shows that at the temperature of 100° C, the biomass with the fraction of 75% also experienced a complete rearrangement in compression tests. Therefore, at 100° C, the curves for 50 and 75% fraction were similar.

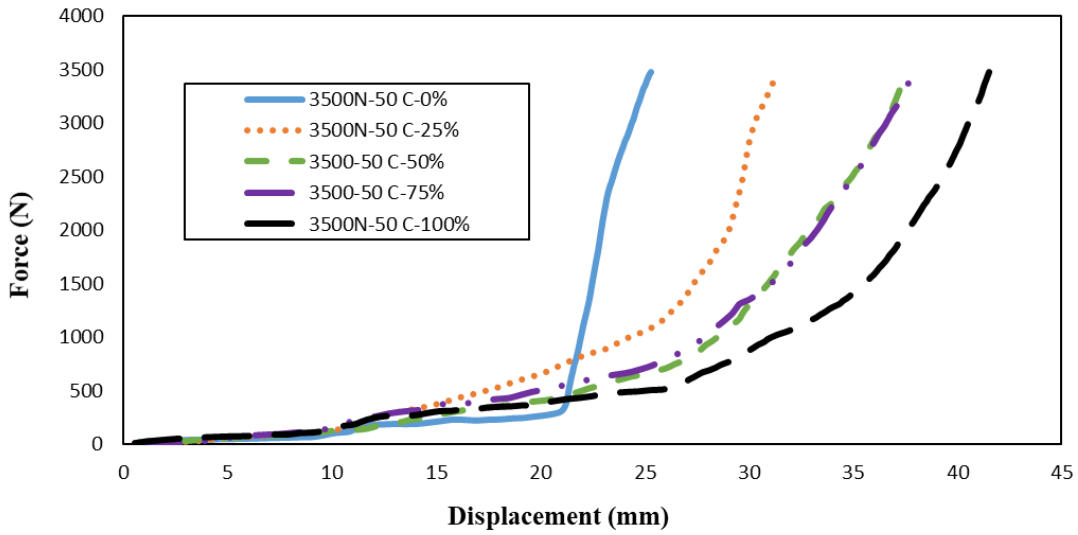

Figure 3.8 Force-displacement graph for compression at maximum pelletization force of 3500 N and temperature of 50° C for pure *Chlorella* (0%), sawdust fraction of 25, 50, 75%, and pure sawdust. Complete rearrangement of particles only happened for pure microalgae.

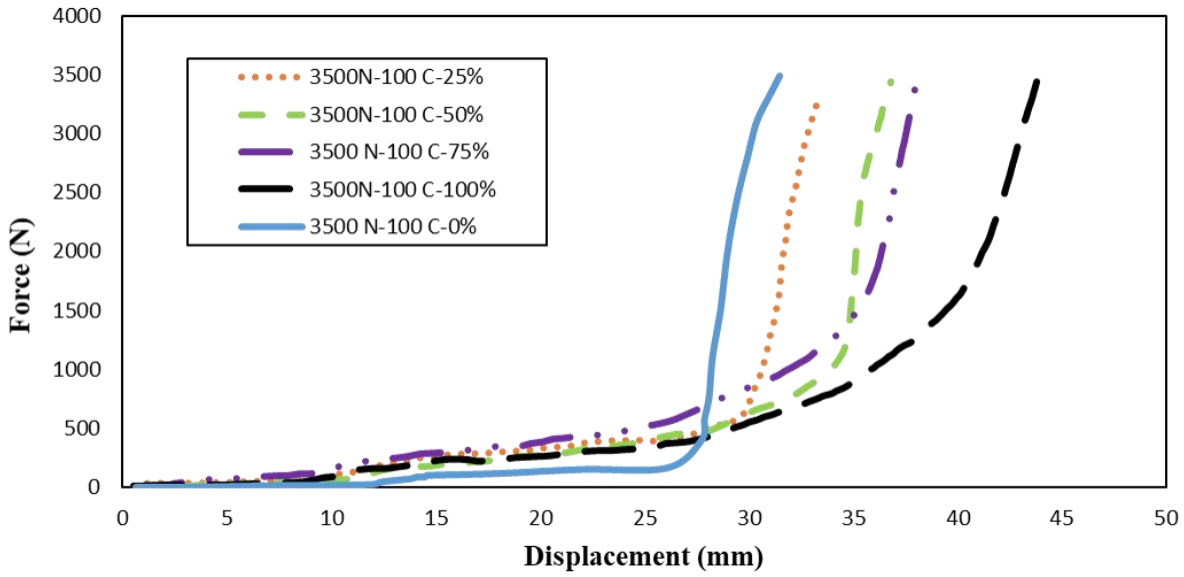

Figure 3.9 Force-displacement graph for compression at maximum pelletization force of 3500 N and temperature of 100° C for pure *Chlorella* (0%), sawdust fraction of 25, 50, 75%, and pure sawdust. Complete rearrangement of particles happened for pure microalgae and sawdust fractions of 25, 50, and 75%.

To further understand the effect of temperature, the compression behavior of biomass at each fraction is shown at three temperatures (Figure 3.10 to Figure 3.14).

For pure microalgae, a complete rearrangement of particles was obvious at 50° C (Figure 3.10). By increasing the temperature further to 100° C, no significant change was observed in the pure microalgae compression mechanism (Figure 3.10). It seems that at 75° C, the natural binders had the maximum bonding effect and further increasing the temperature did not influence their activity.

For pure sawdust (Figure 3.14) a complete rearrangement of particles was not observed. No significant difference between the compression mechanism of pure sawdust at temperatures of 50, 75, and 100° C was observed. The insensitivity of pure sawdust to changing the temperature from 50 to 100° C might be due to the lack of lignin melt prior to reaching about 110° C. As a result, increasing temperature in the range of 50-100° C did not affect compression mechanism of pure sawdust.

Figure 3.11 demonstrates that at 25% sawdust fraction, increasing temperature from 50 to 75° C resulted in a complete rearrangement of particles. However, the behaviors of 75 and 100° C were almost the same at 25% fraction. Similar to 25% fraction, at 50% fraction of sawdust, the

complete rearrangement of particles was observed at 75° C and further increasing the temperature to 100° C did not lead to a change in compression mechanism (Figure 3.12). Interestingly, for 75% fraction of sawdust, increasing the temperature to 75° C did not have an impact on densification mechanism, however, increasing to 100° C resulted in complete particles' rearrangement (Figure 3.13).

My results indicate that increasing the temperature from 50 to 75° C changed the compression mechanism of pellets mainly consisting of microalgae (25%, and 50% sawdust fraction). In other words, changing the temperature from 50 to 75° C did not affect the compression mechanism of pure sawdust and 75% fraction sawdust. On the other hand, increasing the temperature from 75 to 100° C only changed the compression mechanism of 75% fraction sawdust and not pellets dominated with microalgae. The difference in sensitivity of compression behavior to temperature change is related to biomass chemical composition and natural binders present in *Chlorella* and sawdust. It seems that increasing the temperature from 50 to 75° C has resulted in more activity of natural binders (starch gelatinization and protein denaturation) in microalgae, however further increasing the temperature to 100° C did not have an impact on the binders' activity. On the other hand, in the temperature range studied, increasing the temperature did not alter sawdust compaction mechanism. The reason might be that the main natural binder in sawdust, lignin, did not have a significant activity under the studied temperature range.

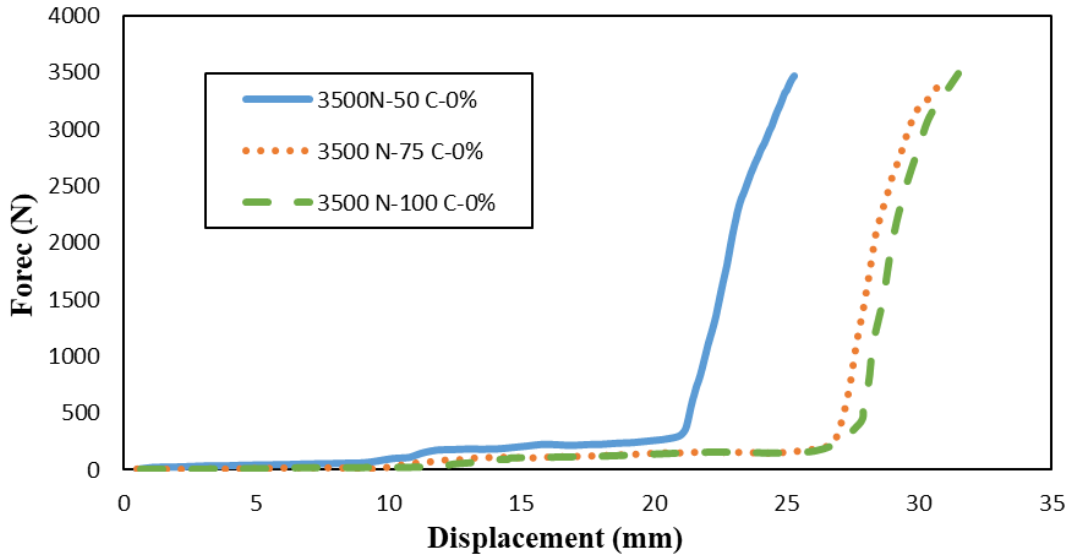

Figure 3.10 Force-displacement graph for compression at maximum pelletization force of 3500 N and different temperatures of 50, 75, and 100° C for pure *Chlorella* (0%). At all three temperatures, pellets experienced complete rearrangement of particles.

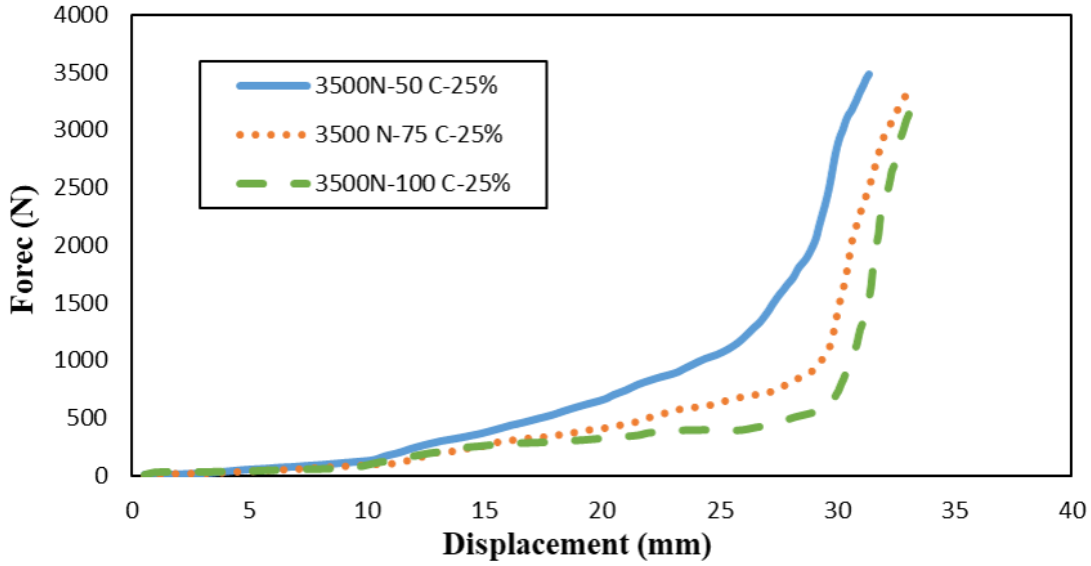

Figure 3.11 Force-displacement graph for compression at maximum pelletization force of 3500 N and different temperatures of 50, 75, and 100° C for 25% sawdust fraction. Increasing the temperature to 75° C resulted in a complete rearrangement of particles. The mechanism at 75 and 100° C were similar.

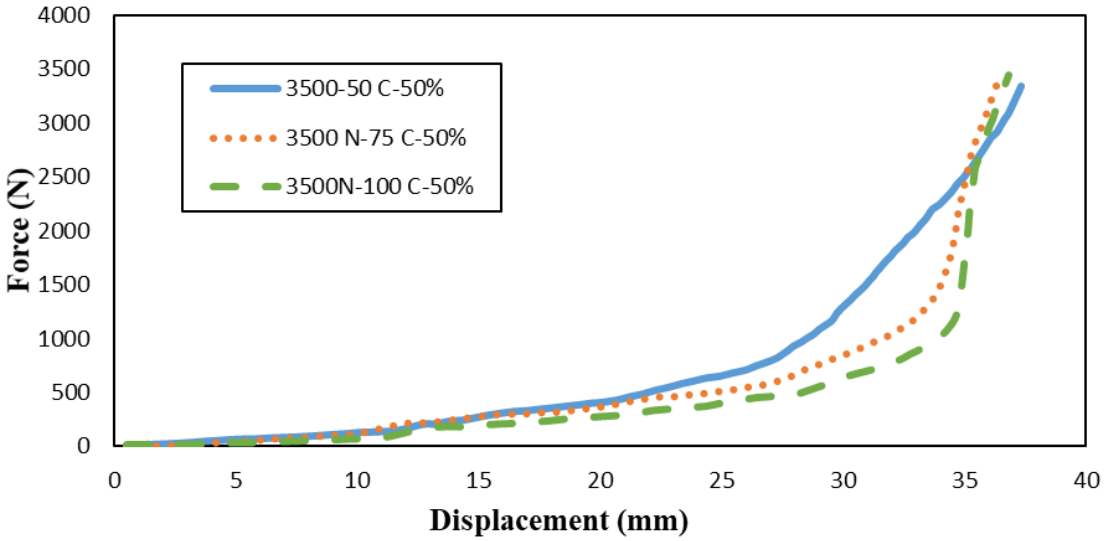

Figure 3.12 Force-displacement graph for compression at maximum pelletization force of 3500 N and different temperatures of 50, 75, and 100° C for 50% sawdust fraction. Increasing the temperature to 75° C resulted in a complete rearrangement of particles. The mechanism at 75 and 100° C were similar.

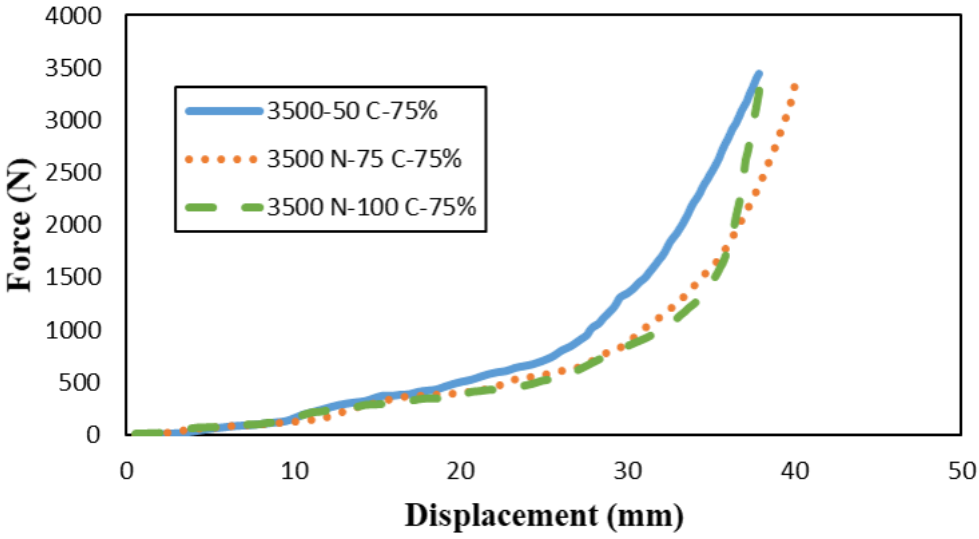

Figure 3.13 Force-displacement graph for compression at maximum pelletization force of 3500 N and different temperatures of 50, 75, and 100° C for 75% sawdust fraction. Increasing the temperature to 100° C resulted in a complete rearrangement of particles. The mechanism at 50 and 75° C were similar.

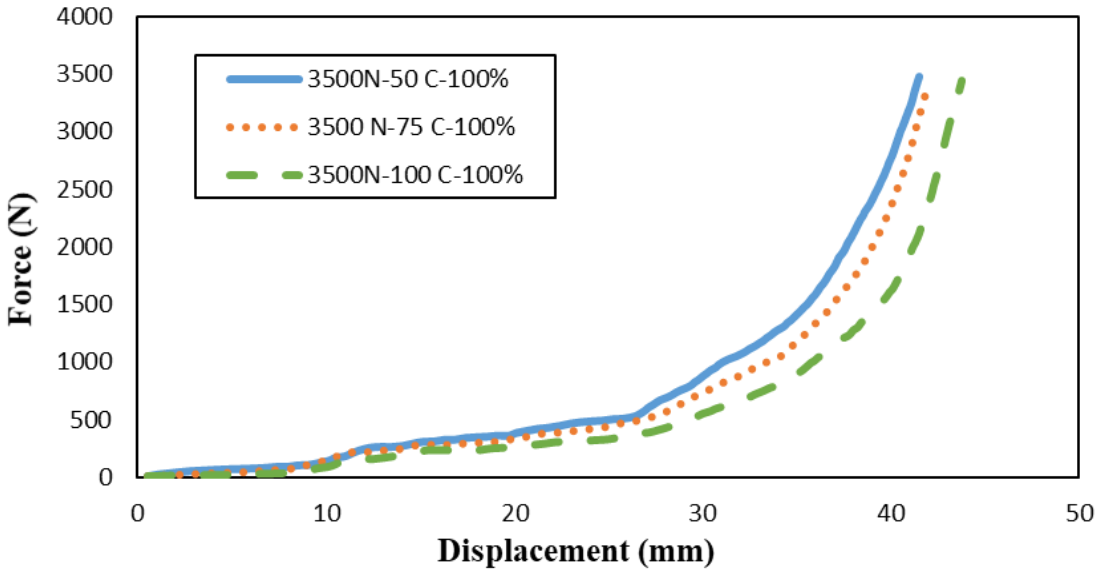

Figure 3.14 Force-displacement graph for compression at maximum pelletization force of 3500 N and different temperatures of 50, 75, and 100° C for pure sawdust. There was no significant difference between pelletization mechanism of sawdust at different temperatures. Increasing the temperature did not affect compaction mechanism.

3.2.3 Energy Consumption

The area under the curve indicates the energy input to form pellets. As shown in Figure 3.15.a, at all operating temperatures and forces by increasing the fraction of sawdust the compression energy increased significantly ($p \leq 0.05$). As an example, the compression energy for pure sawdust at 2500 N and 50° C was 4.8 times higher than the compression energy of pure *Chlorella* under the same conditions. The short displacement in rearrangement phase and the small slope in this stage led to a low compression energy for pure *Chlorella* compared to other biomass (based on Figure 3.4).

Increasing densification temperatures from 50 to 75° C resulted in a significant decrease ($p \leq 0.05$) in compression energy for pure algae and 25 and 50% sawdust blends. However, a significant change was not observed by further increasing the temperature from 75 to 100° C. For 75% sawdust blend and pure sawdust, increasing temperature did not have a significant impact on compression energy, at all ($p > 0.05$). This behavior was similar for both the 2500 and 3500 N force.

The extrusion energy for pure sawdust was significantly higher than other biomass blends and pure algae ($p \leq 0.05$) at all operating temperatures and forces (Figure 3.15.b). For example, at 75° C pelletization temperature and 2500 N maximum force, the extrusion energy of pure sawdust was 1.43 J/g, which was 4.3 times higher than pure *Chlorella*. Increasing temperature from 50 to 75° C caused a decrease in extrusion energy at all biomass blends other than pure sawdust ($p \leq 0.05$) (for both 2500 and 3500 N force).

Similar to compression energy, increasing the fraction of sawdust resulted in a significant rise in total densification energy ($p \leq 0.05$) (Figure 3.15.c). As an example, the total pelletization energy for pure algae, 25%, 50%, 75% blends, and pure sawdust at 75° C and 2500 N were 5.75± 0.38, 10.24± 1.09, 20.67± 1.50, 27.04± 1.67, and 33.63± 2.65 J/g, respectively. For pure microalgae and 25 and 50% sawdust blends, increasing the temperature from 50 to 75° C led to a significant decrease in total densification energy (at both pre-set forces) ($p \leq 0.05$), however, further raising the temperature to 100° C did not have a significant impact on total pelletization energy ($p > 0.05$) (Figure 3.15.c).

The cause for lower pelletization energy of blends containing microalgae could be the oil that squeezes out of the *Chlorella* cells during densification under pressure. It is possible that the oil acted as a lubricant enhancing the pellets' movement in the die and decreasing the densification energy [61,62,102]. Moreover, the denatured proteins and gelatinized starch in the mixed pellet structure enhanced hydrogen bonding and solid bridges among particles, resulting in the improvement of pellets' compactness and reduction of extrusion energy [61,62,102]. Microalgae particles were bound tightly because of going through a complete rearrangement and elastic-plastic deformation. Sawdust particles were not closely packed in pellets' structure. The fibrous structure of sawdust particles is another reason for their larger pelletization energy. In other words, more intertwined fibers on the surface of wood pellets compared to the flat and fine surface of pellets containing microalgae (can be observed in Figure 3.7) led to a higher friction between particles and particles and wall which in turn increased the compaction energy consumption [61,62,102].

(a)

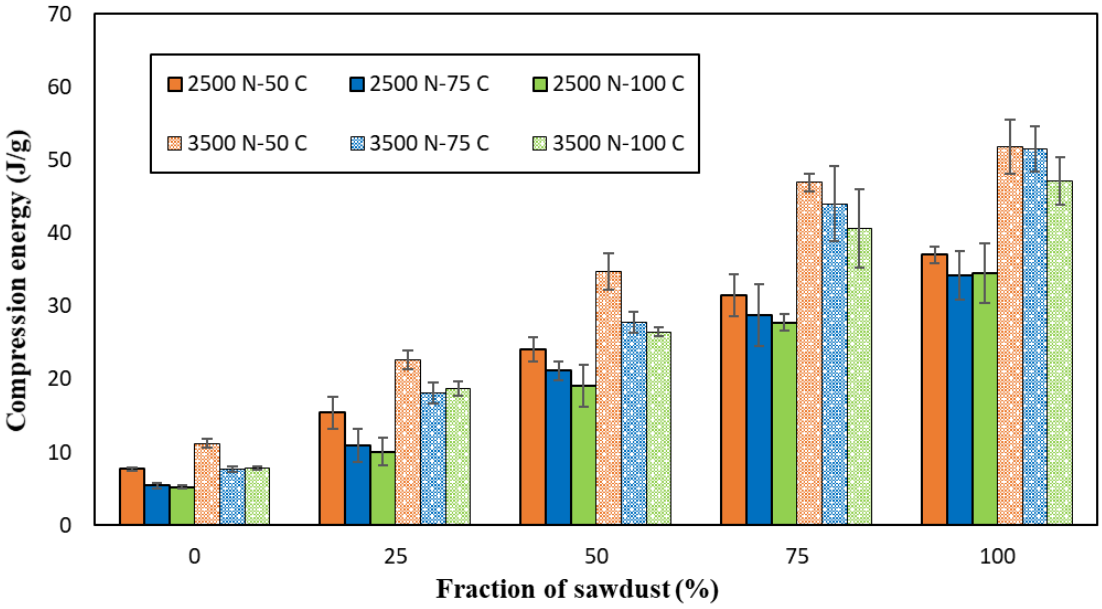
70
60
50
40
30
20
10
0
Compression energy (J/g)
2500 N-50 C
2500 N-75 C
2500 N-100 C
3500 N-50 C
3500 N-75 C
3500 N-100 C
0
25
50
75
100
Fraction of sawdust (%)

(b)

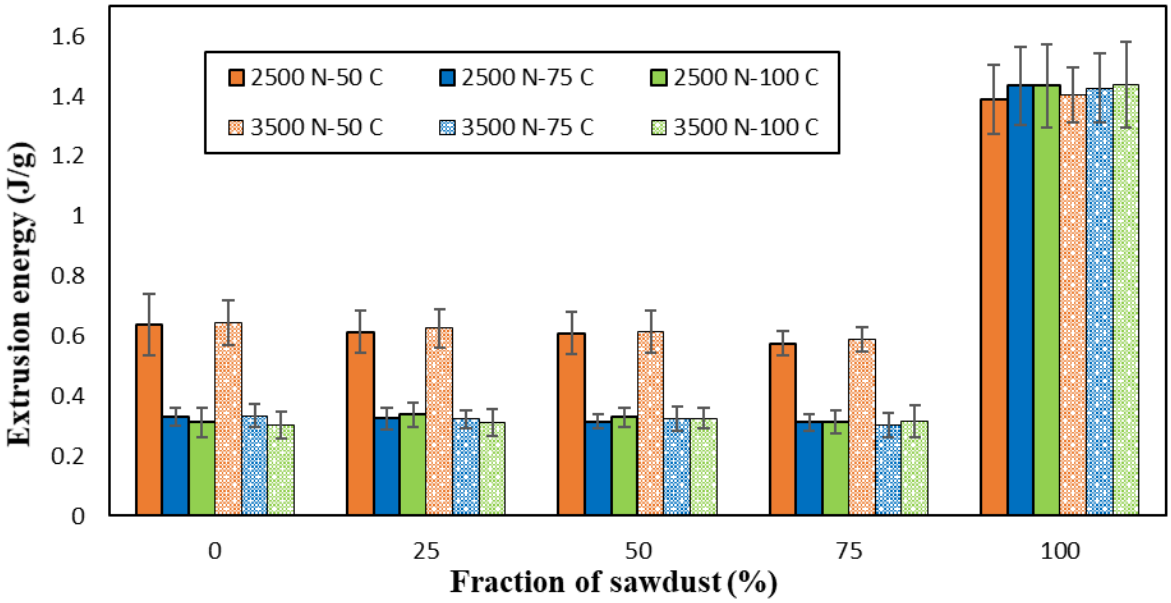
1.6
1.4
1.2
1
0.8
0.6
0.4
0.2
0
Extrusion energy (J/g)
2500 N-50 C
2500 N-75 C
2500 N-100 C
3500 N-50 C
3500 N-75 C
3500 N-100 C
0
25
50
75
100
Fraction of sawdust (%)

(c)

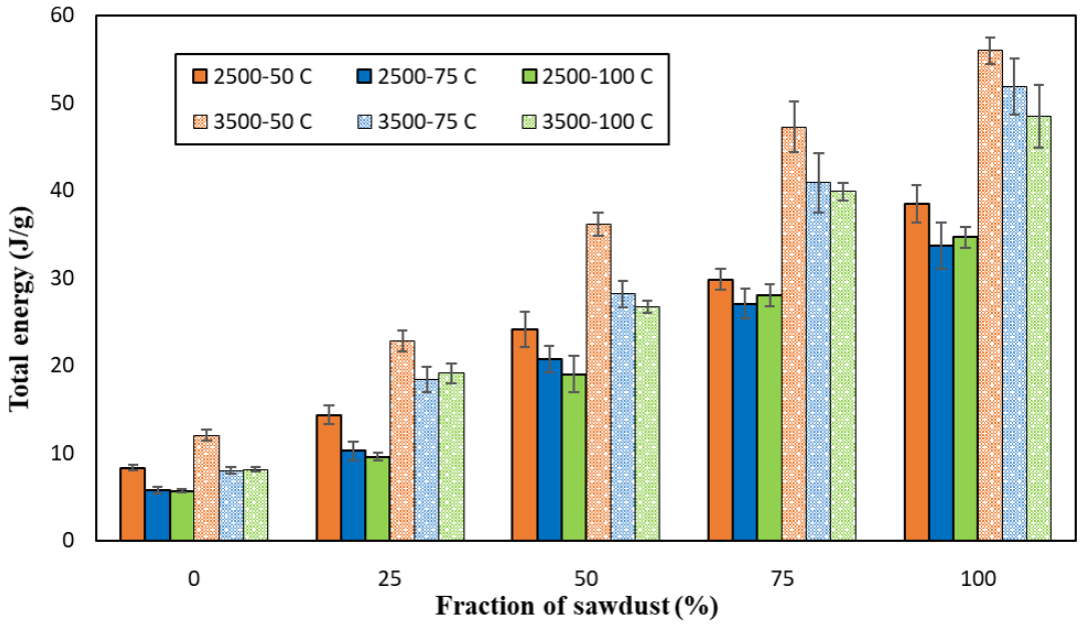

Figure 3.15 Energy consumption for densification of microalgae *Chlorella*/pine wood particles at two different forces of 2500 and 3500 N, temperatures of 50, 75, and 100° C, and five fractions of sawdust: 0, 25, 50, 75, and 100%. (a) compression energy, (b) extrusion energy, (c) total energy. The compression energy increased by increasing the fraction of sawdust (a). Extrusion energy of sawdust was significantly higher that other biomass blends and pure microalgae (b). The total densification energy increased by increasing the ratio of sawdust in the blend (c).

3.3 Summary

The experimental data showed the difference between densification behavior of pure microalgae *Chlorella*, pure pine sawdust, and blends of the two. For *Chlorella*, by increasing the force up to 200 N a substantial rearrangement of particles happened. Applying a higher force up to the maximum pre-set force helped to strengthen the bonds among particles. However, for sawdust, a continuous particles' rearrangement happened over the entire compression process. The smaller required force to overcome friction in the expulsion of pellets from the die, the smaller compression, expulsion, and total densification energy for pure microalgae compared to pure sawdust demonstrated easier compressibility of *Chlorella*. For instance, at 2500 N maximum force and 75° C densification temperature, the total densification energy for pure

Chlorella and pure pine sawdust were 5.75 and 33.63 kJ/kg, respectively. The lipid in microalgae *Chlorella*, which acts as a natural lubricant could explain the mentioned result.

Chapter 4: Characteristics of Microalgae *Chlorella vulgaris* and Pine Sawdust Pellets

The ultimate goal of densification is to produce pellets with improved durability and storage characteristics. This chapter presents pellets' properties like durability, density, porosity, moisture adsorption, and expansion of pellets after a 14-day period. The impact of temperature at three levels of 50, 75, and 100° C and the effect of maximum densification force at two levels of 2500 and 3500 N on pellets' mechanical properties were quantified.

4.1 Methods for Evaluation of Pellets Quality

4.1.1 Dimensions, Density, and Expansion

The diameter, length, and mass of each pellet were measured immediately after each experiment to calculate pellet density. The length and diameter of pellets were measured using a digital caliper with a precision of 0.001 mm (Mastercraft, Miami, FL, USA). An electronic balance (GR200, A&D Inc. Tokyo, Japan) with 0.1 mg precision was utilized to weigh pellets. Single pellet density ($\rho_b=m/V_b$) was calculated by assuming a cylindrical shape for the pellets and by having mass and dimensions of the pellet [103–107]. The length and diameter of the pellets were again measured after storing them for two weeks to determine expansion percentage in diametric and longitudinal directions.

4.1.2 Particle Density

A helium comparison pycnometer (Quantachrome Multipycnometer, Model No: MVP-D160-E, Quantachrome, Boyton Beach, FL, USA) was used to measure the particle density of pellets.

The unit had two chambers, the first one is 11.67 cm^3 volume reference cell, and the second one is the sample cell with the volume of 29.42 cm^3. Pressurized helium penetrated into the pores of material in the sample cell. The pycnometer measured the pressure difference between an empty cell and a cell with the same volume filled with the sample pellets. The volume of the sample's particles was calculated using the measured pressure difference and ideal gas law [96,108]. Particle density measurements were repeated at least three times per sample [100,109–111].

Particle density ($\rho_p=m/V_p$) was obtained by dividing mass by the particle's volume of sample. Interparticle porosity (ε_0) provides packing information of biomass particles and was determined by Equation 12 [76,97].

$$\varepsilon_0 = 1 - \frac{\rho_b}{\rho_p} \quad (12)$$

Where ε_0 is the porosity of a single pellet, ρ_b and ρ_p are the single whole pellet density and solid particle density within the pellet (kg/m^3).

4.1.3 Moisture Adsorption

The moisture adsorption rate of pellets was determined in a humidity chamber (CARON 6010, OH, USA) at 30° C and 90% relative humidity. Prior to the adsorption test, pellets were dried in an oven at 103° C for 24 h [62]. Two pellets in a glass Petri dish were placed in the humidity chamber for at least 5 h. The samples were weighed every 10 minutes for the first hour, followed by every 20 minutes for the next 2 hours, and every 30 minutes for the last 2 hours. The Petri dish was covered with a glass cap during weighing to prevent moisture loss [76].

The kinetics of moisture sorption was studied using thin layer model (Equation 13) [62].

$$\frac{M-M_{eq}}{M_0-M_{eq}} = \exp(-k_{abs}t) \quad (13)$$

Where M, M_{eq}, and M_0 are moisture at time t, equilibrium moisture, and initial moisture content in dry basis, respectively. The coefficient k_{abs} is moisture adsorption constant (min^{-1}) and t is the exposure time (min).

4.1.4 Mechanical Hardness: Durability

The durability of pellets was measured using a single pellet durability tester developed in our laboratory (Figure A.1) [112]. A pre-weighed pellet was placed in a stainless steel box (60×60×60 mm). To increase the mechanical abrasion, an artificial pellet made of tool steel 6 mm in diameter and 12 mm in length was also placed in the box. The box was shaken in a wrist action shaker for 10 minutes. After the test, the contents of the box were poured on a 3.15 mm round-hole sieve and strained through using an antistatic brush. Mass of particles remaining on the sieve was recorded, and the pellet durability was calculated from Equation 14.

$$\text{Durability (\%)} = \frac{\text{Mass left on the screen}}{\text{Initial Mass}} \times 100 \quad (14)$$

Figure 4.1 The single pellet durability tester

4.2 Pelletization Modeling

To characterize the compression behavior of the biomass, experimental data for densification were compared to compaction models. Many empirical equations have been developed to explain the compaction behavior of particulate materials [99,113,114].

Jones proposed a density-pressure relationship (Equation 15) for compacted metal powder [99].

$$\ln \rho = r.\ln P + s \quad (15)$$

Where ρ is the bulk density of compact powder (kg/m^3), P is the compression pressure (MPa), and r and s are constants.

In Cooper-Eaton model (Equation 16) it is assumed that the compression consists of two independent processes, namely, rearrangement of particles and elastic-plastic deformation of particles. Each of the two terms in Equation 16 shows each of the compaction processes [99].

$$\frac{V_0 - V}{V_0 - V_s} = a_1.exp\left(-\frac{p_1}{P}\right) + a_2.exp(-\frac{p_2}{P}) \quad (16)$$

Where V (cm^3) is the volume of the compact at pressure P (MPa), V_0 is the volume at pressure of zero (cm^3), V_s is the void-free volume of compact (cm^3), and a_1, a_2, p_1, and p_2 are model constants.

Kawakita and Ludde observed a relationship between pressure and volume (Equation 17) [99].

$$\frac{P}{C} = \frac{1}{ef} + \frac{P}{e} \quad (17)$$

Where

$$C = \frac{V_0 - V}{V_0}$$

C is the degree of volume reduction, *P* is pressure (MPa), and *e* and *f* are model parameters.

4.3 Results and Discussion

4.3.1 Mechanical Hardness

Figure 4.2 shows that at a densification temperature of 50° C for both operating forces, the durability of pellets decreased significantly by increasing the sawdust fraction ($p \leq 0.05$). At 2500 N and 50° C pelletization conditions, the durability of pure *Chlorella*, 25%, 50%, and 75% sawdust, and pure sawdust pellets were 83.21± 2.28, 72.54± 1.49, 63.08± 2.28, 45.38± 1.98, and 28.64± 1.18%, respectively. However, at temperatures of 75 and 100° C at both forces, there was no significant difference between the durability of pure *Chlorella* and other blends ($p > 0.05$) and this durability was significantly higher than pure sawdust ($p \leq 0.05$). The protein denaturation and starch gelatinization seem to be the major reasons for the better durability of pellets containing microalgae [115]. It is possible that under pressure, protein and starch were squeezed out of microalgae cells and acted as a binder during densification [61,62,102]. When the pellets were left to cool down, the crystalline structure of starch may have been regenerated partially, which enhanced the pellets' strength [102]. Protein in *Chlorella* denatures at 57° C [115]. The degree of protein denaturation and starch gelatinization increased due to the temperature increase beyond 50° C. As a result of higher natural binders' activity in microalgae at 75 and 100° C, even pellets with a smaller amount of microalgae (75% sawdust fraction pellet) had the same durability as pure microalgae pellets. In other words, a higher degree of protein denaturation and starch gelatinization at temperatures greater than 50° C, removed the need for the addition of large amounts of microalgae to sawdust.

Increasing the temperature from 50 to 75° C and from 75 to 100° C resulted in significant durability improvements for pure sawdust pellets ($p \leq 0.05$) (Figure 4.2). It seems that increasing the temperature has caused more softening in cellulose and hemicellulose, which in turn has

resulted in creating a more durable structure. However, for pure algae pellets, 25%, 50%, and 75% blends only increasing the temperature from 50 to 75° C enhanced the pellets durability ($p \leq 0.05$) and a further increase of temperature did not have a significant influence ($p > 0.05$). The observations on the temperature effect on durability were similar at both operating forces.

It was also noticed that only at the low temperature of 50° C, raising the operating force from 2500 to 3500 N caused a significant increase in durability ($p \leq 0.05$) (Figure 4.2). It seems that increasing the temperature removes the need for high values of compression force in pellets containing microalgae. Regarding sawdust pellets, increasing the force is not effective to make durable pellets. It seems that temperature> 100° C is the parameter that results in more durable pellets for pure sawdust.

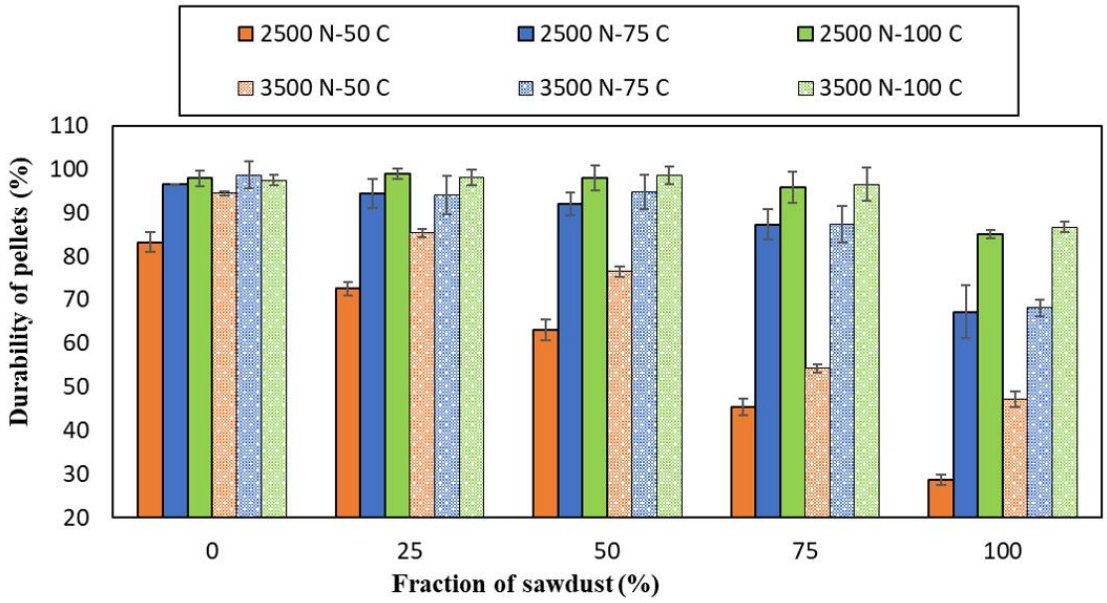

Figure 4.2 The durability of pellets made at two forces (2500 and 3500 N), three pelletization temperatures (50, 75, and 100° C), and five fractions of sawdust (0, 25, 50, 75, 100%). At the pelletization temperature of 50° C, increasing the ratio of sawdust resulted in decreasing the durability of pellets. At all pelletization conditions, the durability of pure microalgae pellets was significantly higher than that of pure sawdust pellets.

4.3.2 Density, Expansion, and Porosity

When studying the effect of microalgae fraction in the blend on pellet density, mixed effects were observed. However, the general trend was that the density of pure microalgae pellets and pellets containing microalgae (25%, 50%, and 75%) was significantly higher than the density of pure sawdust pellets ($p \leq 0.05$) (Figure 4.3). The pellets' density increase was possibly due to the flowing of softened protein and starch into voids and gaps between particles and forming tighter structure [61,62,102].

At both operating forces for 75% blend fractions and pure sawdust, increasing the temperature from 50 to 75° C led to a significant increase in pellets' density ($p \leq 0.05$) (Figure 4.3). Increasing temperature from 50 to 75° C did not influence pellets' density for pure microalgae (0% sawdust), 25%, and 50% fraction blend, significantly ($p > 0.05$). Further temperature increases to 100° C only improved pure sawdust pellets' density ($p \leq 0.05$). At low densification temperatures (50° C), increasing the force to 3500 N resulted in increasing the density of all proportions other than pure microalgae. Also, at a pelletization temperature of 75° C and a blend fraction of 75% and pure sawdust, increasing the force to 3500 N resulted in a significant increase in density ($p \leq 0.05$). Increasing the force to 3500 N at 100° C pelletization temperature, only improved the density of pure sawdust pellets ($p \leq 0.05$). As an example, the density of pellets at 2500 N and 75° C for pure microalgae, blends of 25%, 50%, 75%, and pure sawdust were 1208± 61, 1180± 22, 1157± 22, 1079± 40, and 936± 10 kg/m^3, respectively (Figure 4.3).

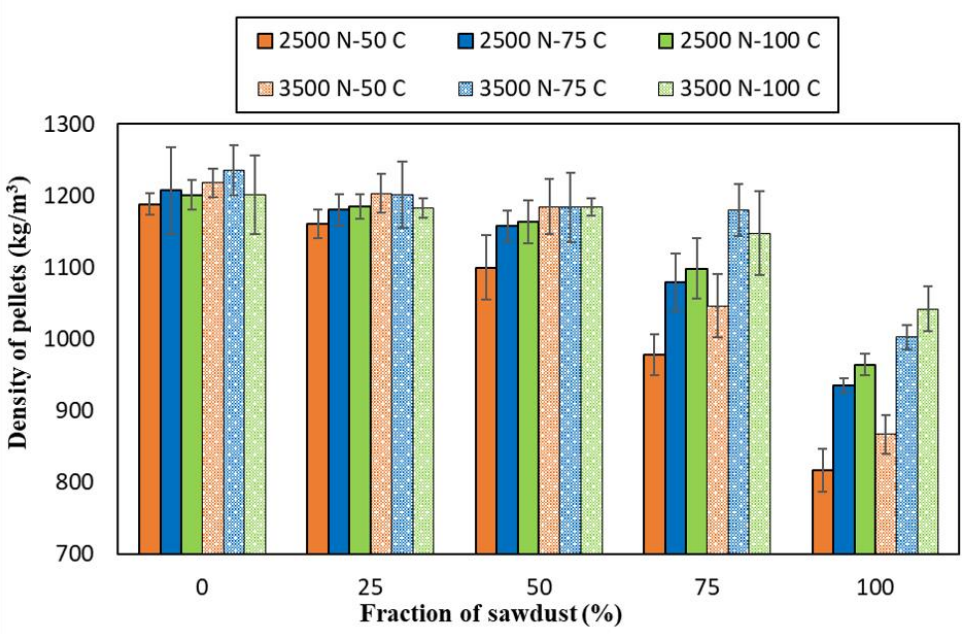

Figure 4.3 The density of pellets at two forces (2500 and 3500 N), three pelletization temperature (50, 75, and 100° C), and five fractions of sawdust (0, 25, 50, 75, 100%). The density of pure microalgae pellets and pellets containing microalgae fraction (25%, 50%, and 75%) was higher than the density of pure sawdust pellets.

The average diameter and length of the pellets made at different operating conditions and fraction of biomass were 6.34± 0.09 and 18.23± 3.9 mm (measured immediately after pellets production), respectively. Figure 4.4 shows a photograph of pellets made at 3500 N maximum force, 75° C pelletization temperature, and different fractions of biomass as an example. It should be noted that the reason for the shorter length of pellets containing sawdust is the smaller mass of biomass that was used for pelletization due to the smaller density compared to microalgae.

Figure 4.4 Pellets made at maximum force of 3500 N and temperature of 75° C. From left to right: pure *Chlorella*, 25%, 50%, and 75% sawdust, and pure sawdust, respectively.

The expansion of pellets in diametrical and longitudinal directions and pellets' density change after 14 days is shown in Figure 4.5.a, b, and c. The expansion in diameter and length direction and the percentage of density reduction increased significantly ($p \leq 0.05$) as a result of increasing the sawdust fraction in the pellet blend. At 2500 N and 75° C, for pure microalgae *Chlorella*, 25%, 50%, 75% blends, and pure sawdust pellets the density decrease after 14 days were 2.90± 0.15, 4.81± 0.19, 7.64± 0.06, 9.98± 0.40, and 11.31± 0.12 %, respectively. The results indicate that pellets dominated by microalgae had good dimensional stability during storage. The strengthened interlocking bonds by adding *Chlorella* may have contributed to the resistance to disruptive forces and reduced longitudinal expansion [61,62,102]. Comparing expansion and density results show that the pellets with larger density, expanded less.

Temperature effect on pellets' expansion at different sawdust fraction and for both forces was as followings (Figure 4.5): for pure *Chlorella* pellets the increased temperature had no impact ($p > 0.05$), at 25% and 50% sawdust fractions with increasing temperature from 50 to 75°C significantly decreased all three parameters (diameter, length, and density expansion) indicating expansion ($p \leq 0.05$); at 75% sawdust fraction and pure sawdust increasing the temperature from 50 to 75 and 75 to 100° C both significantly decreased the degree of expansion ($p \leq 0.05$). Raising the pelletization force from 2500 to 3500 N was effective at decreasing the expansion only with pellets consisting of 75% sawdust or pure sawdust ($p \leq 0.05$).

(a)

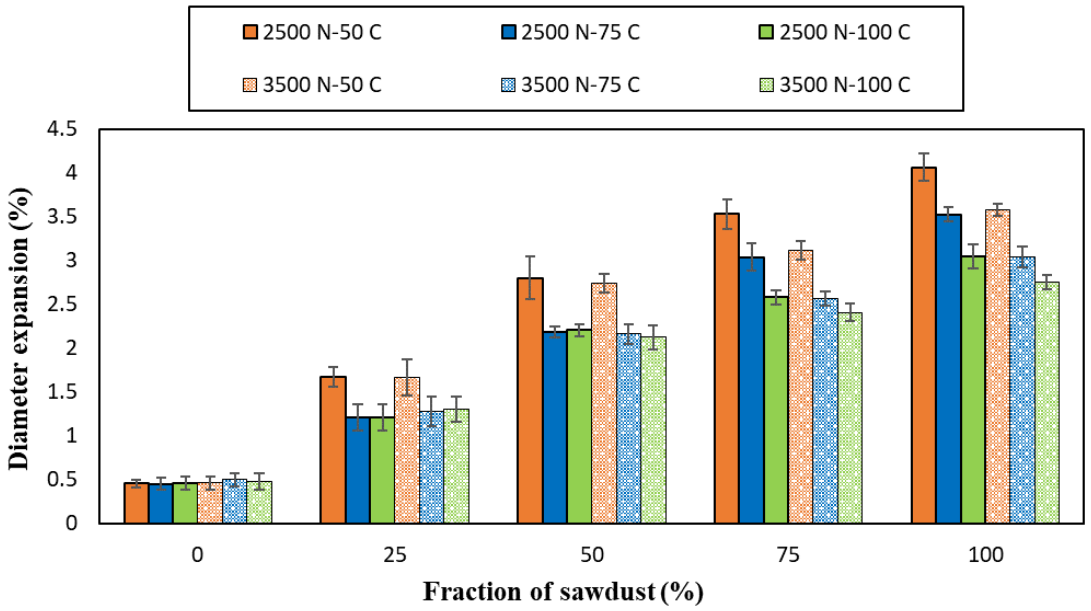
2500 N-50 C
2500 N-75 C
2500 N-100 C
3500 N-50 C
3500 N-75 C
3500 N-100 C
Diameter expansion (%)
4.5
4
3.5
3
2.5
2
1.5
1
0.5
0
0
25
50
75
100
Fraction of sawdust (%)

(b)

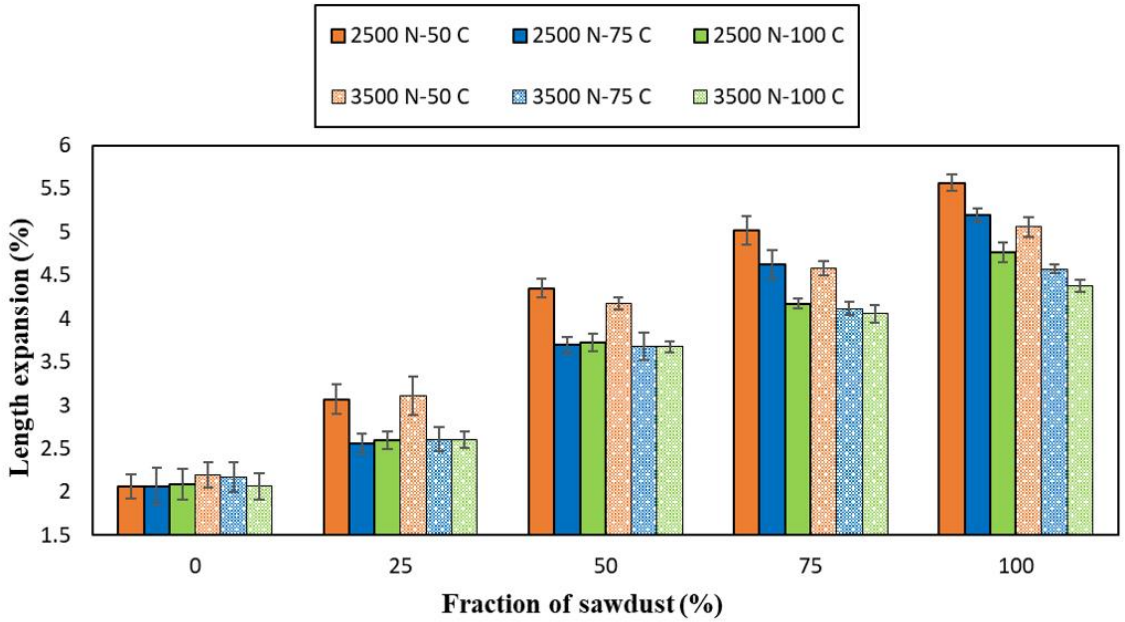
2500 N-50 C
2500 N-75 C
2500 N-100 C
3500 N-50 C
3500 N-75 C
3500 N-100 C
Length expansion (%)
6
5.5
5
4.5
4
3.5
3
2.5
2
1.5
0
25
50
75
100
Fraction of sawdust (%)

(c)

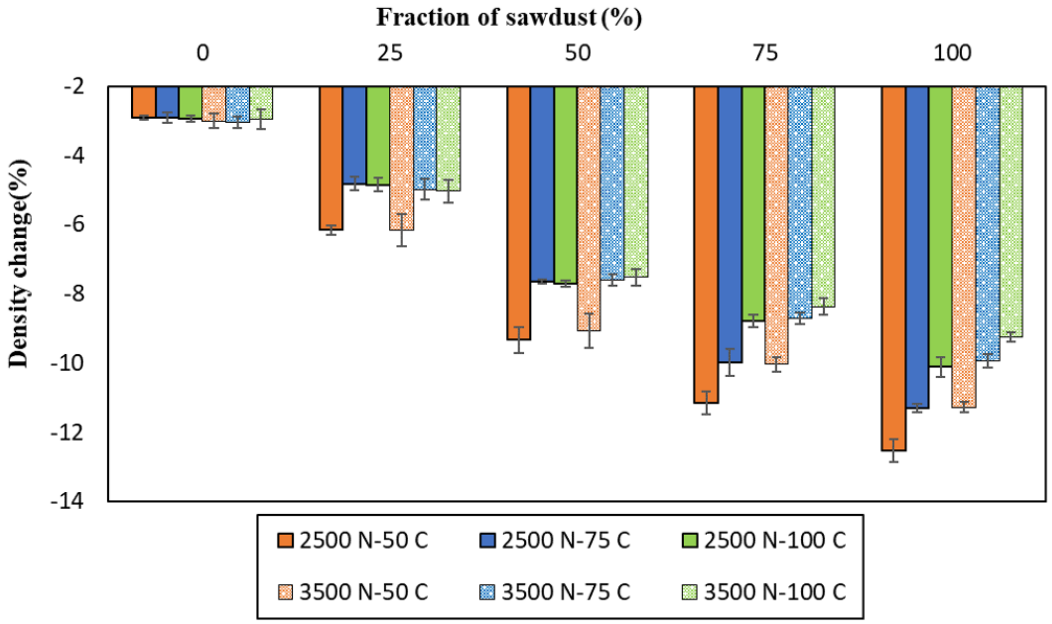

Figure 4.5 Expansion of pellets at two forces (2500 and 3500 N), three pelletization temperatures (50, 75, and 100° C), and five fractions of sawdust (0, 25, 50, 75, 100%). (a) diameter expansion, (b) length expansion, (c) percent density change. Increasing sawdust fraction in the blend resulted in more expansion in diameter and length directions, and overall density decrease of pellets.

By studying the effect of biomass fraction on pellets' porosity, it is apparent that pure microalgae pellets and other pellets containing microalgae (25%, 50%, and 75% sawdust fraction) were less porous than pure sawdust pellets ($p \leq 0.05$) (Figure 4.6). This trend was exactly the same as pellets' density. It seems that the stronger binding between microalgae particles led to a more compact structure with high density and low porosity. Furthermore, increasing temperature from 50 to 75° C led to a significant drop ($p \leq 0.05$) in porosity at 50, 75% blends, and pure sawdust. Increasing temperature further to 100° C did not have a significant impact on porosity at different conditions ($p > 0.05$). The porosity of pellets at 2500 N and 75° C for pure *Chlorella*, 25%, 50%, 75% blends, and pure sawdust were 4.53± 0.4, 6.22± 0.58, 10.55± 2.59, 17.60± 1.95, and 34.13± 1.88 %, respectively.

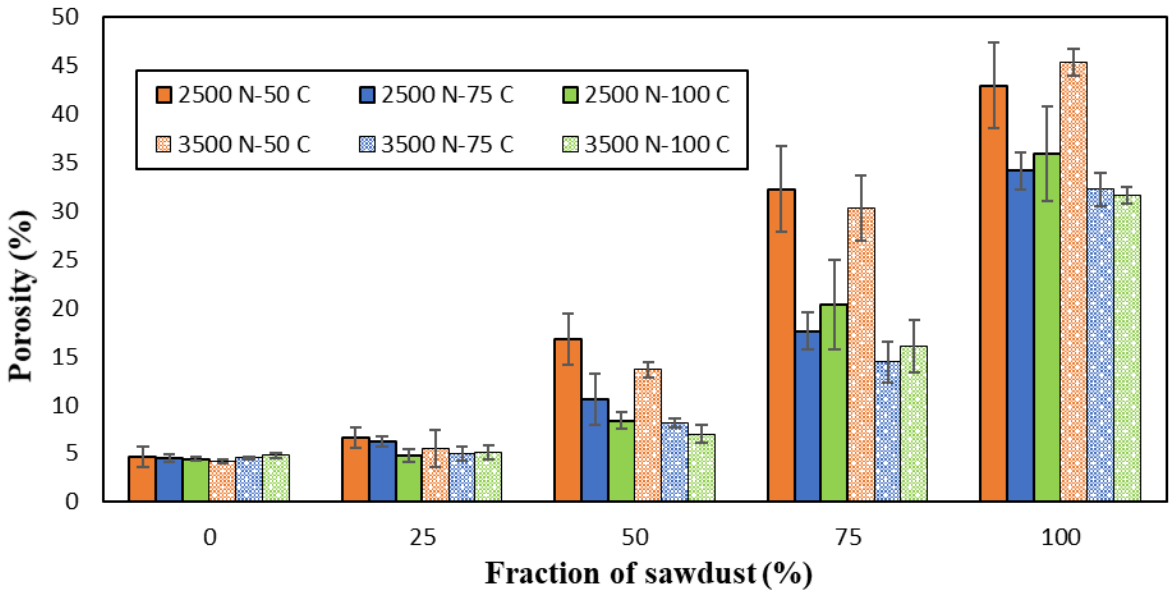

Figure 4.6 Porosity of pellets at two forces (2500 and 3500 N), three pelletization temperatures (50, 75, and 100° C) and five fractions of sawdust (0, 25, 50, 75, 100%). The porosity of pure microalgae pellets and pellets containing microalgae (25%, 50%, and 75%) was lower than the porosity of pure sawdust pellets.

4.3.3 Moisture Adsorption

Moisture adsorption by pellets can loosen the hydrogen bonding and solid bridges in the pellets, producing dust and fines that can ignite and cause an explosion during handling, storage, and transportation [61]. The moisture adsorption kinetics was found to be independent of applied pressure and die temperature, but was affected by sawdust fraction. The moisture adsorption behavior of pellets made at maximum force of 2500 N and pelletization temperature of 75° C as an example for different fractions of biomass are plotted in Figure 4.7. Table 4.1 also lists the moisture adsorption kinetic data. The higher adsorption rate with increasing sawdust fraction might be due to fibrous, porous structure of sawdust and the presence of hydrophilic hemicellulose in sawdust. Moreover, the more compact structure of microalgae pellets compared to sawdust pellets seems to help them resist moisture uptake. Furthermore, the lower equilibrium moisture content of pure *Chlorella* compared to pure sawdust confirmed its lower affinity for moisture (Table 4.1).

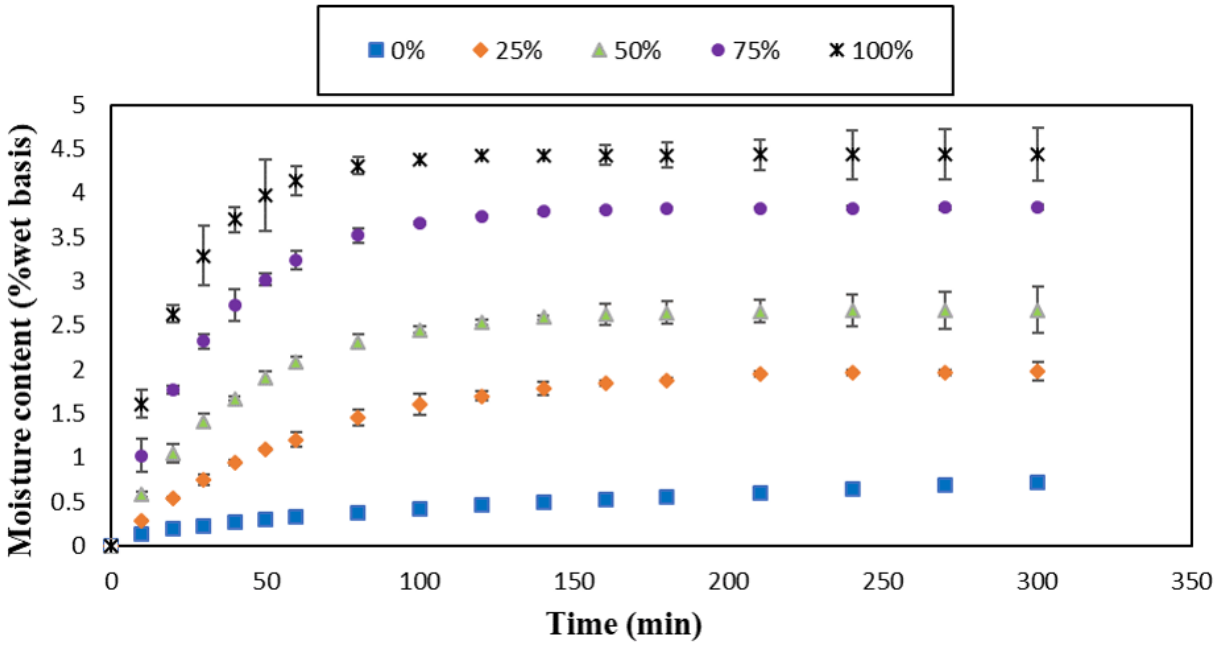

Figure 4.7 Moisture adsorption curves of pellets at 2500 N and 75° C pelletization conditions for pure *Chlorella* 0%, and blended with sawdust at 25%, 50%, 75% and pure sawdust 100%. Conditions inside humidity chamber: 30° C and 90% relative humidity.

Table 4.1 Moisture adsorption kinetic data at 2500 N and 75° C. Conditions inside humidity chamber: 30° C and 90% relative humidity. Pure microalgae had the lowest moisture adsorption rate and equilibrium moisture content.

Pellets' composition	Equilibrium moisture content (%w.b.), After 5 hours	Adsorption rate constant, k_{abs} (min $^{-1}$)	R-square
Pure *Chlorella*	0.72± 0.01	0.009	0.96
25% sawdust	1.98±0.11	0.018	0.98
50% sawdust	2.67±0.27	0.026	0.99
75% sawdust	3.84±0.03	0.029	0.97
Pure sawdust	4.44±0.30	0.034	0.91

4.3.4 Thermochemical Parameters

Since densified biomass may be destined as a fuel for firing or co-firing with coal in existing combined heat and power (CHP) plants, it is necessary to know the thermochemical characteristics of pure and blended biomass [58]. Table 4.2 lists the higher heat value and the ash content of pellets with different blends of biomass at 2500 N and 75° C. The average moisture

content of pellets one weak after making the pellets is also mentioned in Table 4.2 These two parameters were dependent on the fraction of biomass and not on the densification operating conditions (temperature and force). As listed in Table 4.2, pellets ash content and calorific value decreased, significantly ($p \leq 0.05$) by increasing the fraction of sawdust. These results demonstrate that adding microalgae to the sawdust blend increases the pellets energy density and improves their combustion efficiency. On the other hand, the higher ash content of microalgae *Chlorella* compared to woody biomass in this study might be problematic while burning pellets. Ash can cause operational difficulties such as fouling, slagging, and corrosion of burners, which reduces the burning efficiency and results in unwanted shutdowns [116]. However, microalgae ash content can be reduced by changing the formulation of culture media in the cultivation step [117].

Table 4.2 Calorific value and ash content of pellets made at 2500N and 75° C*. Pure microalgae had a significant higher calorific value compared to pure sawdust. Note that adding microalgae to sawdust increased the ash content.

Fraction of sawdust (%)	Higher heating value (MJ/kg)	Ash content (% d.b.)
0	27.80± 0.38	2.47± 0.12
25	25.32± 0.09	1.67± 0.04
50	23.49± 0.28	1.05± 0.08
75	21.44± 0.32	0.65± 0.04
100	19.42± 0.08	0.08± 0.04

*The average moisture content of pellets made at 50, 75, and 100° C was 8.38±0.51, 8.23±0.67, and 7.45±0.43 % w.b, respectively (measured 1 week after pellets' production).

4.3.5 Compaction Modeling

The data of biomass pelletization at 50° C pelletization temperature and maximum pelletization force of 3500 N was used to evaluate density changes during pellet formation with increasing the pressure (Figure 4.8).

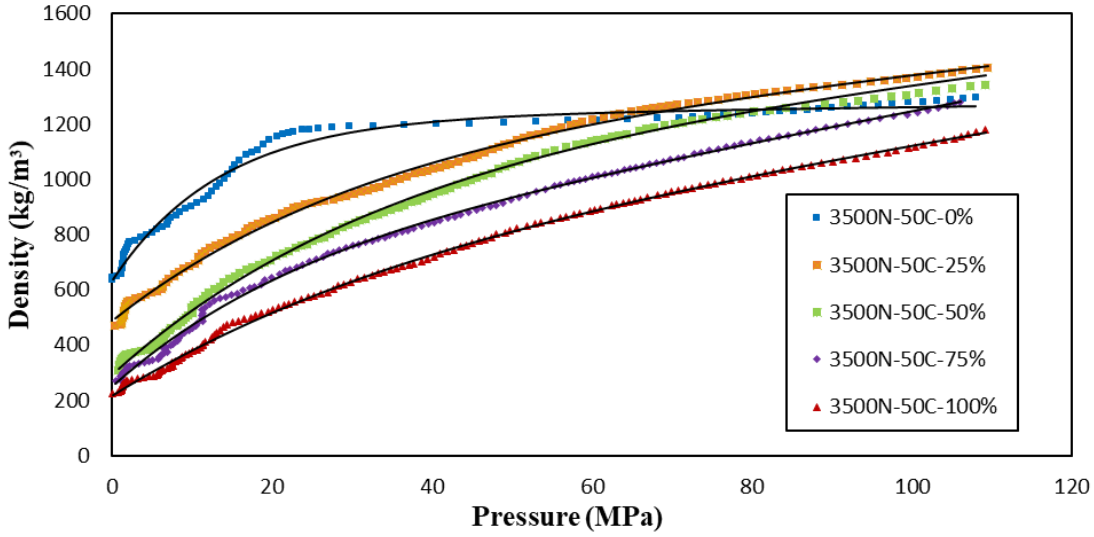

Figure 4.8 Density-pressure data during compression of biomass at pelletization temperature of 50° C, and maximum pelletization force of 3500 N for pure microalgae, 25%, 50%, and 75% sawdust fraction, and pure sawdust. For all fractions of biomass other than pure *Chlorella*, density increased by increasing the pressure in the entire compression phase.

The density-pressure data were modeled using an empirical model (Equation 18).

$$\rho = \rho_0 + (u + vP)(1 - \exp(-wP)) \qquad (18)$$

Where ρ is the pellet density (kg/m^3), P is the applied pressure during compression (MPa), and ρ_0, u, v, and w are model constants. The constants of the model and the goodness of fit are listed in Table 4.3. For pure microalgae, at low pressures < 20 MPa, density increased by increasing pressure, then the density reached a constant value until the end of compression test (Figure 4.8). In contrast, for other biomass blends and pure sawdust, the density increased with increasing pressure during the entire compression phase (Figure 4.8). The constant ρ_0 shows the initial density of biomass before compression.

Table 4.3. The parameters of the empirical model showing the relation of pressure and density (Equation 18) during compression of biomass at pelletization temperature of 50° C, and maximum pelletization force of 3500 N for pellets composed of pure microalgae, 25%, 50%, and 75% sawdust fraction, and pure sawdust.

Sawdust fraction (%)	ρ_0	u	v	w	R-square	SSE
0	636.1	588.9	0.3823	0.0745	0.984	0.068
25	487.4	632.0	2.8230	0.0366	0.997	0.032
50	295.6	766.2	3.1100	0.0344	0.998	0.015
75	250.1	445.9	5.5270	0.0510	0.998	0.031
100	219.9	456.8	4.6260	0.0392	0.999	0.015

The Jones, Cooper and Eaton, and Kawakita and Ludde models were used to model densification of pellets composed of pure or mixture of microalgae at two different compression temperatures of 50 and 100° C. The fitting results of the three models are presented in Table 4.4, Table 4.5, and Table 4.6 and Figure 4.9, Figure 4.10, and Figure 4.11. Mani et al. [113] showed that Cooper and Eaton and Kawakita and Ludde models predicted the compaction behavior of some species of agricultural biomass (wheat and barley straw, corn stover, and switchgrass) well.

The Jones model could explain the pelletization behavior of 25%, 50%, 75% sawdust fraction, and pure sawdust at a temperature of 50° C (Figure 4.9 and Table 4.4). At a compaction temperature of 100° C, only the Jones model fitted pure sawdust compaction behavior. Based on the density results (presented in Section 4.3.2. of this thesis), at densification temperature of 50° C, the density increased with increasing the densification pressure at all proportions of biomass other than pure microalgae. In addition, at 100° C densification temperature, density increases with increasing pressure was only observed for pure sawdust. The findings of pressure-density trends could explain why Jones model does not fit well with pelletization data at some of the conditions. In other words, only at conditions where density increased by increasing pelletization force, Jones model predict pelletization behavior.

Table 4.4 Jones model parameters for densification temperatures of 50 and 100° C and different blends of biomass fractions (Pure *Chlorella*, 25%, 50%, 75% sawdust, and pure sawdust)

Sawdust fraction (%)	Temperature (°C)	Constants		R-square
		r	*s*	
0	50	0.0452	6.8861	0.873
	100	-0.0003	7.0923	0.819
25	50	0.0814	6.7066	0.962
	100	-0.0026	7.08879	0.713
50	50	0.1616	6.3059	0.947
	100	0.0308	6.927	0.822
75	50	0.2316	5.8729	0.993
	100	0.0755	6.6789	0.851
100	50	0.1633	5.9962	0.999
	100	0.2314	5.8637	0.998

(a)

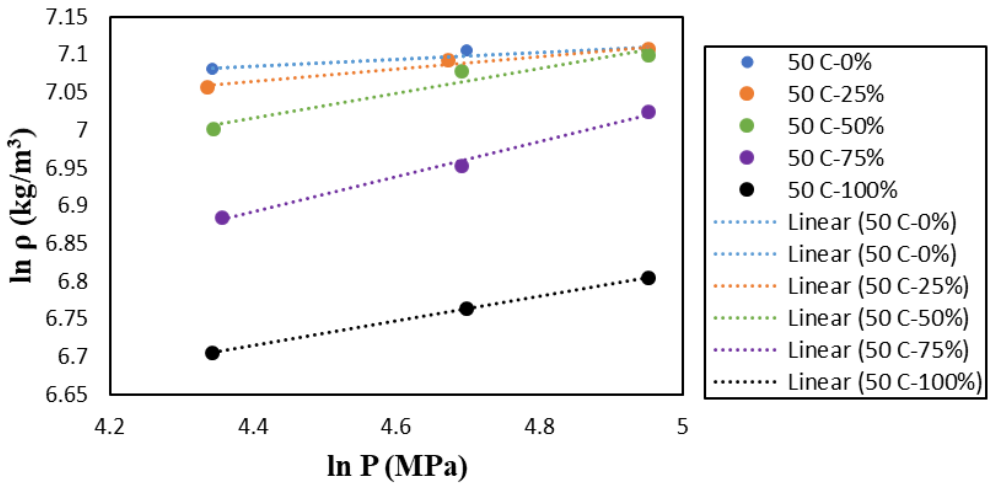

(b)

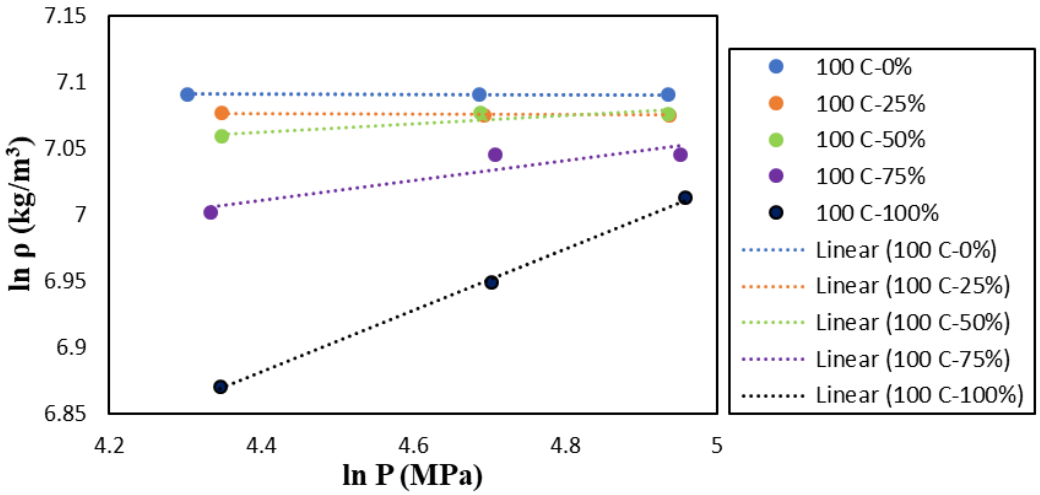

Figure 4.9 Representing the data with Jones model for different proportions of biomass (Pure *Chlorella*, 25%, 50%, 75% sawdust, and pure sawdust). (a) densification temperature of 50° C, (b) densification temperature of 100° C.

Cooper-Eaton parameters explain the prominent mechanism of biomass compaction and the corresponding pressure requirement. The parameter a_1 indicates the relative density of biomass after particle rearrangement and a_2 indicates the relative density after deformation. Since elastic-plastic deformation creates a more compact structure in comparison to particle rearrangement, usually a_1 value is lower than that of a_2. Parameters p_1 and p_2 represent the pressure required to initiate densification by particle rearrangement and deformation, respectively [99].

Similar to Jones model, Cooper-Eaton model fitted to the compaction data of pure sawdust at 100 °C and 25%, 50%, 75%, and pure sawdust at 50° C (Table 4.5 and Figure 4.10). At 50° C densification temperature for pure sawdust, the a_1 value was smaller and a_2 value was larger compared to parameters of the pellet containing 25% sawdust. Interestingly, this result shows that the particles deformation mechanism was needed to increase the pellets' density when the ratio of sawdust in the blend increased. Moreover, at 50° C densification temperature, the required pressure to induce particle deformation (p_2) in pure sawdust was much larger compared

to pellet containing 25% sawdust. At all compaction conditions that were successfully fitted by Cooper-Eaton model, the p_2 value was larger than p_1 value. In other words, the required pressure to initiate particles deformation was larger than the pressure required to initiate particle rearrangement.

Table 4.5 Cooper-Eaton model parameters for densification temperatures of 50 and 100° C and fractions of biomass blends (Pure *Chlorella*, 25%, 50%, 75% sawdust, and pure sawdust)

Sawdust fraction (%)	Temperature (°C)	Constants				R-square
		a_1	a_2	p_1	p_2	
0	50	0.0019	0.7373	0.0706	1.5150	0.704
	100	0.1145	0.6221	7.5000	0.0740	0.730
25	50	0.4319	0.5872	5.2830	8.4850	0.994
	100	0.4566	0.5083	0.2779	0.5083	0.053
50	50	0.1699	0.7932	0.00042	6.8040	0.914
	100	0.0517	0.9106	1.0100	1.2280	0.761
75	50	0.2259	0.8582	0.0002	32.7200	0.995
	100	0.4454	0.4800	0.9314	0.2106	0.137
100	50	0.2846	0.8182	0.0010	53.8300	0.942
	100	0.3945	0.5544	0.0003	17.8300	0.951

(a)

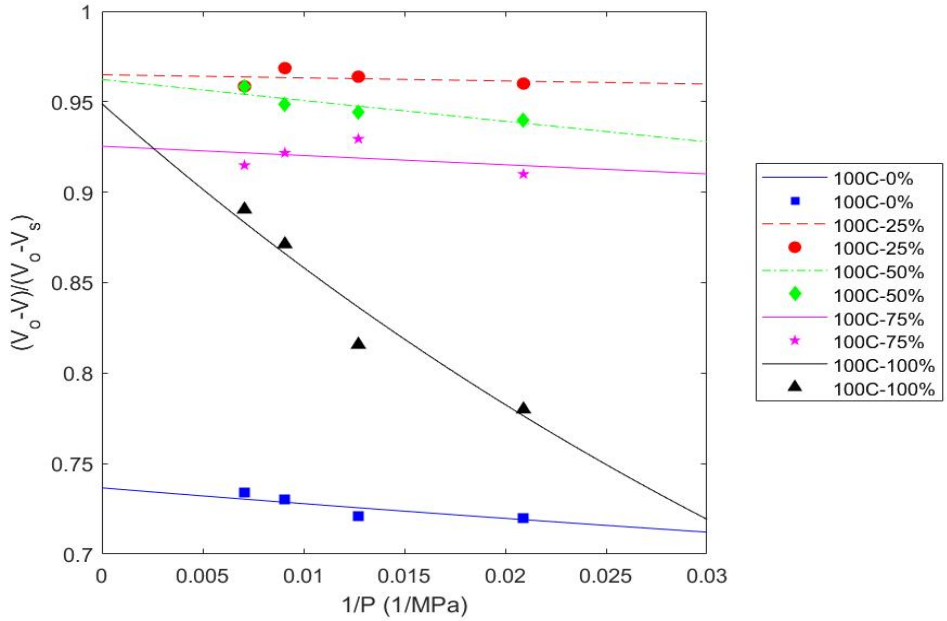

(b)

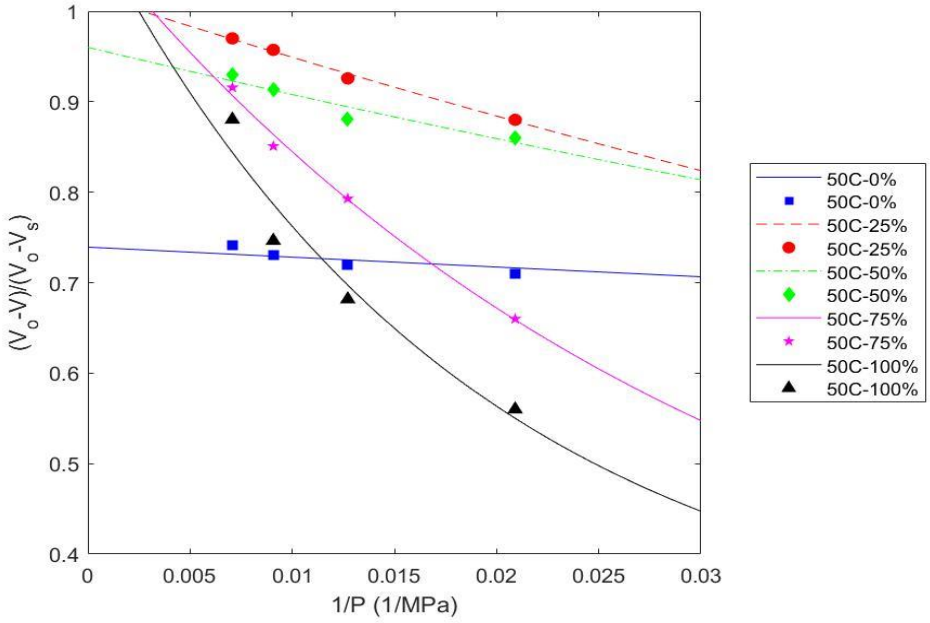

Figure 4.10 Representing the data with Cooper-Eaton model for different proportions of biomass (pure *Chlorella*, 25%, 50%, 75% sawdust, and pure sawdust). (a) densification temperature of 50° C, (b) densification temperature of 100° C.

The Kawakita- Ludde model fitted compaction data at both densification temperatures and all biomass proportions (Figure 4.11 and Table 4.6). Based on the literature [113], parameter *e* is an indicator of initial porosity of biomass grinds. The results in Table 4.6 show that the *e* value increased by increasing the proportion of sawdust in the blend, which is in accordance with the higher porosity of sawdust compared to microalgae particles, however, in this research the *e* values did not exactly show the porosity of biomass particles. Other researchers [113] reported that 1/*f* indicates the failure stress of pellet, which means a pellet with higher 1/*f* value is harder to break. However, the trend in 1/*f* value in my study did not confirm the finding from other papers. In other words, a mixed trend was observed between the different ratio of biomass and 1/*f* value.

Table 4.6 Kawakita- Ludde model parameters for densification temperatures of 50 and 100° C and fractions of biomass blends (Pure *Chlorella*, 25%, 50%, 75% sawdust, and pure sawdust)

Sawdust fraction (%)	Temperature (°C)	Constants		R-square
		e	*1/f*	
0	50	0.3145	-31.4203	0.996
	100	0.6183	-5.2190	0.970
25	50	0.7684	24.5520	0.992
	100	0.7528	18.4899	0.995
50	50	0.9235	31.7538	0.999
	100	0.8408	19.7108	1
75	50	1.0122	38.8269	0.971
	100	0.8705	13.7239	0.999
100	50	0.9180	24.5249	0.973
	100	0.9234	18.4912	0.998

(a)

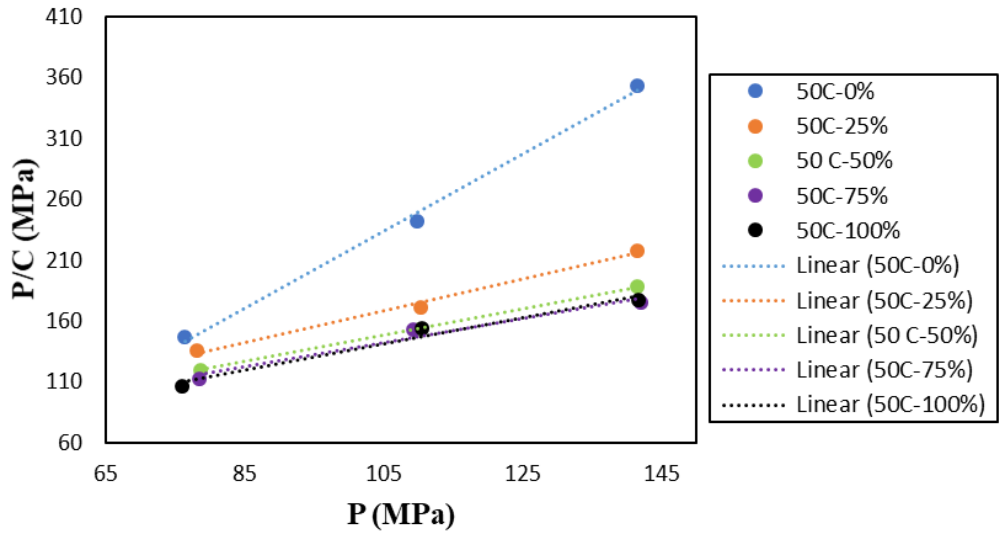

(b)

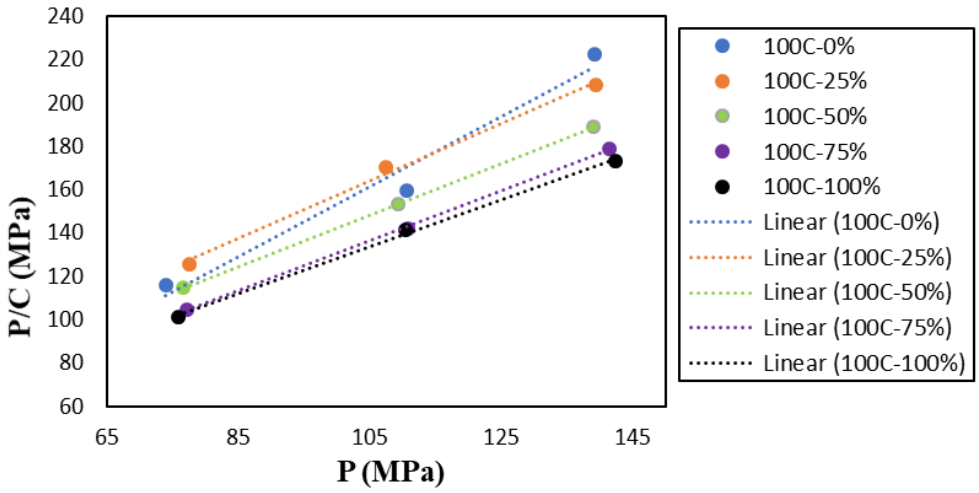

Figure 4.11 Representing the data with Kawakita- Ludde model for different proportions of biomass (Pure *Chlorella*, 25%, 50%, 75% sawdust, and pure sawdust). (a) densification temperature of 50° C, (b) densification temperature of 100° C.

4.4 Summary

The higher durability of pure *Chlorella* pellets compared to pure sawdust indicated that more durable pellets can be made by adding microalgae to wood. The protein and starch molecules in microalgae structure, which acts as natural binders are probably responsible for this improvement in durability. The experimental results of density, porosity, expansion, and moisture adsorption showed similar trends to pellets durability regarding the effect of microalgae addition to sawdust.

The pelletization data along with temperature and force data demonstrated that adding microalgae to woody biomass results in producing durable pellets even at moderate densification temperature (75° C) and force (2500 N). This is a noteworthy result because previous research has shown the need for elevated temperatures (more than 100° C) and force (about 4500 N) to make strong pure wood pellets [76]. In addition, the higher calorific value of *Chlorella* compared to sawdust is another advantage of adding microalgae to woody biomass in order to have a more valuable fuel.

The results showed that Jones and Cooper-Eaton models were fitted to the experimental compression data at biomass proportions that density increases by pressure, namely, at 50° C for 25%, 50%, 75% sawdust fraction, and pure sawdust, and at 100° C for pure sawdust. The Kawakita-Ludde model was fitted successfully to the experimental data at all temperatures and biomass proportions.

Chapter 5: Concluding Remarks and Recommendations

5.1 Discussion and conclusions

The new data generated in this thesis lead to an improved understanding of the drying behavior of microalgae *Chlorella vulgaris*. The unique knowledge gained from this research helps to choose an optimum drying temperature – time and moisture content for drying *Chlorella*. The thesis gives insight on the impact of drying on microalgae characteristics like lipid, carbohydrate, protein, and surface color. Changes in composition and surface color are indicators of the deterious effect of thermal drying on microalgae. Modifications in lipids and carbohydrates are important for using microalgae as a feedstock for liquid fuels. On the other hand, protein content and surface color determine the material's suitability for high-value products like supplements for human food or animal feed and cosmetics.

From the thermo-gravimetric analysis of *Chlorella*, it was learned that *Chlorella* loses water until 112^{o} C and volatiles at 941^{o} C with some ash (2.2%) and 14.7% fixed carbon left at the end. The micrographs (SEM) taken from dried microalgae at several drying temperatures showed that microalgae cells burst at 140^{o} C.

From thin layer drying, we learned that *Chlorella* at an initial moisture content of 70% dries in a falling rate manner during the entire drying cycle in the temperature range of 40-140° C. The drying was controlled by a diffusion mechanism. Oliveira et al. and Viswanathan et al. observed the same mechanism when drying *Spirulina* and a mixed consortium of green microalgae, respectively [26,43]. The drying rate of *Chlorella* is similar to published drying rates for other microalgae species.

The drying experiments in this work showed that all the moisture in *Chlorella* below 70% can be considered bound moisture. This means applying more energy to non-thermal dewatering steps is a waste of energy and money. In other words, thermal drying should be applied to further remove the water. In addition, it was observed that at a moderate temperature of 80° C, lipid, protein, carbohydrate, and surface color of *Chlorella* were better preserved compared to extremely low (40° C) or high (140° C) drying temperatures. This was an important finding that helps to obtain a high quality dried product for high-value applications.

Another contribution of this study is generating new empirical knowledge on the rheology of blends of microalgae and pine. The research revealed that a bulk of microalgae under axial forces initially undergoes rearrangement of cells with a large bulk volume deformation. The force-deformation curve then shows a sharp increase in densification forces with a small volumetric deformation. Pure sawdust shows a gradual increase in force deformation representing an elastic-plastic type material. The plot of volume ratio vs. inverse of pressures (Cooper-Eaton model) showed that pure microalgae was a straight line whereas pure sawdust was an exponentially decreasing curve. The volume changes vs. inverse pressure for blends of microalgae and pine sawdust fell in between the two plots.

There was a distinct difference between the densification behavior of *Chlorella* and sawdust. For sawdust, the pelletization was a continuous rearrangement of particles by increasing the force, however, for pure microalgae, the main rearrangement happened in the first phase of pelletization, followed by strengthening the bonds by further increasing the force. Blending sawdust with *Chlorella* demonstrated that by increasing microalgae in the blend, less densification energy was required. In other words, *Chlorella* was easier to compress because of its lipid content, which acts as a natural lubricant. Pellets that contained more microalgae had higher durability, density, and lower porosity, expansion, and moisture adsorption compared to pellets dominated with sawdust. The latter result can be explained by starch gelatinization and protein denaturation, which is responsible for creating strong bonds between particles.

It was observed that when *Chlorell*a was added to the biomass blend, lower levels of heat (lower temperature) and force was required to produce durable pellets compared to pure sawdust pellets. This finding demonstrated that pellets dominated with microalgae not only have superior properties like high heating value and durability but also need less energy for production.

In the drying section, it was expected to see more deterioration of biomass properties as a result of increasing the temperature. In other words, it was believed that at the lowest studied drying temperature (40° C), microalgae characteristics would be best preserved. However, the results deviated from expectations because the effect of time was not considered. In drying practices, the combined effect of time and temperature should be studied in order to find a suitable drying temperature and maintain biomass properties. In the densification section, it was expected that by applying the force during microalgae pelletization, the particles move toward

each other in the entire compaction phase. However, the results demonstrated that the movement of particles stops after reaching a specific force. The reason for the latter fact is the small porosity between microalgae particles.

The analysis on drying of microalgae on a belt conveyor using recycled heat from a power plant showed that the total cost to dry microalgae from 55% to 10% ranged from $46.13 to $109.64 per ton of dried product. The drying cost of a comparable spray dryer was estimated at $109.05 per ton of dried product. The results showed that integrating waste heat recovery with conveyor belt dryer decreased the drying costs of *Chlorella* drying.

It is stipulated that a power plant with an exhaust flue gas as the waste heat and CO_2 source is a great opportunity for co-location with algae and wood processing plants. The carbon dioxide emitted in the exhaust gas can be utilized to grow microalgae, then microalgae can be dried in a conveyor belt dryer using waste heat from flue gas as the heat source. The waste heat from the flue gas can also be used for wood drying. After drying, part of microalgae will be stored for high-value applications like for food, feed, and pharmaceuticals. The rest may enter the biofuel conversion processes. For thermo-chemical conversion steps, dried biomass can be pelletized as pure or mixed with woody biomass. Finally, the pelletized biomass can be combusted in the power plant to produce energy.

The co-location of drying, power plant and wood pellet plant example helps to decrease CO_2 emission of the power plant by using it for growing microalgae, a sustainable energy source, and at the same time using the processed microalgae and wood as a fuel in the same system. Currently, woody biomass is used as the fuel for some power plants, especially in Europe. Using microalgae-wood pellet combination can improve the conversion reaction efficiency because of improved properties of the pellets like heating value, durability, and density.

Some of the applications of my research in future research or industrial practices can be summarized as follows. The drying results give insight on the effect of temperature and time on microalgae characteristics. The drying constant developed from thin layer drying experiments can be used in the diffusional heat and mass transfer modeling of the thicker layers of biomass on belts or the drying rate of microalgae in a fluidized environment like rotary drum dryers.

In addition, the drying mechanism results indicate the need for industry to be cautious about the energy that they spend on mechanical dewatering techniques. My results showed that since moisture is entrapped inside the cells, thermal drying is necessary to reach a safe moisture content for storage (usually 10% wet basis). The pelletization results in my thesis may help industry to decrease their costs by using appropriate microalgae-sawdust blends. In addition, durability, density, and other results of pellets' characteristics are useful in the storage and transportation sectors.

The data and subsequent analysis on co pelletization provide practical guidelines on the functional characteristics of blends of microalgae and pine sawdust on making durable pellets. The data helps to optimize operating conditions (force and temperature) for producing high-quality pellets. The developed knowledge could help to decrease pelletization costs by avoiding application of unnecessary high force and heat. Moreover, the results of co-pelletization of *Chlorella* and pine sawdust could lead to faster commercialization of algae-based fuels since using pure microalgae for energy applications does not look to be economical, at present.

5.2 Recommendations

The author makes the following recommendations for further research on the topic of this thesis:

The main goal of thin-layer drying experiments was to investigate the optimum drying temperature, the effect of temperature on dried microalgae properties, and to generate new kinetics data for the design of large-scale dryers. These objectives were well addressed in Chapter 2. However, it is necessary to validate the thin-layer empirical results in a lab-scale industrial dryer. It is suggested that (1) a complete drying model consisting of heat and mass transfer including the kinetic data is developed; (2) a small-scale conveyor belt dryer is built based on the results of this study and the drying model to validate the thin layer drying results.

It is recommended to study the thermal decomposition of microalgae pellets and the co-pellets with sawdust. For this purpose, the combustion and pyrolysis behavior of pellets can be characterized in a thermo-gravimetric analyzer. These experiments provide information for thermochemical conversion of microalgae as a fuel. In direct fuel production from high oil *Chlorella*, the remaining residue contains protein and carbohydrates. This material can be mixed

with sawdust and other fibrous lignocellulosic material for feed and bioenergy applications. Co-pelletization of these blends can be developed in the future.

It is highly recommended to conduct an integrated cost analysis for microalgae processing. An economic analysis of microalgae drying in a conveyor belt dryer using waste heat is provided in Appendix A, however, in order to be able to make decisions and choose the appropriate algae processing and conversion pathway, a complete economic analysis is required.

In the suggested study, the economics of cultivation, dewatering, thermal drying, and densification should be investigated. In addition, the price of microalgae-based fuels and high-value products from microalgae should be considered.

Bibliography

[1] R. Razeghifard, Algal biofuels, Photosynthesis Research. 117 (2013) 207–219. doi:10.1007/s11120-013-9828-z.

[2] J.S. Tumuluru, L. Tabil, A. Opoku, M.R. Mosqueda, O. Fadeyi, Effect of process variables on the quality characteristics of pelleted wheat distiller's dried grains with solubles, Biosystems Engineering. 105 (2010) 466–475. doi:10.1016/j.biosystemseng.2010.01.005.

[3] J. Yan, T. Lin, Biofuels in Asia, Applied Energy. 86 (2009) 1–10. doi:10.1016/j.apenergy.2009.07.004.

[4] P. Prawisudha, T. Namioka, K. Yoshikawa, Coal alternative fuel production from municipal solid wastes employing hydrothermal treatment, Applied Energy. 90 (2012) 298–304. doi:10.1016/j.apenergy.2011.03.021.

[5] J. Gong, F. You, Value-added chemicals from microalgae: Geener, more economical, or both?, ACS Sustainable Chemistry & Engineering. 3 (2015) 82–96. doi:10.1021/sc500683w.

[6] G. Markou, E. Nerantzis, Microalgae for high-value compounds and biofuels production: A review with focus on cultivation under stress conditions, Biotechnology Advances. 31 (2013) 1532–1542. doi:10.1016/j.biotechadv.2013.07.011.

[7] P. Spolaore, C. Joannis-Cassan, E. Duran, A. Isambert, Commercial applications of microalgae., Journal of Bioscience and Bioengineering. 101 (2006) 87–96. doi:10.1263/jbb.101.87.

[8] Y. Sumi, Microalgae pioneering the future-application and utilization, Biotechnology Journal. 4 (2009) 9–21.

[9] P. Chen, M. Min, Y. Chen, L. Wang, Y. Li, Q. Chen, C. Wang, Y. Wan, X. Wang, Y. Cheng, S. Deng, K. Hennessy, X. Lin, Y. Liu, Y. Wang, B. Martinez, R. Ruan, Review of the biological and engineering aspects of algae to fuels approach, International Journal of Agricultural and Biological Engineering. 2 (2009) 1–30. doi:10.3965/j.issn.1934-6344.2009.04.001-030.

[10] M.F. Demirbas, Biofuels from algae for sustainable development, Applied Energy. 88

(2011) 3473–3480. doi:10.1016/j.apenergy.2011.01.059.

[11] T. Aysu, O. Ola, M.M. Maroto-Valer, A. Sanna, Effects of titania based catalysts on in-situ pyrolysis of Pavlova microalgae, Fuel Processing Technology. 166 (2017) 291–298. doi:10.1016/j.fuproc.2017.05.001.

[12] M.A. Borowitzka, High-value products from microalgae—their development and commercialisation, Journal of Applied Phycology. 25 (2013) 743–756. doi:10.1007/s10811-013-9983-9.

[13] I. Rawat, R. Ranjith Kumar, T. Mutanda, F. Bux, Biodiesel from microalgae: A critical evaluation from laboratory to large scale production, Applied Energy. 103 (2013) 444–467. doi:10.1016/j.apenergy.2012.10.004.

[14] J.J. Milledge, S. Heaven, Methods of energy extraction from microalgal biomass: a review, Reviews in Environmental Science and BioTechnology. 13 (2014) 301–320. doi:10.1007/s11157-014-9339-1.

[15] K.-Y. Show, D.-J. Lee, A.S. Mujumdar, Advances and challenges on algae harvesting and drying, Drying Technology. 33 (2015) 386–394. doi:10.1080/07373937.2014.948554.

[16] R. Harun, M. Singh, G.M. Forde, M.K. Danquah, Bioprocess engineering of microalgae to produce a variety of consumer products, Renewable and Sustainable Energy Reviews. 14 (2010) 1037–1047. doi:10.1016/j.rser.2009.11.004.

[17] N.K. Singh, D.W. Dhar, Microalgae as second generation biofuel. A review, Agronomy for Sustainable Development. 31 (2011) 605–629. doi:10.1007/s13593-011-0018-0.

[18] P.J. le B. Williams, L.M.L. Laurens, Microalgae as biodiesel & biomass feedstock: Review & analysis of the biochemistry, energetics & economics, Energy & Environmental Science. 3 (2010) 554. doi:10.1039/b924978h.

[19] K. De Boer, N.R. Moheimani, Extraction and conversion pathways for microalgae to biodiesel : a review focused on energy consumption, Journal of Applied Phycology. (2012) 1681–1698. doi:10.1007/s10811-012-9835-z.

[20] Aban Infrastructure Pvt Ltd, (n.d.). http://www.aban.com/ABANBIOTECH/about-us.html.

[21] C. Chen, J. Chang, D. Lee, Dewatering and drying methods for microalgae, Drying Technology. 33 (2015) 443–454. doi:10.1080/07373937.2014.997881.

[22] M.L. Gerardo, S. Van Den Hende, H. Vervaeren, T. Coward, S.C. Skill, Harvesting of microalgae within a biorefinery approach: A review of the developments and case studies from pilot-plants, Algal Research. 11 (2015) 248–262. doi:10.1016/j.algal.2015.06.019.

[23] H. Hosseinizand, C.J. Lim, E. Webb, S. Sokhansanj, Economic analysis of drying microalgae Chlorella in a conveyor belt dryer with recycled heat from a power plant, Applied Thermal Engineering. 124 (2017) 525–532. doi:10.1016/j.applthermaleng.2017.06.047.

[24] H. Hosseinizand, S. Sokhansanj, C.J. Lim, Studying the drying mechanism of microalgae Chlorella vulgaris and the optimum drying temperature to preserve quality characteristics, Drying Technology. 36 (2018) 1049–1060. doi:10.1080/07373937.2017.1369986.

[25] K.-Y. Show, D.-J. Lee, J.-S. Chang, Algal biomass dehydration, Bioresource Technology. 135 (2013) 720–729. doi:10.1016/j.biortech.2012.08.021.

[26] T. Viswanathan, S. Mani, K.C. Das, S. Chinnasamy, A. Bhatnagar, Drying characteristics of a microalgae consortium developed for biofuels production, Transactions of ASABE. 54 (2011) 1–8.

[27] M.K. Weschler, W.J. Barr, W.F. Harper, A.E. Landis, Process energy comparison for the production and harvesting of algal biomass as a biofuel feedstock, Bioresource Technology. 153 (2014) 108–115. doi:10.1016/j.biortech.2013.11.008.

[28] S.D. Varfolomeev, L.A. Wasserman, Microalgae as source of biofuel, food, fodder, and medicines, Applied Biochemistry and Microbiology. 47 (2011) 789–807. doi:10.1134/S0003683811090079.

[29] J.R. Miranda, P.C. Passarinho, L. Gouveia, Pre-treatment optimization of Scenedesmus obliquus microalga for bioethanol production, Bioresource Technology. 104 (2012) 342–348. doi:10.1016/j.biortech.2011.10.059.

[30] A. Sathish, B.R. Smith, R.C. Sims, Effect of moisture on in situ transesterification of microalgae for biodiesel production, Journal of Chemical Technology & Biotechnology. 89 (2014) 137–142. doi:10.1002/jctb.4125.

[31] E.A. Ehimen, Z.F. Sun, C.G. Carrington, Variables affecting the in situ transesterification of microalgae lipids, Fuel. 89 (2010) 677–684. doi:10.1016/j.fuel.2009.10.011.

[32] M.B. Johnson, Z. Wen, Production of biodiesel fuel from the microalga Schizochytrium

limacinum by direct transesterification of algal biomass, Energy & Fuels. 23 (2009) 5179–5183. doi:10.1021/ef900704h.

[33] G.H. Huang, F. Chen, D. Wei, X.W. Zhang, G. Chen, Biodiesel production by microalgal biotechnology, Applied Energy. 87 (2010) 38–46. doi:10.1016/j.apenergy.2009.06.016.

[34] S. Jones, Y. Zhu, D. Anderson, R. Hallen, D. Elliott, A. Schmidt, K. Alberecht, T. Hart, M. Butcher, C. Drennan, L. Snowden-Swan, R. Davis, C. Kinchin, Process design and economics for the conversion of algal biomass to hydrocarbons : Whole algae hydrothermal liquefaction and upgrading, 2014. doi:10.2172/1126336.

[35] A.C. Guedes, H.M. Amaro, F.X. Malcata, Microalgae as sources of carotenoids, Marine Drugs. 9 (2011) 625–644. doi:10.3390/md9040625.

[36] M.L. Van Emon, D.D. Loy, S.L. Hansen, Determining the preference , in vitro digestibility , in situ disappearance , and grower period performance of steers fed a novel algae meal derived from heterotrophic microalgae, Animal Science. 93 (2015) 3121–3129. doi:10.2527/jas2014-8654.

[37] V.T. Duong, F. Ahmed, S.R. Thomas-Hall, S. Quigley, E. Nowak, P.M. Schenk, High protein and high lipid-producing microalgae from northern Australia as potential feedstock for animal feed and biodiesel, Frontiers in Bioengineering and Biotechnology. 3 (2015) 1–7. doi:10.3389/fbioe.2015.00053.

[38] S.L. Lodge-Ivey, L.N. Tracey, A. Salazar, The utility of lipid extracted algae as a protein source in forage or starch-based ruminant diets, American Society of Animal Science. 92 (2014) 1331–1342. doi:10.2527/jas2013-7027.

[39] J.J. Milledge, S. Heaven, A review of the harvesting of micro-algae for biofuel production, Reviews in Environmental Science and Biotechnology. 12 (2013) 165–178. doi:10.1007/s11157-012-9301-z.

[40] L. Bennamoun, P. Arlabosse, A. Léonard, Review on fundamental aspect of application of drying process to wastewater sludge, Renewable and Sustainable Energy Reviews. 28 (2013) 29–43. doi:10.1016/j.rser.2013.07.043.

[41] S. Basu, U.S. Shivhare, A.. Mujumdar, Models for sorption isotherms for foods: A review, Drying Technology. 24 (2006) 917–930.

[42] G. V Barbosa-c, H. Vega-Mercado, Dehydration of foods, Chapman and Hall, London,

1996.

[43] E.G. Oliveira, G.S. Rosa, M. a. Moraes, L. a a Pinto, Characterization of thin layer drying of Spirulina platensis utilizing perpendicular air flow, Bioresource Technology. 100 (2009) 1297–1303. doi:10.1016/j.biortech.2008.05.052.

[44] G. Leach, G. Oliveira, R. Morais, Spray-drying of Dunaliella salina to produce a beta-carotene rich powder, Journal of Industrial Microbiology and Biotechnology. 20 (1998) 82–85. doi:10.1038/sj.jim.2900485.

[45] R. Sarada, M.G. Pillai, G. a. Ravishankar, Phycocyanin from Spirulina sp: Influence of processing of biomass on phycocyanin yield, analysis of efficacy of extraction methods and stability studies on phycocyanin, Process Biochemistry. 34 (1999) 795–801. doi:10.1016/S0032-9592(98)00153-8.

[46] a. Morist, J.L. Montesinos, J. a. Cusidó, F. Gòdia, Recovery and treatment of Spirulina platensis cells cultured in a continuous photobioreactor to be used as food, Process Biochemistry. 37 (2001) 535–547. doi:10.1016/S0032-9592(01)00230-8.

[47] G. Leach, G. Oliveira, R. Morais, Production of a carotenoid-rich product by alginate entrapment and fluid-bed drying of Dunaliella salina, Journal of the Science of Food and Agriculture. 76 (1998) 298–302.

[48] C. Tello-Ireland, R. Lemus-Mondaca, A. Vega-Gálvez, J. López, K. Di Scala, Influence of hot-air temperature on drying kinetics, functional properties, colour, phycobiliproteins, antioxidant capacity, texture and agar yield of alga Gracilaria chilensis, LWT - Food Science and Technology. 44 (2011) 2112–2118. doi:10.1016/j.lwt.2011.06.008.

[49] A. Vega-Gálvez, A. Ayala-Aponte, E. Notte, L. De la Fuente, R. Lemus-Mondaca, Mathematical modeling of mass transfer during convective dehydration of brown algae Macrocystis Pyrifera, Drying Technology. 26 (2008) 1610–1616. doi:10.1080/07373930802467532.

[50] G. Shelef, A. Sukenik, Microalgae harvesting and processing:A literature review, Haifa, 1984.

[51] E.W. Becker, Microalgae: Biotechnology and microbiology, 1st ed., Cambridge University Press, New York, 1994.

[52] A.I. Liapis, R. Bruttini, Freeze drying, in: A.S. Mujumdar (Ed.), Handbook of Industrial

Drying, 3rd ed., Taylor and Francis, New York, 2007: pp. 257–284. doi:10.1016/B978-0-12-374951-2.00019-6.

[53] I. Johnson, W. T. Choate, Waste heat recovery: Technology and opportunities in U.S. industry, 2008.

[54] Q. Zheng, J.O. Martin, S.E. Kentish, Energy efficient transfer of carbon dioxide from flue gases to microalgal systems, Energy & Environmental Science. (2016). doi:10.1039/C5EE02005K.

[55] D. Butler, Use of low grade heat from existing coal plants in Alberta, 2013.

[56] I.C. Kemp, Reducing dryer energy use by process integration and pinch analysis, Drying Technology. 23 (2005) 2089–2104. doi:10.1080/07373930500210572.

[57] A. Odukoya, G.F. Naterer, Upgrading waste heat from a cement plant for thermochemical hydrogen production, International Journal of Hydrogen Energy. 39 (2014) 20898–20906. doi:10.1016/j.ijhydene.2014.10.096.

[58] J.S. Tumuluru, C.T. Wright, J.R. Hess, K.L. Kenney, A review of biomass densification systems to develop uniform feedstock commodities for bioenergy application, Biofuels, Bioproducts and Biorefining. 5 (2011) 683–707. doi:10.1002/bbb.

[59] Z. Liu, A. Quek, R. Balasubramanian, Preparation and characterization of fuel pellets from woody biomass, agro-residues and their corresponding hydrochars, Applied Energy. 113 (2014) 1315–1322. doi:10.1016/j.apenergy.2013.08.087.

[60] S. Mani, L.G. Tabil, S. Sokhansanj, Specific energy requirement for compacting corn stover, Bioresource Technology. 97 (2006) 1420–1426. doi:10.1016/j.biortech.2005.06.019.

[61] Z.L. Huang, H. Li, X.Z. Yuan, L. Lin, L. Cao, Z.H. Xiao, L.B. Jiang, C.Z. Li, The energy consumption and pellets' characteristics in the co-pelletization of oil cake and sawdust, Royal Society of Chemistry Advances. 6 (2016) 19199–19207. doi:10.1039/C5RA23346A.

[62] H. Li, L.B. Jiang, C.Z. Li, J. Liang, X.Z. Yuan, Z.H. Xiao, Z.H. Xiao, H. Wang, Co-pelletization of sewage sludge and biomass: The energy input and properties of pellets, Fuel Processing Technology. 132 (2015) 55–61. doi:10.1016/j.fuproc.2014.12.020.

[63] L. Kumar, Z. Tooyserkani, S. Sokhansanj, J.N. Saddler, Does densification influence the

steam pretreatment and enzymatic hydrolysis of softwoods to sugars?, Bioresource Technology. 121 (2012) 190–198. doi:10.1016/j.biortech.2012.06.049.

[64] H. Li, X. Liu, R. Legros, X.T. Bi, C. Jim Lim, S. Sokhansanj, Pelletization of torrefied sawdust and properties of torrefied pellets, Applied Energy. 93 (2012) 680–685. doi:10.1016/j.apenergy.2012.01.002.

[65] N. Kaliyan, R.V. Morey, Natural binders and solid bridge type binding mechanisms in briquettes and pellets made from corn stover and switchgrass, Bioresource Technology. 101 (2010) 1082–1090. doi:10.1016/j.biortech.2009.08.064.

[66] W. Stelte, A.R. Sanadi, L. Shang, J.K. Holm, J. Ahrenfeldt, U.B. Henriksen, Recent Developments in Biomass Pelletization –A review, Bioresources. 7 (2012) 4451–4490.

[67] N. Kaliyan, R. Vance Morey, Factors affecting strength and durability of densified biomass products, Biomass and Bioenergy. 33 (2009) 337–359. doi:10.1016/j.biombioe.2008.08.005.

[68] W.B. Cavalcanti, K.C. Behnke, Effect of composition of feed model systems on pellet quality:A mixture experimental approach, Cereal Chemistry. 82 (2005) 462–467.

[69] J.L. Briggs, D.E. Maier, B.A. Watkins, K.C. Behnke, Effect of ingredients and processing parameters on pellet quality, Poultry Science. 78 (1999) 1464–1471.

[70] M.T. Carone, A. Pantaleo, A. Pellerano, Influence of process parameters and biomass characteristics on the durability of pellets from the pruning residues of Olea europaea L, Biomass and Bioenergy. 35 (2011) 402–410. doi:10.1016/j.biombioe.2010.08.052.

[71] T. Filbakk, G. Skjevrak, O. Høibø, J. Dibdiakova, R. Jirjis, The influence of storage and drying methods for Scots pine raw material on mechanical pellet properties and production parameters, Fuel Processing Technology. 92 (2011) 871–878. doi:10.1016/j.fuproc.2010.12.001.

[72] P. Gilbert, C. Ryu, V. Sharifi, J. Swithenbank, Effect of process parameters on pelletisation of herbaceous crops, Fuel. 88 (2009) 1491–1497. doi:10.1016/j.fuel.2009.03.015.

[73] L. Tabil, Binding and pelleting characteristics of alfalfa, University of Saskatchewan, 1996. http://ecommons.usask.ca/handle/10388/etd-10202004-235937.

[74] S. Thapa, D.B. Johnson, P.P. Liu, T. Canam, Algal biomass as a binding agent for the

densification of miscanthus, Waste and Biomass Valorization Journal. 6 (2015) 91–95. doi:10.1007/s12649-014-9326-3.

[75] J. Bradfield, M. P. Levi, Effect of species and wood to bark ratio on pelleting of southern woods, Forest Products Journal. 34 (1984) 61–63.

[76] P.S. Lam, Steam explosion of biomass to produce durable pellets, University of British Columbia, 2011.

[77] S. Sadaka, S. Negi, Improvements of biomass physical and thermochemical characteristics via torrefaction process, Environmntal Progress and Sustainable Energy. 28 (2009) 427–434.

[78] S. Van Wychen, L.M.L.L. Nrel, Determination of total solids and ash in algal biomass, Laboratory analytical procedure (LAP), 2013.

[79] M.M. Phukan, R.S. Chutia, B.K. Konwar, R. Kataki, Microalgae Chlorella as a potential bio-energy feedstock, Applied Energy. 88 (2011) 3307–3312. doi:10.1016/j.apenergy.2010.11.026.

[80] Z. Bi, B.B. He, Characterization of microalgae for the purpose of biofuel production, American Society of Agricultural and Biological Engineers. 56 (2013) 1529–1539.

[81] S.S. Nielsen, Food analysis laboratory manual, 2nd ed., Springer, 2013. doi:10.1017/CBO9781107415324.004.

[82] M. Dubois, K.A. Gilles, J.K. Hamilton, P.A. Rebers, F. Smith, Colorimetric method for determination of sugars and related substances, Analytical Chemistry. 28 (1956) 350–356.

[83] L.Q. Zepka, E. Jacob-Lopes, R. Goldbeck, M.I. Queiroz, Production and biochemical profile of the microalgae Aphanothece microscopica Nageli submitted to different drying conditions, Chemical Engineering and Processing: Process Intensification. 47 (2008) 1311–1316. doi:10.1016/j.cep.2007.04.013.

[84] E. Jacob Lopes, L.Q. Zepka, L.A.A. Pinto, M.I. Queiroz, Characteristics of thin-layer drying of the cyanobacterium Aphanothece microscopica Nägeli, Chemical Engineering and Processing: Process Intensification. 46 (2007) 63–69. doi:10.1016/j.cep.2006.04.004.

[85] D.I. Onwude, N. Hashim, R.B. Janius, N.M. Nawi, K. Abdan, Modeling the thin-layer drying of fruits and vegetables: A review, Comprehensive Reviews in Food Science and Food Safety. 15 (2016) 599–618. doi:10.1111/1541-4337.12196.

[86] H. Kucuk, A. Midilli, A. Kilic, I. Dincer, A review on thin-layer drying-curve equations, Drying Technology. 32 (2014) 757–773. doi:10.1080/07373937.2013.873047.

[87] J. Tang, S. Sokhansanj, A model of thin layer drying of lentils, Drying Technology. 12 (1994) 849–867.

[88] S. Sokhansanj, R.T. Patil, Kinetics of dehydration of green alfalfa, Drying Technology. 14 (1996) 1197–1234.

[89] A.O. Dissa, H. Desmorieux, P.W. Savadogo, B.G. Segda, J. Koulidiati, Shrinkage, porosity and density behaviour during convective drying of spirulina, Journal of Food Engineering. 97 (2010) 410–418. doi:10.1016/j.jfoodeng.2009.10.036.

[90] D. Lee, A. Su, A.S. Mujumdar, Bound water content in wet materials, Drying Technology. 31 (2013) 202–206. doi:10.1080/07373937.2012.694946.

[91] L. Ait Mohamed, C.S. Ethmane Kane, M. Kouhila, a. Jamali, M. Mahrouz, N. Kechaou, Thin layer modelling of Gelidium sesquipedale solar drying process, Energy Conversion and Management. 49 (2008) 940–946. doi:10.1016/j.enconman.2007.10.023.

[92] G. Chen, P.L. Yue, A.S. Mujumdar, Sludge dewatering and drying, Drying Technology. 20 (2006) 883–916. doi:10.1081/DRT-120003768.

[93] D.. Brooker, F.W. Bakker-Arkema, Drying ceral grains, The AVI publishing company, Westport, 1984.

[94] E. Ryckebosch, K. Muylaert, M. Eeckhout, T. Ruyssen, I. Foubert, Influence of drying and storage on lipid and carotenoid stability of the microalga Phaeodactylum tricornutum, Journal of Agricultural and Food Chemistry. 59 (2011) 11063–11069. doi:10.1021/jf2025456.

[95] Y.Y. Neoh, P. Matanjun, J.S. Lee, Comparative study of drying methods on chemical constituents of Malaysian red seaweed, Drying Technology. 34 (2016) 1745–1751. doi:10.1080/07373937.2016.1212207.

[96] H. Rezaei, Physical and thermal characterization of ground wood chip and ground wood pellet particles, University of British Columbia, 2017.

[97] S. Mani, A system analysis of biomass densification process, University of British Columbia, 2005.

[98] B. Ghiasi, L. Kumar, T. Furubayashi, C.J. Lim, X. Bi, C.S. Kim, S. Sokhansanj, Densified

biocoal from woodchips: Is it better to do torrefaction before or after densification?, Applied Energy. 134 (2014) 133–142. doi:10.1016/j.apenergy.2014.07.076.

[99] S. Mani, L.G. Tabil, S. Sokhansanj, An overview of compaction of biomass grinds, Powder Handling and Processing. 15 (2003) 1–9.

[100] P.S. Lam, P.Y. Lam, S. Sokhansanj, X.T. Bi, C.J. Lim, Mechanical and compositional characteristics of steam-treated Douglas fir (Pseudotsuga menziesii L.) during pelletization, Biomass and Bioenergy. 56 (2013) 116–126. doi:10.1016/j.biombioe.2013.05.001.

[101] E.L. Back, N.L. Salmen, Glass transitions of wood components hold implications for molding and pulping processes, The Journal of the Technical Association of the Pulp and Paper Industry. 65 (1982) 107–110.

[102] L. Jiang, J. Liang, X. Yuan, H. Li, C. Li, Z. Xiao, H. Huang, H. Wang, G. Zeng, Co-pelletization of sewage sludge and biomass: The density and hardness of pellet, Bioresource Technology. 166 (2014) 435–443. doi:10.1016/j.biortech.2014.05.077.

[103] R. Razuan, K.N. Finney, Q. Chen, V.N. Sharifi, J. Swithenbank, Pelletised fuel production from palm kernel cake, Fuel Processing Technology. 92 (2011) 609–615. doi:10.1016/j.fuproc.2010.11.018.

[104] J.T. Shankar, C.T. Wright, K.L. Kenny, J.R. Hess, J.S. Tumuluru, A review on biomass densification technologies for energy application, 2010. doi:INL/EXT-10-18420.

[105] F. Yazdanpanah, Evolution and stratification of off-gasses in stored wood pellets, University of British Columbia, 2013.

[106] D. Bergstrom, S. Israelsson, M. Ohman, S.-A. Dahlqvist, R. Gref, C. Boman, I. Wasterlund, Effects of raw material particle size distribution on the characteristics of Scots pine sawdust fuel pellets, Fuel Processing Technology. 89 (2008) 1324–1329. doi:10.1016/j.fuproc.2008.06.001.

[107] S. Mani, L.G. Tabil, S. Sokhansanj, Effects of compressive force, particle size and moisture content on mechanical properties of biomass pellets from grasses, Biomass and Bioenergy. 30 (2006) 648–654. doi:10.1016/j.biombioe.2005.01.004.

[108] P.S. Lam, P.Y. Lam, S. Sokhansanj, C.J. Lim, X.T. Bi, J.D. Stephen, A. Pribowo, W.E. Mabee, Steam explosion of oil palm residues for the production of durable pellets,

Applied Energy. 141 (2015) 160–166. doi:10.1016/j.apenergy.2014.12.029.

[109] P.Y. Lam, P.S. Lam, S. Sokhansanj, X.T. Bi, C.J. Lim, S. Melin, Effects of pelletization conditions on breaking strength and dimensional stability of Douglas fir pellet, Fuel. 117 (2014) 1085–1092. doi:10.1016/j.fuel.2013.10.033.

[110] Z. Tooyserkani, S. Sokhansanj, X. Bi, C.J. Lim, J. Saddler, A. Lau, S. Melin, P.. Lam, L. Kumar, Effect of steam treatment on pellet strength and the energy input in pelleting of softwood particles, American Society of Agricultural and Biological Engineers. 55 (2012) 2265–2272.

[111] P.S. Lam, S. Sokhansanj, X. Bi, C.J. Lim, S. Melin, Energy input and quality of pellets made from steam-exploded douglas fir (Pseudotsuga menziesii), Energy and Fuels. 25 (2011) 1521–1528. doi:10.1021/ef101683s.

[112] C. Schilling, M. Wohler, F. Yazdanpanah, X. Bi, A. LAu, J. Lim, S. Sokhansanj, S. Pelz, Development of a novel wood pellet durability tester for small samples, in: World Sustainable Energy Days, 2015.

[113] S. Mani, L.G. Tabil, S. Sokhansanj, Evaluation of compaction equations applied to four biomass species, Canadian Biosystems Engineering. 46 (2004) 55–61.

[114] P.J. Denny, Compactation equations: A comparison of the Heckel and Hawakita equations, Powder Technology. 127 (2002) 162–172.

[115] D. Porter, F. Vollrath, Water mobility, denaturation and the glass transition in proteins, Biochimica et Biophysica Acta. 1824 (2012) 785–791. doi:10.1016/j.bbapap.2012.03.007.

[116] S. Fournel, J. Palacios, S. Godbout, M. Heitz, Effect of additives and fuel blending on emissions and ash-related problems from small-scale combustion of reed canary grass, Agriculture. 5 (2015) 561–576. doi:10.3390/agriculture5030561.

[117] J.P. Maity, J. Bundschuh, C.-Y. Chen, P. Bhattacharya, Microalgae for third generation biofuel production, mitigation of greenhouse gas emissions and wastewater treatment: Present and future perspectives – A mini review, Energy. 78 (2014) 104–113. doi:10.1016/j.energy.2014.04.003.

[118] http://www.stela.de/, (n.d.).

[119] Y. a Castro, Optimization of wastewater microalgae pretreatment for acetone, butanol, and ethanol fermentation, Utah State University, 2014.

[120] I.C. Kemp, Fundamentals of energy analysis of dryers, in: E. Tsotsas, A.S. Mujumdar (Eds.), Modern Drying Technology, 1st ed., Wiley-VCH Verlag GmbH & Co KGaA, 2012.

[121] R.L. Shilling, P.M. Bernhagen, V.M. Goldschmidt, P.S. Hrnjak, D. Johnson, K.D. Timmerhaus, Heat-transfer Equipment, in: 8 (Ed.), Perry's Chemical Engineers' Handbook, McGraw-Hill, 2008: pp. 1–125. doi:10.1036/0071511342.

[122] J.R. Couper, D.W. Hertz, F.L. Smith, Process economics, in: Perry's Chemical Engineering Handbook, 8th ed., McGraw-Hill, New York, 2008: pp. 1–56. doi:10.1036/0071511326.

[123] http://metalsupermarkets.com/, (n.d.).

[124] http://www.condexenergy.com/advantages.htm, (n.d.).

[125] H.P. Loh, J. Lyons, C.W. White, Process equipment cost estimation, 2002.

[126] S.M. Walas, Chemical process equipment, selection and design, Butterworth-Heinemann, Newton, 1990.

[127] Z.T. Sztabert, T. Kudra., Cost estimation methods for dryers, in: A.S. Mujumdar (Ed.), Handbook of Industrial Drying, 3rd ed., Taylor and Francis, New York, 2007: pp. 1247–1258.

[128] M.S. Peters, K.D. Timmerhaus, Plant design and economics for chemical engineers, 4th ed., McGraw-Hill, New York, 1991.

[129] C. J.M., J.F. Richardson, Coulson and Richardson's chemical engineering, Particle technology and separation processes, 5th ed., Butterworth-Heinemann, Woburn, 2002.

[130] I. Obernberger, G. Thek, The pellet handbook: The production and thermal utilisation of biomass pellets, 2010. http://bios-bioenergy.at/uploads/media/The-Pellet-Handbook-Flyer.pdf.

Appendices

Appendix A Economic Analysis of Drying Microalgae *Chlorella* in a Conveyor Belt Dryer with Recycled Heat from a Power Plant

The main goal of this chapter was to investigate the economics of microalgae *Chlorella* drying in a conveyor belt dryer using recycled heat for possible cost reductions. The proposed drying system was a continuous conveyor belt dryer, and the drying took place in a convective heat transfer mode at 80°C. The dryer was modeled to find the key design parameters like bed length. The recycling system consisted of a run around thermal fluid between two tube heat exchangers. The dryer and heat recovery system were designed for the production of 1000 kg/h dried microalgae at a moisture content of 10% (wet basis, w.b.). The input moisture content ranged from 35 to 75% (wet basis). The economics of the proposed system was compared with drying in conveyor belt dryer using natural gas instead of recycled heat. The cost of spray dryer at the specific conditions mentioned in the chapter was also included in calculations.

A.1 Approach and Assumptions for Analysis: Description of the System

A single-pass conveyor belt dryer for the present analysis was used. A counter-current air flow passed through the microalgae *Chlorella vulgaris* distributed on the moving belt and the drying took place at a temperature of 80° C (based on the results of chapter 2). The dryer was equipped with blowers for air circulation through the product.

For the present analysis, the heat was transferred from the exhaust stack to the dryer through a run-around thermal liquid and two heat exchangers, one at the exhaust stack of the power plant and one at the dryer side. Figure A.1 shows the process configuration. The conveyor belt dryer was modeled mathematically. Thin-layer drying results (chapter 2) were used to obtain the necessary parameters for the system design.

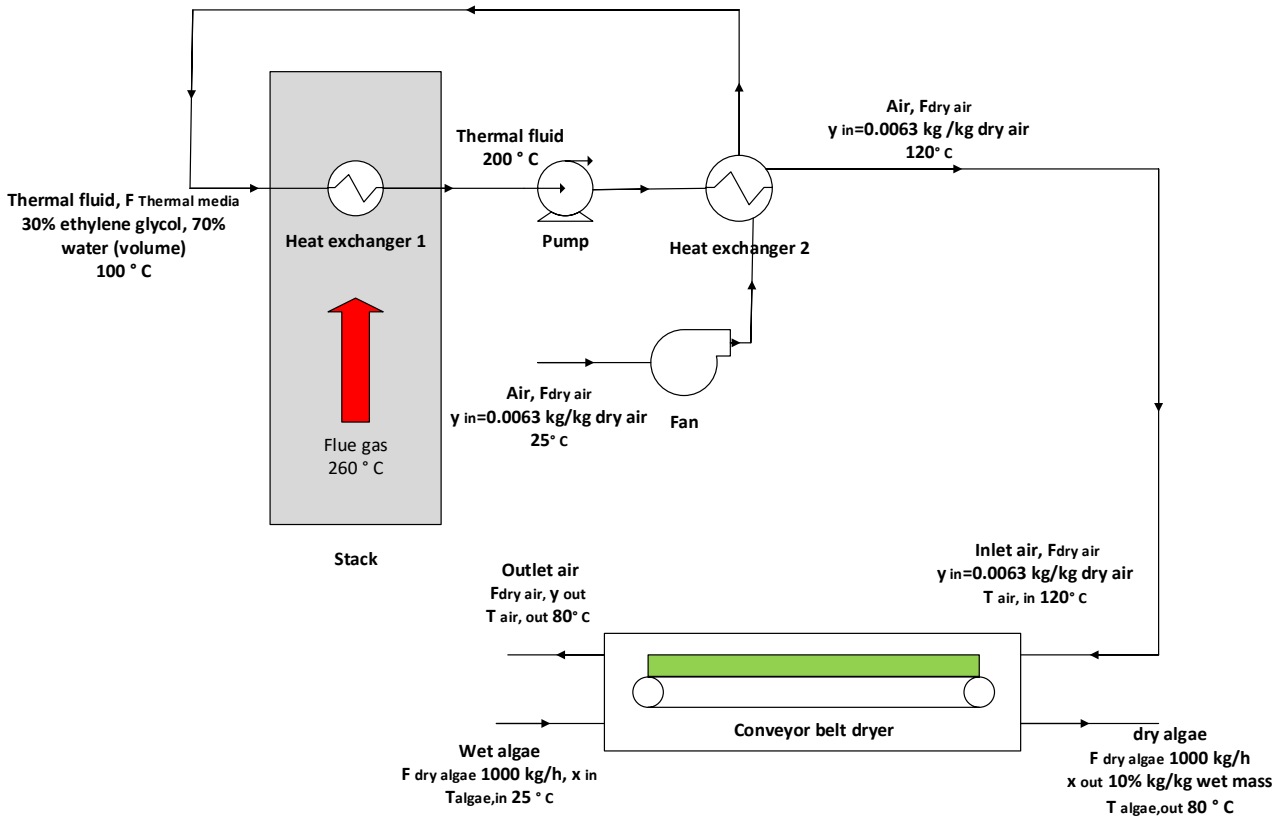

Figure A.1 Schematic diagram of the conveyor belt dryer with the heat exchanger coupled with a liquid thermal loop for recovering waste heat from the power plant. Components of the diagram are not to scale.

A.2 Approach and Assumptions for Analysis: Drying Mass Transfer Coefficient

Empirical kinetic data of Chapter 2 at a temperature of 80 °C and air velocities of 0.5, 1, and 1.5 m/s were used to estimate the internal mass transfer coefficient ($K_{internal}$). The $K_{internal}$, a parameter describing moisture transfer during the falling-rate period, was calculated based on Equation A.1. The difference between average moisture content in the bulk of the material and the moisture on the surface (Equilibrium moisture content) was the driving force for mass transfer.

$$K_{internal} = \frac{m_{dry\ algae}\,(-\frac{dx}{dt})_x}{\mathrm{A}\,(\mathrm{x}-x_{eq})} \qquad \text{(A.1)}$$

Where $K_{internal}$ is the internal mass transfer coefficient in kg/m^2. s, $m_{dry\ algae}$ is the dry weight of the biomass in thin-layer drying experiments (kg), A is the surface area of the material in thin-layer drying experiments (m^2), x is the moisture content (d.b.), and x_{eq} is the equilibrium moisture content (d.b.).

A.3 Approach and Assumptions for Analysis: Dryer Design

To find the basic design parameters of the conveyor belt dryer (bed length, required air, total residence time, and moisture profile along the bed) the dryer was mathematically modeled. Based on the presented results in chapter 2, *Chlorella* drying happens in the falling-rate period, so there was only one region on the belt. In the falling-rate period, moisture migration is controlled by solid phase, so the mass transfer coefficients of solid phase were used.

Table A.1 summarizes the key input assumptions with respect to the dryer design. There is typically a wide range of reported moisture content for the dewatered microalgae paste. In this study, the effect of initial moisture content in the range of 35 to 75% was investigated. The target final moisture content was 10% (w.b.) as a safe storage moisture content [51].

Table A.1 List of process assumptions and input data for dryer and heat recovery system design

Parameter	Value
Microalgae final moisture content (% w.b.)	10
Ambient air temperature (˚C)	25
Ambient air humidity (kg water/kg dry air)	0.0063
Inlet drying air temperature (˚C)	120
Outlet drying air temperature (˚C)	80
Drying temperature (˚C)	80
Ambient pressure (kPa)	101.325
Material depth on conveyor belt (m)	0.05
Belt width (m)	3
Dryer duct height (m)	1
Outer diameter of tubes for heat exchangers (mm)	25
Inlet thermal fluid temperature (heat exchanger 1) (˚C)	200
Outlet thermal fluid temperature (heat exchanger 1) (˚C)	100
Inlet thermal fluid temperature (heat exchanger 2) ˚C)	100
Outlet thermal fluid temperature (heat exchanger 2) (˚C)	200
Flue gas temperature exhausting from stack (˚C)	260
Inner diameter of pipes between heat exchangers (mm)	95
Distance between heat exchangers (m)	200
Heat transfer coefficient of heat exchangers (W/m^2.K)	100

The dryer was designed to produce1000 kg/h dried microalgae at 10% moisture content. The assumption of 3 m width of the belt was based on a manufacturer data [118]. The material depth on the belt was assumed to be 0.05 m. Although the thickness of material on the bed was larger than the one used in thin-layer experiments since the air velocity along the bed was way larger than the thin-layer experiments the assumption of thin-layer drying was still valid [85].

An element was considered in the solid phase as shown in Figure A.2 and two mass balances were written in this element (Equation A.2 and Equation A.3). It was assumed that the surface moisture content of the biomass was almost the same as final moisture content (equilibrium moisture content). Because of the movement of solid phase on the belt, the molecular diffusion was neglected in comparison to convective term in writing the mass balance along the bed.

$$\frac{dx}{dz} - \frac{K_{internal}W}{F_{dry\ algae}}(x - x_{eq}) = 0 \qquad \text{(A.2)}$$

$$\frac{dy}{dz} - \frac{K_{internal}W}{F_{dry\ air}}(x - x_{eq}) = 0 \qquad \text{(A.3)}$$

Where x is algae moisture content in the element (d.b.), y is air humidity (kg water/kg dry air). W is the bed width (m), $F_{dry\ air}$ is the flow rate of dry air (kg/s), $F_{dry\ algae}$ is the flow rate of dry algae (kg/s), z is the distance (m), and x_{eq} is the equilibrium moisture content (d.b.).

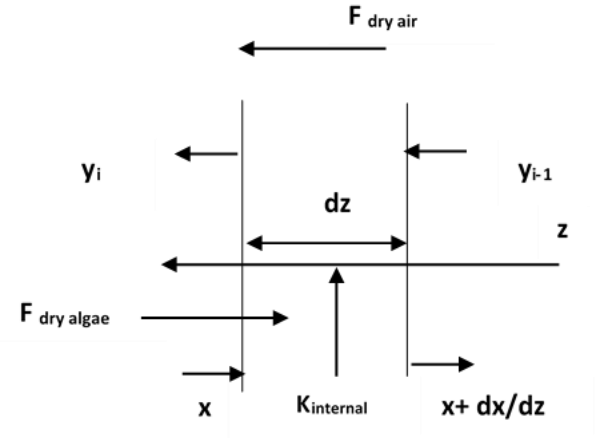

Figure A.2 Element of the wet solid on the belt

A macroscopic energy balance was also written for the whole dryer (Equation A.4).

$$F_{air}\ cp_{air}\left(T_{air,in} - T_{air,out}\right) = F_{algae,product}\ cp_{algae}\ \left(T_{algae,out} - T_{algae,in}\right) + (x_{in} - x_{out})F_{dry\ algae}\ \Delta H^{lv} \quad \text{(A.4)}$$

Where $T_{air,in}$ and $T_{air,out}$ are the temperature of the air at inlet and outlet of the dryer (K), and $T_{algae,in}$ and $T_{algae,\ out}$ are the temperature of algae at the inlet and outlet of the dryer (K). F_{air} and $F_{algae,\ product}$ are the mass flow rate of inlet air and outlet algae (kg/s). x_{in} and x_{out} are the dry basis moisture content of algae at the inlet and outlet of the dryer (kg water/kg dry algae), respectively. cp_{air}, cp_{algae}, and ΔH^{lv} are specific heat capacity of air, specific heat capacity of algae at 10% moisture content (J. kg^{-1}. K^{-1}) [119], and water heat of vaporization (J/kg), respectively.

In this work, the temperature distribution of microalgae and air was not studied. It was assumed that the drying air entered the dryer at 120° C and its temperature decreased 40° C along the bed based on a rule of thumb available in the literature [120]. Therefore, the bulk temperature of the air was 100° C and based on the available literature drying occurred at a temperature almost 20°C lower than the bulk of air, so in this case, drying happened at 80° C [120].

By assuming lumped coordinates for width and thickness directions, the moisture content changed only along the bed. The 1-D steady-state problem was solved using finite difference method. The initial and final algae moisture contents (x_{in} and x_{out}) were used as inlet and outlet boundary conditions, respectively. The bed length was divided into 0.01 m long segments. Statistical analysis showed that smaller mesh size did not have a considerable impact on the moisture distribution along the bed. The internal mass transfer coefficient was obtained from Equation A.1. For each segment, moisture content was calculated in an iterative manner. First, it was assumed that the moisture content of cell center was equal to inlet moisture. The outlet moisture in each segment was obtained by calculating water evaporation with the mass balance equation (Equation A.2). Then, cell moisture content was updated by using the averaged inlet and outlet moisture content. The convergence of numerical solution was assured by monitoring the residuals of two consecutive iterations to a criterion of at least 10^{-5} for the moisture content. The bed length was obtained from cumulating of distance segments once the moisture content on the bed was less than final moisture content.

A.4 **Approach and Assumptions for Analysis: Heat Recovery System**

In the United States, the total unrecovered heat from industrial boiler exhaust gas is about 1200 TBtu/year [53]. The temperature exhausted from the stack ranges from 232-650˚ C with an average of around 260˚ C. For the present study a run-around loop was proposed to recover the sensible waste heat from flue gas and transfer it to the drying air (Figure A.1). The system consisted of two sets of heat exchangers connected with a pipe. A high-pressure pump pushed the heat transport medium water-ethylene glycol (30% volume) solution between the two heat exchangers. Table A.1 lists the assumed conditions for the heat recovery system. The inefficiency of heat exchangers was considered in order to include heat losses from the heat recovery system in cost calculations. The 100 $W/m^2.K$ heat transfer coefficient for air-cooled exchanger on bare-tube basis was extracted from Perry handbook [121].

The economics of the conveyor belt dryer coupled with waste heat recovery was compared with the conveyor belt dryer of the same dimensions and operating conditions using natural gas and also with the spray dryer using natural gas.

To study the performance of conveyor belt dryer using natural gas, in the calculations the entire recovery system was replaced with an industrial air heating furnace. The furnace provided heat to the drying air to raise the temperature to 120° C as in the heat recovery system. The heat load and required air flow rate of spray dryer with inlet and outlet air temperatures of 200 and 121° C were also calculated. The biomass inlet flow rate for the spray dryer was assumed the same flow rate at 55% initial moisture content in conveyor belt dryer case and the results were compared with conveyor belt dryer at 55% initial moisture content.

A.5 Approach and Assumptions for Analysis: Economic Analysis

The resulting mass and energy balance outputs were used to evaluate the capital and operating costs in order to estimate total drying cost using waste heat. The capital cost is independent of fluctuations in operating conditions. The total capital investment includes costs required to purchase land, design, purchase, shipment, and installation of equipment, structures, building and bringing the facility into operation [122]. The cost estimation method and assumptions used were all according to Jones et al.'s study [34]. Table A.2 lists all the input cost data and assumptions.

Table A.2 List of economic assumptions and cost data

Parameter	Value
Electricity cost ($/kWh)	0.10
Operation time (h/y)	7920
Interest rate (%)	6
Lifetime period (y)	10
Natural gas price ($/1000 ft^3)	6.27
Hand factor for spray dryer	3.5
Hand factor for pump	4.0
Hand factor for conveyor belt, pipelines, fan and cyclone	2.5
Hand factor for fire heater and heat exchanger	2.0
Pipe cost (stainless steel 304-SC10-0.75 in) ($/ft)	5.06
Pipe cost (stainless steel 304-SC10-3.5 in) ($/ft)	27.79
Labor hourly wage ($/h)	15

The major part of the capital investment is fixed capital investment (FCI); and equipment purchasing, delivery, and installation is the most important compartment of fixed capital investment. In this study, Hand factors were used to estimate the total installed cost (TIC) for the equipment. Based on Hand method, equipment was categorized into different groups, and a factor was assigned to each group [122]. The TIC of each unit was calculated by multiplying its purchase cost by its Hand factor.

For the drying coupled with heat recycling, main pieces of equipment were conveyor belt dryer, heat exchangers, pipe, pump, and fan. For the spray dryer case, major equipment was spray dryer, fan, gas heater furnace, and cyclone. The main pieces of the conveyor belt using natural gas were conveying system, blowers, and furnace. The Hand factors (installed cost/purchase price) for conveyor, heat exchanger, pump, pipe, blower, gas heater, cyclone, and spray dryer are listed in Table A.2 [28]. The values of Hand factor depend on the size of the project, vendor, complexity of installations, and the distance between supplier and microalgae plant. Therefore, in addition to cost estimation by applying Hand factors, the cost was also estimated with assuming the value of 1 for Hand factors. The cost of building, additional piping, and site development were calculated as 1%, 4.5%, and 9% of TIC. The total direct cost (TDC), was the sum of the total installed cost, building, additional piping, and site development costs. Fixed capital investment (FCI) of the plant included direct and indirect cost (55% of TDC). Finally, total capital investment (TCI) was calculated by summation of FCI and working capital (5% of FCI) [34].

The purchased cost of the heat exchanger, conveyor belt dryer, and pipe was estimated based on vendor quotes [118,123,124]. The purchased cost of gas heater furnace, pump and fan were calculated based on the graphs in Loh et al.'s report [125], Purchased cyclone cost was extracted from Walas text book [126] and cost reference for spray dryer was Sztabert and Kudra's book [127]. In cases where purchased equipment cost for the exact capacity was not available, Equation A.5 was used to scale purchased cost with a capacity factor [128].

$$Cost_{eq} = \alpha S^{\beta} \quad \text{(A.5)}$$

Where α is the unit cost of equipment, β is a factor and S is a capacity parameter. The purchase costs of various years were converted to 2015 dollars, Chemical Engineering Plant Cost Index (CE Index) was used [128]. Equation A.6 was applied to update the cost.

$$Cost_{year\ A} = Cost_{year\ B} \frac{\text{CE Index at year A}}{\text{CE Index at year B}} \quad \text{(A.6)}$$

Operating costs depend on throughput and consist of the costs associated with raw material, utilities including heat and electricity, labor, supervision, maintenance, and insurance [23,24]. Variable operating costs were utility, fuel (in spray dryer case and belt dryer using natural gas), and raw material. Fixed operating costs were labor, supervision, maintenance, benefits, insurance, and taxes. Benefits were calculated as 90% of total salaries. Maintenance and insurance and taxes were estimated as 3% and 0.7% of the fixed capital investment, respectively [34]. The supervision cost was calculated as 20% of labor cost [128]. Utility cost was dependent on the annual running time and the price of energy. The assumption of 330 operating days per year was made from Jones et al. [34]. The raw material is usually the largest cost in manufacturing of a product, but in this study, it was excluded from annual operating expenses because drying was one of the operations along the supply chain. The annual operating cost was calculated based on Equation A.7:

$$Cost_{operating} = (C_s Q + C_e P)t_y + Cost_{fuel} + Cost_{Labor} + Cost_{supervision} + Cost_{benefits} + Cost_{maintenance} + Cost_{insurance\ and\ taxes} \quad \text{(A.7)}$$

where t_y is the annual running time assumed to be 7920 h/year C_s and C_e are the price of a unit of heat and a unit electricity, respectively. Q and P are the amount of required heat and electrical power (kWh), respectively. The total annual cost was obtained by the sum of annual operating cost and annualized capital cost (Equation A.8):

$$Cost_{annual-Total} = Cost_{annual-\ capital} + Cost_{operating} \quad \text{(A.8)}$$

To calculate the annual capital cost, capital recovery factor (e) was used [128] (Equation A.9 and Equation A.10):

$$Cost_{annual\ capital} = e.Cost_{capital} \quad \text{(A.9)}$$

$$e = \frac{i_r(1+i_r)^{l_f}}{(1+i_r)^{l_f}-1} \quad \text{(A.10)}$$

where i_r is interest rate and l_f is a lifetime of the dryer (see Table A.2) [128].

Finally, the cost of drying a unit of final product in $/ton (w.b.) in heat recycled system, belt dryer using natural gas, and spray dryer were estimated from Equation A.11.

$$Cost_{drying} = \frac{Cost_{annual-Total}}{t_y * F_p} \quad \text{(A.11)}$$

where F_p is the mass flow of the microalgae at its final target moisture content in a year (ton/year).

A.6 Design Results and Discussion

From the numerical differentiation of empirical drying data, $K_{internal}$ was calculated. Figure A.3 shows the values derived for internal mass transfer coefficient at different air velocities. By decreasing the moisture content in falling- rate period, the values of $K_{internal}$ increased, due to a small driving force at low moisture contents, which in turn led to large $K_{internal}$ values.

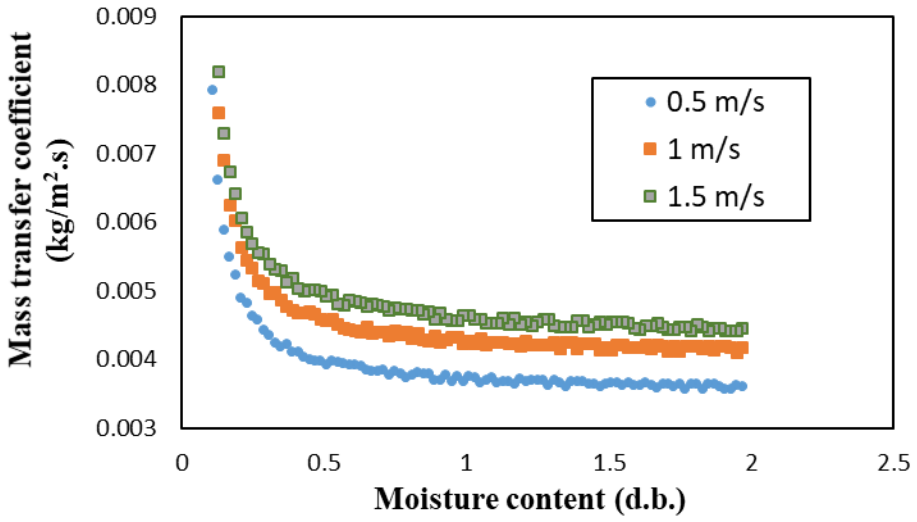

Figure A.3 The experimental internal mass transfer coefficient for microalgae dried at 80° C

Since the air velocities used in industrial conveyor belt dryers were higher than those applied in thin-layer drying experiments, the effect of air velocity on the internal mass transfer coefficient should be considered. The dependency of the mass transfer coefficient at 80° C on velocity is described using Equation A.12.

$$K_{internal} = 7.586 \times 10^{-4} . \frac{x}{x-0.0622} . (1 + \ln \frac{u_{air}}{0.01389}) \quad \text{(A.12)}$$

Where u_{air} is the air velocity (m/s). By substitution of $K_{internal}$ from Equation A.12 in Equation A.2 and Equation A.3, the model was solved mathematically. The moisture distribution along the bed for the initial moisture content of 55% as a specific case is presented in Figure A.4. To include the effect of heat loss from the dryer, the thermal inefficiency of conveyor belt dryer was considered and the parameters obtained from the mathematical model were updated. Table 5.3 presents the final results for different input moisture contents of biomass.

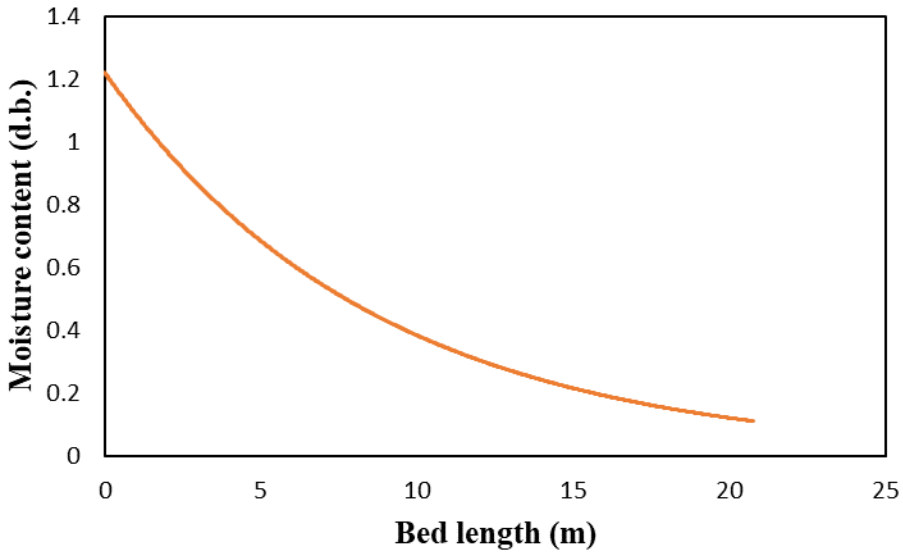

Figure A.4 Moisture profile along the bed for initial moisture content of 55% and final moisture content of 10% (w.b.)

Table 5.3 Design parameters of conveyor belt dryer coupled with waste heat recovery system at initial moisture contents of 35, 45, 55, 65, and 75% (w.b.)

Initial moisture content (% w.b.)	35	45	55	65	75
Wet feed flowrate (kg/h)	1385	1636	2000	2571	3600
Dry product flowrate (kg/h)	1000	1000	1000	1000	1000
Evaporation rate (kg/h)	384.6	636.6	1000	1571	2600
Residence time (min)	165.7	194.3	217.2	242.2	263.1
Bed length (m)	20.7	24.3	27.2	30.3	32.9
Air flowrate (kg/s)	6.6	10.7	16.5	25.7	42.3

A.7 **Economics Results and Discussion**

Table A.4 lists the purchase cost of major pieces of equipment. Figure A.5 presents the capital and operating costs per ton of dry product for conveyor belt dryer coupled with heat recycling system, conveyor belt dryer using natural gas, and drying with spray dryer at an initial moisture content of 55%. The three sets of data on the right of the plot were based on the assumption of Hand factor equal to one, and the three sets on the left were based on Hand factors other than one extracted from Table A.2. By considering the Hand factors (Installed cost/purchased cost) listed in Table A.2, the annual total cost of drying in conveyor belt dryer using waste heat recovery was 109.64 $/ton of dried biomass. The annual total cost under the same conditions using a spray dryer and conveyor belt dryer using natural gas was 1.7 and 1.29 times higher than the recycled system at 187.67 and 141.5 $/ton, respectively.

Table A.4 Purchase cost of equipment to produce 1000 kg/h of microalgae at 10% moisture content from the initial moisture content of 55% (wet basis). The costs were converted to 2015 dollars.

Equipment	Purchase cost (1000 x $)
Conveyor belt dryer	712.73
Heat recycling system (including heat exchangers, pump, fan, and piping)	419.39
Indirect natural gas heating system	365.02
Spray dryer (including dryer, fan, and cyclone)	684.11

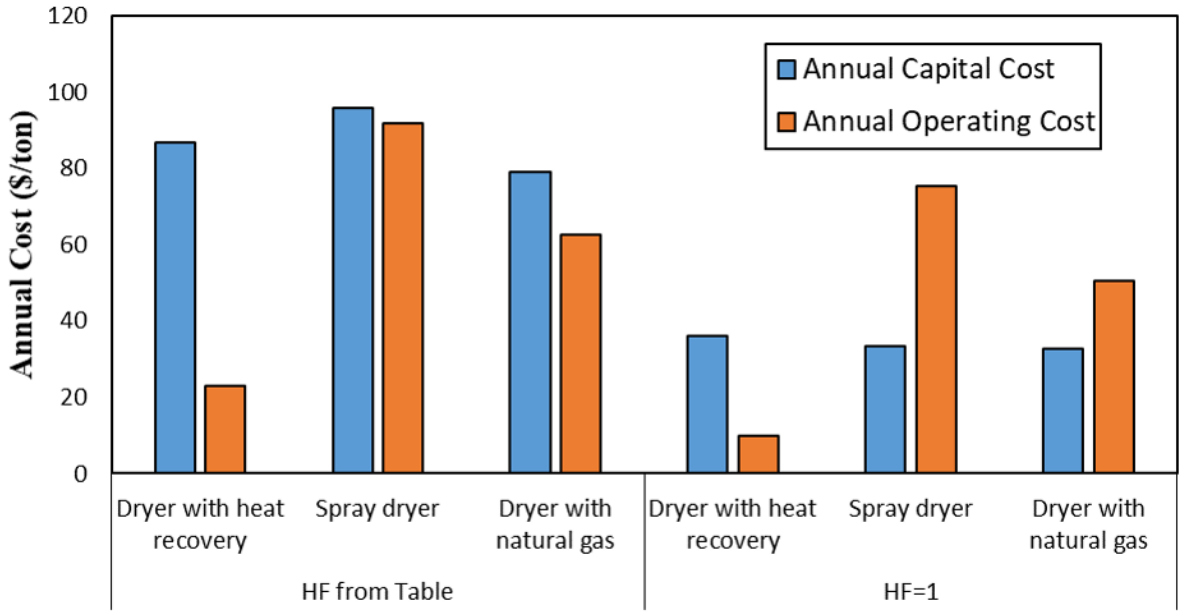

Figure A.5 Annual capital, operating, and total cost per ton of dried product for different drying systems by considering Hand factor (HF) from Figure A.2 (three data set on the left) and HF=1 (three data set on the right). (input moisture content 55% w.b)

Applying heat integration system provided the opportunity to use waste heat in order to warm up the air rather than consuming fuel for this purpose. The flue gas waste heat can be captured to decrease the operating costs and to improve the microalgae drying economics. If spray dryer or conveyor belt dryer without any heat integration is used, a fuel like coal, natural gas, or biomass should be burnt to provide the required energy for increasing air temperature. Increased fuel consumption results in high operating costs. As Figure A.5 shows, the annual capital cost of three dryers was almost the same. However, significantly higher operating costs of a spray dryer (91.7 $/ton) and conveyor belt dryer using natural gas (62.57 $/ton) in comparison to conveyor belt dryer using recycled heat (23.02 $/ton) made them less cost-effective. The major difference in operating costs in the spray dryer and heat recycled system was the huge amount of natural gas needed to increase the air temperature to desired inlet temperature (about 200° C based on [129]).

The costs based on all the Hand factors equal to 1 were also presented in Figure A.5. By removing the Hand factors, the costs of all three systems declined. The total annual cost of

conveyor belt dryer using waste heat, spray dryer, and conveyor belt dyer using natural gas was 46.13, 109.05, and 83.47 $/ton, respectively when HF=1. Probably the real cost is a value between these two extremes [37]. In an economic analysis [130] for sawdust pellet production that used a belt dryer with a water evaporative capacity of 5000 kg/h, to dry biomass from 55% to 10%, the total drying cost was quoted as 950,000 Euros (2010) or 48.10 Euro /ton of output, equal to $66.00 per ton in 2015 dollars.

The economics of drying using natural gas was mainly dependent on natural gas price, and the recycled system would be more economical at high prices of natural gas. Comparing the cost of microalgae drying in three systems revealed that utilizing recycled heat instead of natural gas improved drying economics. Moreover, it was realized that drying cost in conveyor belt dryer with recycled heat was significantly lower than spray drying cost which is mostly applied in industry.

The effect of moisture content variation was investigated in the range of 35 to 75% because there are a variety of dewatering methods which can remove biomass water to different final values. The results are plotted in Figure A.6. The reduction in drying cost was significant when input moisture content decrease from 75% to 35%, the cost went down from $91.13 to $31.88 per dry ton.

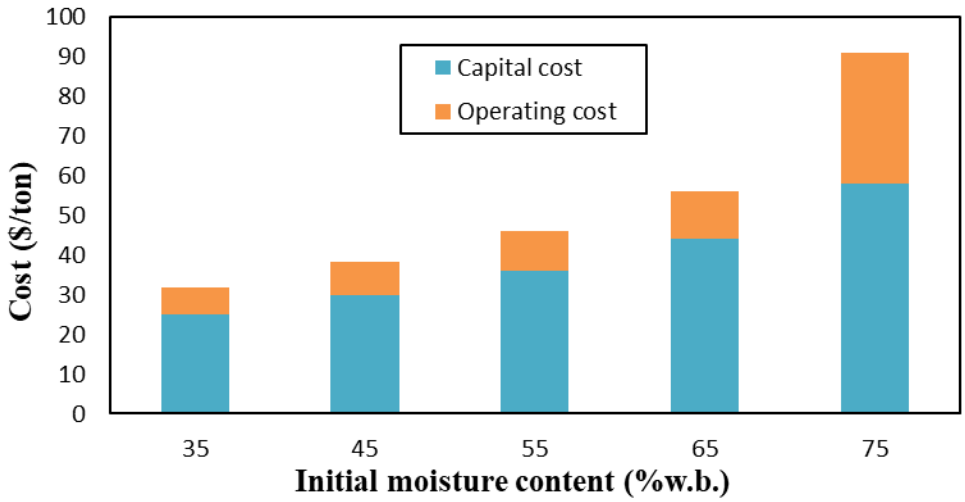

Figure A.6 Sensitivity of drying cost to initial (input) moisture content for the belt dryer with recycled heat (HF=1)

A.8 **Summary**

Depending upon the applied Hand factor, the total cost to dry microalgae from 55% to 10% ranged from $46.13 to $109.64 per ton of dried product. Using natural gas assumed at $6.27/GJ, the drying cost increased to $83.47 per ton (using hand factor equal to 1). The drying cost using a commercial spray dryer was $109.05 per ton of dried product (using hand factor equal to 1). The results showed that integrating waste heat recovery with conveyor belt dryer decreased the drying costs of *Chlorella* drying in comparison to two other drying methods.